PCRLB-BASED RADAR RESOURCE MANAGEMENT FOR MULTIPLE TARGET TRACKING

PCRLB-BASED RADAR RESOURCE MANAGEMENT FOR MULTIPLE TARGET TRACKING

By ANBANG DENG, M.Sc

A Thesis Submitted to the School of Graduate Studies in Partial Fulfillment of the Requirements for the Degree Doctor of Philosiphy

McMaster University

DOCTOR OF PHILOSIPHY (2023)

Hamilton, Ontario, Canada (Electrical and Computer Engineering)

TITLE:	PCRLB-based Radar Resource Management for Multiple Target Tracking
AUTHOR:	Anbang Deng M.Sc. (Electrical and Computer Engineering), Western University, London, Canada
SUPERVISOR:	Prof. T. Kirubarajan
NUMBER OF PAGES:	xv, 149

Abstract

As a crucial factor in improving radar performance for multiple target tracking (MTT), resource management problems are analyzed in this thesis with regard to sensor platform path planning, beam scheduling, and burst parameter design. This thesis addresses problems to deploy or adapt radar configurations for multisensor-multitarget tracking, including 1) the path planning of movable receivers and power allocation of transmitted signals, 2) the optimal beam steering of high-precision pencil beams, and 3) the pulsed repetition frequency (PRF) set selection and waveform design.

Firstly, the coordinated sensor management on the ends of both receivers and transmitters for a multistatic radar is studied. A multistatic radar system consists of fixed transmitters and movable receivers. To form better transmitter-target-receiver geometry and to establish an effective power allocation scheme to illuminate targets with different priorities, a joint path planning and power allocation problems, which determines the moving trajectories of receivers mounted on unmanned airborne vehicles (UAVs) and the power allocation scheme of transmitted signals over a limited time horizon, is formulated as a weighted-sum optimization. The problem is solved with a genetic algorithm (GA) with a novel pre-selection operator. The pre-selection operator, which takes advantage of the receding horizon control (RHC) framework

to improve population structures prior to the next generation, can accelerate the convergence of GA.

Secondly, the beam steering strategies for a cooperative phased array radar system with high-precision beams are developed. Pencil beams with narrow beamwidth, which are designated to track targets for a phased array radar, offer efficient performance in an energy-saving design, but can cause partial observations. The novel concept of expected Cramér-Rao lower bound (EPCRLB) is proposed to model partial observations. A formulation based on PCRLB is given and solved with a hierarchical genetic algorithm (HGA). An optimal strategy based on EPCRLB, which is effective in performance and efficient in time, is proposed.

Finally, a joint pulsed repetition frequency (PRF) set selection and waveform design is studied. The problem tries to improve blind zone maps while preventing targets from falling into blind zones. Waveform parameters are then optimized for the system to provide better tracking accuracy. The problem is first formulated as a bi-objective optimization problem and solved with a multiple-objective genetic algorithm. Then, a two-step strategy that prioritizes the visibility of targets is developed. Numerical results demonstrate the effectiveness of proposed strategies over simple approaches.

To my family

Acknowledgements

It is a privilege to acknowledge my deepest gratitude to my supervisor, Prof. T. Kirubarajan, for accepting me as a Ph.D. student, for supporting me financially and spiritually, for suggesting the topic of this thesis, and for his advice and guidance throughout the course of my academic career. Working under his supervision is one of my deepest honors.

I would like to thank Dr. R. Tharmarasa, for the insightful advice and generous help during these years. His comprehensive knowledge and kind personality inspired me during my days working in the lab. I would also like to express my sincere gratitude and appreciation to my committee members, Prof. T. Field and Prof. S. Dumitrescu, for their helpful and professional suggestions during the study. I appreciate all your time spent on my supervisory meetings and reading this thesis. I would like to thank our sponsors and collaborators from Defence Research and Development Canada (DRDC) and Aselsan Inc., for sharing their knowledge on the real-world problems which motivate the research covered in this thesis.

I would like to thank all my colleagues in the Estimation, Tracking and Fusion research laboratory for their help throughout my Ph.D. studies. Specially, I would like to thank David and Nikhil. I accumulated knowledge and appreciated kindness during my days working with them. I would also like to give special thanks to Hong

in our lab, who has been a true friend. I am thankful to the administrative staff of the ECE department, specially Ms. C. Gies and Ms. T. Coop, for their administrative support.

Finally, I would like to express my sincere gratitude to my parents for their unconditional love and consistent support.

Table of Contents

List of Figures

List of Tables

Abbreviations

Abbreviations

2D	Two-dimensional
AI	Artificial intelligence
B&B	Branch-and-bound
CRLB	Cramér-Rao lower bound
EA	Evolutionary algorithm
ESA	Electrically steered antennas
EKF	Extended Kalman filter
FA	False alarm
FIM	Fisher information matrix
GA	Genetic algorithm
HGA	Hierarchical genetic algorithm

IRF	Information reduction factor
KF	Kalman filter
LPI	Low probability of intercept
MINP	Mixed-integer nonlinear programming
MOU	Measurement origin uncertainty
MTT	Multiple target tracking
PAR	Phased array radar
PCRLB	Posterior Cramér-Rao lower bound
PF	Particle filter
PRF	Pulse repetition frequency
PRI	Pulse repetition interval
RCS	Radar cross section
RFS	Random finite set
RMSE	Root mean squared error
RRM	Radar resource management
SA	Simulated annealing
SAT	Search and track
SNR	Signal-to-noise ratio
UKF	Unscented Kalman filter
UT	Unscented transform

Declaration of Academic Achievement

This research presents analytical and computational work carried out solely by Anbang Deng, herein referred to as the "author", with advice and guidance provided by the academic supervisor Prof. T. Kirubarajan. Information that is presented from outside sources which has been used towards analysis or discussion, has been cited when appropriate, all other materials are the sole work of the author.

Chapter 1

Introduction

1.1 Introduction

1.1.1 Background of Multisensor-multitarget Tracking

Multiple target tracking (MTT) has a long history of almost a century and draws consistent research interests due to recent advancements in computer vision and artificial intelligence areas. Multisensor-multitarget tracking refers to the joint estimation of multiple targets' state by using observation data from multiple sensors in a simultaneous or sequential manner. MTT aims to monitor targets of interest and obtain their accurate state estimation over time.

Tracking algorithms generally solve the tracking problem in two stages: data association, which establishes target-measurement association in the presence of missed detection or clutters, and state estimation, which updates the target's state with the given measurements. In the scenarios where multiple media are used, characteristic

extraction must be performed to convert complex information, i.e., videos, into kinematic measurements, i.e., angle-of-arrival, for the tracker to process. Classic data association techniques include the global nearest neighbor (GNN)[41], joint probabilistic data association (JPDA)[7] and multiple hypothesis tracking (MHT)[9]. GNN associates the nearest measurement in the gate to the target. JPDA fuses all valid measurements with different weights in the gate to update the track. In MHT, every hypothesis of measurement-target association is propagated into the future in anticipation that future observations will solve the uncertainty[9]. The computational load of MHT is high due to the exploding increase of hypotheses.

Under the framework of recursive Bayesian filtering, Kalman filter (KF)[8] and its variations have shown effectiveness in handling state estimation problems. KF is the optimal linear minimum mean squared error (LMMSE) under the Gaussian assumption. Extend Kalman filter (EKF) and unscented Kalman filter (UKF) are used to handle nonlinear tracking problems. EKF uses the Jacobian matrix as a linear approximation of the state and/or measurement equations while UKF uses sigma points to represent the Gaussian distribution of the target and unscented transform (UT) to approximate the nonlinear evolution between the state and measurement spaces. Particle filter (PF)[5], as a Monte-Carlo realization of Bayesian filter that generates numbers of particles to represent the target distribution, has also shown efficiency in target tracking. PF is feasible for nonlinear tracking and it does not require Gaussian assumption. Multiple model filters, such as generalized pseudo Bayesian (GPB) filter[28] and interacting multiple model (IMM) filter[48], are developed to handle tracking problems of maneuvering target, where the target's motion is complex and cannot be described by a single kinematic model. The basic idea of these filters is to

use multiple motion models with respective weights to describe the target's motion. The state estimation is obtained by running multiple local filters for each motion model and then fusing the outputs of all filters.

1.1.2 Radar Resource Management for Multiple Target Tracking: A Brief Review

Technological advances in radar systems have enabled the diversification of radar functions and configurations. Multiple functionalities and complicated deployments have become a trend in the civil and military radar industries. Requirements arise for effective and efficient radar resource management algorithms to meet the need for accurate detection and tracking abilities.

In the narrow sense, radar resource management (RRM) refers to the methods with which the sensors are deployed or configured, such as path planning[90, 80], sensor selection[82, 85] or sensor placement[25]. These problems are also called sensor management. With the advancement of radar technologies, sensor management problems are extended rapidly into fields of resource-aware system design. Problems are studied on the allocation of limited radar resources, such as time[49] and power[94, 92]. Furthermore, problems related to the configuration or selection of radar parameters, such as beamforming[44] are also classified into RRM problems.

This thesis considers the optimization of path planning, power allocation, beam scheduling, and burst beam design, in the context of target tracking. Algorithms and strategies are developed to allocate resources or adapt radar parameters accordingly in the dynamic environments of target tracking.

Although considerable effort has been dedicated to sensor path planning for target

localization, search, or tracking, existing algorithms have not considered the multi-static radar system due to the complex transmitter-target-receiver geometry or combined the path planning problem with RRM from the fixed transmitter side. Therefore, it is worth studying a joint optimization of both receivers and transmitters and combining the power allocation of transmitted signals into the RRM problem design.

In the current literature, it is often assumed that a beam can cover the entire area of interest. However, this assumption no longer holds with the utilization of pencil-beams. Therefore, we investigate the characteristics of pencil-beams and propose the concept of expected PCRLB, with which an effective and efficient strategy is developed to guide the steering of beams.

RRM problems are typically formulated into optimization problems where one or more objective functions are to be minimized subject to system constraints. In radar resource management problems, the objective function is generally referred to as quality of service (QoS), which explicitly defines what task qualities are required. The Cramér-Rao lower bound (CRLB), which is defined by the inverse of the Fisher Information Matrix (FIM), provides a lower achievable minimum estimation of the mean squared error (MSE) for any unbiased estimator of an unknown parameter[86]. The posterior Cramér-Rao lower bound (PCRLB) gives a lower bound on the MSE for an unbiased estimator of an unknown variable. The PCRLB can be calculated recursively[86] and it is shown in [57] that the estimation error asymptotically approaches the PCRLB in areas with high signal-to-noise ratio (SNR) if the measurement noise is Gaussian. Therefore, many optimal resource management problems, as this thesis, use PCRLB as a criterion to optimize[94, 96, 82, 62, 55, 54]. The selection of objectives is highly dependent on the mission profiles and the requirements of users.

In[74], information gain is used as the objective function instead of estimated error. Tracking completeness is more important than tracking accuracy for surveillance and tracking missions of large numbers of targets.

For the solution techniques, some problems are solved analytically[92, 94, 95] with necessary convex relaxation[10]. Others, however, use heuristic algorithms to obtain rapid and near-optimal results due to the complexity of objective functions. Heuristic algorithms refer to a set of methods characterized by self-learning and discovery. These methods are usually inspired by selection processes in nature. They have the advantage of quick search at the cost of optimality. Classic heuristic algorithms include genetic algorithm (GA)[64, 1, 60, 14], particle swarm optimization (PSO)[64], simulated annealing (SA)[2] and ant colony optimization (ACO). GA mimics the process of natural evolution and the optimal candidate is found by eliminating other individuals that fail the competition. PSO is inspired by birds searching for food, every candidate tries to reach the optimal point through individual learning and group learning. SA and ACO, search for the optimum by imitating annealing and ant colony, respectively. In this thesis, where PCRLB is selected as the objective, convexity can hardly be preserved due to complex matrix operations such as multiplication and inversion. Therefore, we use strategies based on genetic algorithms as solvers. Despite its effectiveness, GA suffers from early maturing and may be trapped in a local optimum. In this thesis, a custom pre-selection operator is developed to take advantage of the information in the RHC framework and accelerate the convergence of the algorithm.

1.2 Theme and Objectives of Dissertation

In compliance with the terms and regulations of McMaster University, this dissertation has been written in sandwich thesis format by assembling three articles. These articles represent the independent research performed by the author of this dissertation, Anbang Deng.

The articles in the dissertation focus on the resource management algorithms for multisensor networks. The general theme is based on the following:

1. To propose a joint path planning and power allocation strategy of multitarget tracking for a multistatic radar system (Paper I).

2. To propose the concept and derive the expression of expected PCRLB (EPCRLB) and validate its utilization in describing partial observation (Paper II).

3. To propose beam scheduling algorithms for phased array radars with high-precision pencil beams (Paper II).

4. To propose burst parameter designing strategies for pulsed Doppler radars (Paper III).

5. To design closed-loop multisensor-multitarget tracking frameworks with incorporated resource management algorithms (Paper I, II, and III).

1.3 Summary of Enclosed Articles

The papers enclosed in this thesis are listed as follows:

1.3.1 Paper I (Chapter 2)

A. Deng, R. Tharmarasa, T. Kirubarajan

Joint Path Planning and Power Allocation for Multitarget Tracking in Multistatic Radar System, submitted to *Elsvier Signal Processing*, Oct 2022.

Preface: Multistatic radar systems have the advantage of practicability and potential tracking capabilities over traditional monostatic radar systems. They can be improved by optimizing limited power and efficient deployment of sensors for multitarget tracking applications. This paper presents a joint path planning and power allocation (JPPPA) strategy for tracking multiple targets in a multistatic radar system having a fixed transmitter and multiple moving receivers.

The proposed approach optimizes and controls the allocation scheme for transmitted power and the receivers' path to obtain accurate speed and heading angle estimation. To measure the optimal performance of an unbiased estimating approach, the Posterior Cramer-Ratio Lower Bound (PCRLB) is derived and used as the basis for the resource management strategy. A modified genetic algorithm (GA) with a custom pre-selection operator is developed to determine the power allocation scheme and sensor movement simultaneously. A receding horizon control (RHC) framework is applied to offer fault tolerance and provide the system with long-term guidance. Results show that the tracking performance in terms of estimation accuracy can be improved using the JPPPA strategy. The effectiveness of the proposed pre-selection operator is verified through comparison with the ordinary genetic algorithm.

1.3.2 Paper II (Chapter 3)

A. Deng, F. Pektas, F. Kumru, R. Tharmarasa, M. Efe, T. Kirubarajan

Adaptive Beam Scheduling for Cooperative Phased Array Radars with High-Precision Pencil-Beam, accepted in final form for to *IEEE Transactions on Aerospace and Electronic Systems*, Aug 2023. (doi: 10.1109/TAES.2023.3308549)

*Preface:*Phased array radar (PAR) has attracted considerable attention in civil and military applications due to its capability of performing multiple tasks such as surveillance, tracking, and weapon engagement simultaneously. To make better use of limited radar resources and to offer the best operating performance, an efficient resource allocation strategy is necessary. Traditional PAR schedulers are inefficient in using pencil-beams with super narrow beamwidth to cover areas of interest, especially in cases of maneuvering targets with high motion uncertainty, which results in missed detection. To utilize the limited time and energy resources required for PAR with pencil beams, it is necessary to provide an efficient beam scheduling algorithm. However, existing works often assume that a beam can cover the entire area of interest; thus, the problem of scheduling small-beamwidth pencil-beam to perform search and track (SAT) efficiently is barely discussed or addressed in the literature. In this paper, the problems of tracking with a pencil-beam and its beam scheduling optimization are addressed. Three beam scheduling strategies, fixed linear wipe, open-loop linear wipe that uses a hierarchical genetic algorithm (HGA), and expected posterior Cramér–Rao lower bound (EPCRLB) based optimal solution, are proposed to solve the mixed integer nonlinear problem (MINP). To handle the partially covered target existence area by pencil-beam, a new concept of predicted expected posterior Cramér–Rao lower bound (P-EPCRLB) is proposed and used as the main optimization criterion for the scheduling strategy. Numerical results demonstrate the superior performance of the proposed EPCRLB-based optimal solution strategy and its effectiveness as a proposed

solution.

1.3.3 Paper III (Chapter 4)

A. Deng, R. Tharmarasa, T. Kirubarajan

Joint PRF Set Selection and Waveform Design for Pulsed Doppler Radars, to be submitted to *IEEE Transactions on Aerospace and Electronic Systems*, Aug 2023.

*Preface:*This paper considers the problem of pulse repetition frequency (PRF) selection and waveform design for pulsed Doppler radars. Burst parameter design is an essential step in radar resource management. A proper configuration of burst parameters, including PRF, pulse width, and waveform bandwidth, significantly impacts the system performance on target tracking and detection. We address the problem of comprehensive waveform design by jointly optimizing the radar blind rate and tracking accuracy. The posterior Cramér-Rao lower bound (PCRLB) is utilized as the performance metric and a joint PRF set selection and waveform design (JPSSWD) problem is formulated. Two formulations and corresponding solution methodologies based on genetic algorithm (GA) are proposed. Numerical simulations are conducted to evaluate the performance of proposed strategies.

Chapter 2

Joint Path Planning and Power Allocation for Multitarget Tracking in Multistatic Radar System

2.1 Introduction

Multistatic radar systems, characterized by the separation between transmitters and receivers, have attracted considerable interest in recent years. Since passive receivers are cheap and hard to detect, multistatic radars provide the capability to handle more difficult tasks, especially in dangerous or hostile environments. Multistatic radars offer significant advantages over traditional monostatic radars in civil and military applications such as surveillance and environmental monitoring by utilizing illuminators of opportunity with passive receivers and working cooperatively with several transmitters and receivers[23].

With the discovery of new applications for multistatic radars, there is a rising

challenge in the system's resource management, which ensures that better tracking performance and adequate resource allocation are met. The configuration of resources in radar systems affects the capability of trackers, especially in multistatic radars where tracking accuracy is affected by the bistatic geometry, and a small change in the receivers' position may bring significant improvement.

The aim of resource management, in the field of target tracking, is to achieve accurate state estimation by properly deploying limited resources and to lower the the estimation errors to a certain threshold[27]. Originally, resource management only focused on the deployment of sensors, and is commonly referred to as sensor management. Based on the configuration of sensors, the main problems of sensor management include optimal sensor selection[85, 97, 84], optimal sensor placement[93, 54] and path planning of mobile sensors[83, 24, 30, 67]. The objective of sensor management is to determine the behaviors of sensors, such as the trajectories of movable sensors, to optimize the tracking performance subject to their operational constraints. Sensor management has been studied for decades, considerable concepts and algorithms have been addressed in the literature[82, 85, 25, 16, 17]. Recently, other resources such as power and communication channels are incorporated into sensor management, making them more practical in real-life scenarios.

Multistatic radar systems could integrate the use of receivers mounted on small and affordable Unmanned Aerial Vehicle (UAVs). UAVs have been well studied in literature and widely employed in real-life applications[61]. Studies on UAV path planning have provided fundamental background for sensor management problems in multistatic radar systems. The positions or trajectories of sensors are important in multistatic radars due to the complicated transmitter-target-receiver triangle.

In [26], an optimal path planning problem using bearing-only measurement was presented and a searching technique was developed. This work provided a basic framework for the path planning problem in multistatic radar systems. In [18], a nonlinear programming problem that maximizes the determinant of the Fisher Information Matrix (FIM) to minimize localization uncertainty was presented. Conventional optimization algorithms such as gradient descent are used to solve the path planning problem[11]. In [63], path planning is modeled as a partially observable Markov decision process and solved through nominal belief-state optimization (NBO) approximation. Convex relaxation is also studied in some papers[92][95]. Heuristic methods such as Genetic Algorithm (GA) and Particle Swarm Optimization (PSO) were presented in [64]. Although heuristic algorithms cannot guarantee an optimal solution, they are suitable for problems with complicated objective functions that are hard to solve analytically. Besides, their computational budgets are decent compared to exhaustive search approaches.

Power allocation is another critical problem in resource-aware systems. In a radar system, the transmitters have limited power budgets to generate multiple beams that illuminate different targets. Proper allocation of the power resources determines the optimal performance of the radar system. Some UAVs that carry the receivers are equipped with batteries, however, the UAVs' trajectories need to be optimized under the constraint of a limited power supply.

Several authors have focused on the power allocation problem in radar systems[4, 47]. In [95], a joint beam selection and power allocation strategy that minimizes the trace of Posterior Cramer-Rao Lower Bound (PCRLB) was proposed to handle the scenario where the transmitter cannot launch enough beams to track all the targets

simultaneously. The nonconvex problem was solved by a two-step gradient projection method after variable partitioning.

In [92], a similar problem where the selection of fusion nodes was considered in a decentralized radar network. A large number of studies regarding the low probability of interception (LPI) address the issue of power allocation[71][22].

Although path planning and power allocation are both important issues to address in multistatic radar systems, they are barely considered together to the best of our knowledge. In a multi-static radar system, it is practically meaningful and technically feasible to consider the path planning problem from the receiver side and the power allocation problem from the transmitter side jointly. In the literature, the criteria used for these two problems are generally different. Therefore, it is hard to formulate them into an integral problem. A common approach would be the adoption of a weighted-sum model where multiple objectives are integrated into one metric with respective user-defined weights. The result of such an optimization problem is essentially a Pareto trade-off that depends on how much weight the user gives to each individual problem. Therefore, the result is subjective and does not offer adequate guidance to the system. Besides, measurement origin uncertainty (MOU) is often neglected in similar works because it will change the convexity of functions that contain PCRLB, making it hard to use convex optimization techniques to solve the problem, while MOU is a realistic issue that needs to be considered in general situations.

The Posterior Cramér-Rao lower bound (PCRLB), which is defined as the inverse of the Fisher Information Matrix, provides a lower bound of the estimation mean squared error (MSE) for any unbiased estimator. The PCRLB can be calculated in a recursive manner[86], and it is shown in[57] that under the assumption, that the

measurement noise is Gaussian, the estimation error asymptotically approaches the PCRLB in high SNR. Therefore, PCRLB is a suitable criterion where the tracking performance is the objective to optimize[25, 82, 62]. Error covariance is also used in some works[17].

In this paper, a multistatic radar system with one fixed transmitter and several movable receivers tracking multiple airborne targets is presented. The transmitter is capable of launching multiple beams to illuminate all the targets simultaneously. A beam with more power allocated will lead to more accurate measurements of the target it illuminates. The total power to launch these beams is limited and needs to be allocated properly. Besides, the receivers are mounted on UAVs whose trajectories need to be optimized so that the radar system can achieve better tracking performance. The system is designed as a closed-loop signal processing framework. A receding horizon control (RHC) framework[20] where the system makes decisions for a continuous time sequence is used. At each time step, three processes are carried out. First, the state estimations of targets are achieved by trackers. Second, decisions regarding how much power the transmitter should allocate to each launched beam, and what speed and angle the receiver should move are made. Finally, the decision variables are sent back to the system.

A solution based on GA is developed to solve the JPPPA optimization problem. A custom pre-selection is developed to improve the structure of the initial population by taking advantage of the decisions obtained by the RHC framework on future steps. Comparisons are made between the proposed JPPPA and an approach that makes decisions on path planning and power allocation separately to verify the effectiveness of our algorithm. The modified GA is compared with the traditional GA to verify

the effectiveness of the custom pre-selection operator.

This paper makes the following contributions:

1) *A joint path planning and power allocation (JPPPA) strategy is comprehensively analyzed and formulated as an optimization problem.* The JPPPA strategy solves the problem of maximizing a performance metric subject to constraints on UAV kinematics and power budgets.

2) *A modified GA with user-customized operators that take advantage of prior information is developed to solve the nonconvex JPPPA problem.* The JPPPA problem is hard to solve with gradient-based methods due to the complexity of the objective function and the existence of both equality and inequality constraints. We use GA to obtain real-time solutions and develop a custom operator to accelerate the algorithm.

3) *A JPPPA-based framework for multitarget tracking is developed.* A particle filter is employed to handle the nonlinear filtering. A closed-loop signal processing framework is established for the radar system. Details of the framework are illustrated in Fig.2.1.

The remainder of the paper is organized as follows. Section II presents a description of the problem and introduces the system model. The problem is mathematically formulated in Section III. In Section IV, the solution technique of the JPPPA optimization problem is presented and a multitarget tracking algorithm based on the JPPPA strategy is developed. The simulation results are presented and discussed in Section V and conclusions and recommendations are stated in Section VI.

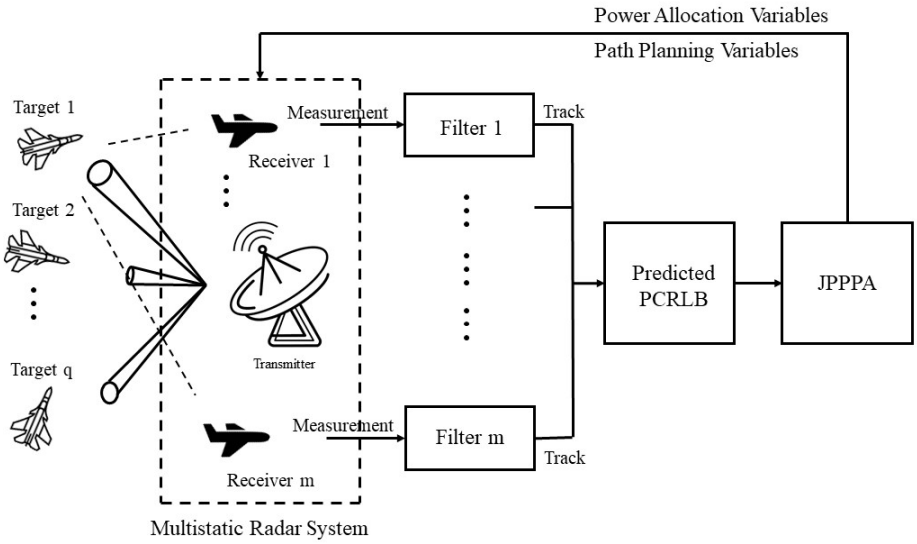

Figure 2.1: JPPPA-based multitarget tracking framework in a multistatic radar system

2.2 Problem Description

Consider a 2-D surveillance area where a multistatic radar system with one transmitter and N receivers is deployed. The position of the transmitter is denoted by $(x^{\mathrm{Tx}}, y^{\mathrm{Tx}})$. The receivers are mounted on UAVs. The nth receiver has the initial position $(x^{\mathrm{R}}_{n,1}, y^{\mathrm{R}}_{n,1})$, initial velocity $(\dot{x}^{\mathrm{R}}_{n,1}, \dot{y}^{\mathrm{R}}_{n,1})$ and initial heading angle $\theta_{n,1}$. There are Q airborne targets in the surveillance area. The qth target is intially located at $(x_{q,1}, y_{q,1})$ with a initial velocity $(\dot{x}_{q,1}, \dot{y}_{q,1})$. At time step k, the qth target is located at $(x_{q,k}, y_{q,k})$ with velocity $(\dot{x}_{q,k}, \dot{y}_{q,k})$.

For simplicity, it is assumed that the number of targets is fixed and known to the system and all the trackers are already initialized. The multistatic radar should track all the targets in the surveillance area while efficiently utilizing limited resources. The

transmitter launches multiple beams that point at different targets simultaneously. The signal-to-noise ratio (SNR) level of the echoes is proportional to the power radiation that is allocated to generate that beam. Let $P_{q,k}$ denote the power that is allocated to launch the beam, which tracks target q at time step k, then we define a power allocation vector $\mathbf{P}_k = [P_{1,k}, P_{2,k}, ..., P_{q,k}]$ that denotes the power scheme at time step k.

Meanwhile, the trajectories of UAVs that carry the receivers need to be optimized for the system to obtain better tracking performance. The maneuver of receiver n at time step k is described by two variables: speed $V_{n,k}$ and heading angle $\theta_{n,k}$

2.2.1 Signal Model

The transmitter launches all beams to track different targets simultaneously. The transit beam for target q at time step k is given by the following equation.

$$s_{q,k}(t) = \sqrt{P_{q,k}} E_{q,k}(t) e^{-j2\pi f_c t} \tag{2.2.1}$$

where f_c is the carrier frequency, and $P_{q,k}$ is the transmit power. $E_{q,k}(t)$ is the normalized complex envelope of the transmit signal, which has an effective bandwidth of β_N

$$\beta_N^2 = \frac{\int f^2 |E_{q,k}(f)|^2 df}{\int |E_{q,k}(f)|^2 df} \tag{2.2.2}$$

and an effective time duration T_N

$$T_N^2 = \frac{\int t^2 |E_{q,k}(t)|^2 dt}{\int |E_{q,k}(t)|^2 dt} \tag{2.2.3}$$

The signal received by the nth receiver is an attenuated version of the transmit signal, which is delayed by

$$\begin{aligned} r_{n,q,k}(t) =& h_{n,q,k}\sqrt{\alpha_{n,q,k}P_{q,k}}E_{q,k}(t-\tau_{n,q,k})e^{-j2\pi f_{n,q,k}t} \\ &+ \omega_{n,q}^{k}(t) \end{aligned} \tag{2.2.4}$$

The term $\alpha_{n,q,k} \propto 1/(R_{n,q,k})^4$ denotes the variation in the signal strength due to loss effects along the signal transmission path (transmitter-target-receiver), where $R_{n,q,k}$ is the bistatic, i.e. the sum of the distance from the transmitter to the target and the distance from the target to the receiver. $h_{n,q,k}$ denotes target RCS, also referred to as reflectivity, which is a random variable. $\omega_{q,k}^{n}$ is a zero-mean complex Gaussian noise.

The time delay is proportional to the bistatic range, and it is given by

$$\begin{aligned} \tau_{n,q,k} &= \frac{1}{c}R_{n,q,k} \\ &= \frac{1}{c}(\left\|(x^{\mathrm{Tx}},y^{\mathrm{Tx}})-(x_{q,k},y_{q,k})\right\| \\ &+ \left\|(x_{q,k},y_{q,k})-(x_{n,k}^{\mathrm{R}},y_{n,k}^{\mathrm{R}})\right\|) \end{aligned} \tag{2.2.5}$$

where $\|\cdot\|$ denotes the Euclidean norm. c is the speed of light. The Doppler shift $f_{n,q,k}$ is proportional to the derivative of the bistatic range, which is given by

$$\begin{aligned} f_{n,q,k} = -\frac{f_c}{c}\Bigg\{ & \frac{\dot{x}_{q,k}\left(x_{q,k}-x^{\mathrm{Tx}}\right)+\dot{y}_{q,k}\left(y_{q,k}-y^{\mathrm{Tx}}\right)}{\left\|(x^{\mathrm{Tx}},y^{\mathrm{Tx}})-(x_{q,k},y_{q,k})\right\|} \\ & + \frac{\dot{x}_{q,k}\left(x_{q,k}-x_{n,k}^{\mathrm{R}}\right)+\dot{y}_{q,k}\left(y_{q,k}-y_{n,k}^{\mathrm{R}}\right)}{\left\|(x_{n,k}^{\mathrm{R}},y_{n,k}^{\mathrm{R}})-(x_{q,k},y_{q,k})\right\|}\Bigg\} \end{aligned} \tag{2.2.6}$$

2.2.2 Target Dynamics

Let $\mathbf{x}_{q,k} = [x_{q,k}, \dot{x}_{q,k}, y_{q,k}, \dot{y}_{q,k}]^T$ denote the state vector of the qth target, where $[x_{q,k}, y_{q,k}]$ and $[\dot{x}_{q,k}, \dot{y}_{q,k}]$ denote the position and velocity of the target respectively.

The target's motions are assumed to follow a constant-velocity (CV) model in which the state of the target evolves as:

$$\mathbf{x}_{q,k+1} = \mathbf{F}_k \mathbf{x}_{q,k} + \mathbf{w}_{q,k} \tag{2.2.7}$$

$\mathbf{F}_k$ is the transition matrix

$$\mathbf{F}_k = \mathbf{I}_2 \otimes \begin{bmatrix} 1 & T \\ 0 & 1 \end{bmatrix} \tag{2.2.8}$$

where $\otimes$ is the Kronecker operator, and $\mathbf{I}_2$ denotes the 2×2 identity matrix. $\mathbf{w}^k$ is the process noise that describes the inaccuracy of the motion model. It is assumed to be zero-mean Gaussian distributed with a known covariance $\mathbf{\Gamma}^k$.

The covariance matrix is denoted by

$$\mathbf{\Gamma}_k = \kappa \mathbf{I}_2 \otimes \begin{bmatrix} \frac{1}{3}T^3 & \frac{1}{2}T^2 \\ \frac{1}{2}T^2 & T \end{bmatrix} \tag{2.2.9}$$

where κ is the intensity of process noise.

2.2.3 UAV Kinematic Model

UAVs are constrained by their kinematic capacities. In this paper, a 2-D maneuvering model is used. The heading angle and speed of each UAV might change at each

observation point, while within the time interval, the UAVs are assumed to move at a constant velocity with fixed heading angles.

Let $\theta_{n,k}$ and $V_{n,k}$ denote the heading angle and the speed of the nth receiver at time step k, then the position of this receiver $[x^{\mathrm{R}}_{n,k}, y^{\mathrm{R}}_{n,k}]^T$ evolves as:

$$[x^{\mathrm{R}}_{n,k}, y^{\mathrm{R}}_{n,k}]^T = [x^{\mathrm{R}}_{n,k-1}, y^{\mathrm{R}}_{n,k-1}]^T + V_{n,k}T[\cos(\theta_{n,k}), \sin(\theta_{n,k})]^T \tag{2.2.10}$$

where T is the time interval.

At each time step, the maneuver of each UAV must satisfy the kinematic constraints, i.e., the acceleration and the angular acceleration must be within a specified interval, given by:

$$\begin{cases} |\theta_{n,k} - \theta_{n,k-1}| \leq \theta_{max} \\ |V_{n,k} - V_{n,k-1}| \leq a_{max} \end{cases} \tag{2.2.11}$$

θ_{max} and a_{max} are the maximum angular and linear accelerations of each UAV, which are assumed to be constants.

2.2.4 Measurement Model

In a general case where measurement origin uncertainty(MOU) exists, measurements originate from one of the targets or clutter. The measurement is given by:

$$\mathbf{z}_{n,q,k} = \begin{cases} h_n(\mathbf{x}_{q,k}) + \mathbf{w}_{n,q,k} & \text{if originated from target } q \\ \upsilon_{n,q,k} & \text{if false alarm} \end{cases} \tag{2.2.12}$$

where $\mathbf{z}_{n,q,k}$ is the measurement of target q at time step k that is obtained by the nth receiver, h_n is the nonlinear observation function. The measurements consist of bistatic range $R_{n,q,k}$, bearing from target to sensor $\theta_{n,q,k}$, and Doppler shift $f_{n,q,k}$, i.e.,

$$h_n(\mathbf{x}_{q,k}) = [R_{n,q,k}, \theta_{n,q,k}, f_{n,q,k}]^T \tag{2.2.13}$$

The bearing is given by:

$$\theta_{n,q,k} = \arctan\left(\frac{y_{q,k} - y^{\mathrm{R}}_{n,k}}{x_{q,k} - x^{\mathrm{R}}_{n,k}}\right) \tag{2.2.14}$$

and the expressions of $R_{n,q,k}$ and $f_{n,q,k}$ can be found in equations (2.2.5) and (2.2.6). $\mathbf{w}_{n,q,k}$ is the measurement noise, which is assumed to be a zero-mean Gaussian random variable with covariance $\mathbf{\Sigma}_{n,q,k}$.

$$\mathbf{\Sigma}_{n,q,k} = \mathrm{diag}\left(\sigma^2_{R_{n,q,k}}, \sigma^2_{\theta_{n,q,k}}, \sigma^2_{f_{n,q,k}}\right) \tag{2.2.15}$$

where $\sigma^2_{R_{n,q,k}}$, $\sigma^2_{\theta_{n,q,k}}$ and $\sigma^2_{f_{n,q,k}}$ are the Cramér-Rao Lower Bounds (CRLBs) on the estimation MSE of the qth target's bistatic range, bearing and Doppler shift estimates, which satisfy

$$\begin{cases} \sigma^2_{R_{n,q,k}} \propto (\mu_{n,q,k}\beta_N^2)^{-1} \\ \sigma^2_{\theta_{n,q,k}} \propto (\mu_{n,q,k}/B_W)^{-1} \\ \sigma^2_{f_{n,q,k}} \propto (\mu_{n,q,k}T_N^2)^{-1} \end{cases} \tag{2.2.16}$$

where B_W is the null-to-null width of the receiver antennas, β_N and T_N are the effective bandwidth and time duration of the transmit signal respectively as previously defined in equations (2.2.2) and (2.2.3). $\mu_{n,q,k}$ is the SNR which satisfies $\mu_{n,q,k} \propto$

$\alpha_{n,q,k}P_q^k|h_{n,q,k}|^2$, thus we have

$$\begin{cases} \sigma^2_{R_{n,q,k}} \propto \left(\alpha_{n,q,k}P_q^k|h_{n,q,k}|^2\beta_N^2\right)^{-1} \\ \sigma^2_{\theta_{n,q,k}} \propto \left(\alpha_{n,q,k}P_q^k|h_{n,q,k}|^2/B_W\right)^{-1} \\ \sigma^2_{f_{n,q,k}} \propto \left(\alpha_{n,q,k}P_q^k|h_{n,q,k}|^2T_N^2\right)^{-1} \end{cases} \tag{2.2.17}$$

Note that the elements in equation (2.2.16) are inversely proportional to the allocated power P_q^k, which yields an intuitive conclusion that for a single target, the covariance of the measurement noise is inversely proportional to the power that is assigned to track it, i.e., the more power assigned to track a target, the more accurate the measurements of that target will be.

The term $\upsilon_{n,q,k}$ in equation (2.2.12) represents the measurement generated by clutters, which is a zero-mean Gaussian random variable uniformly distributed in the measurement space (within the observation volume V). The number of false alarms at each frame satisfies the Poisson distribution, given by

$$p(n_{fa}) = \frac{e^{-\lambda V}(\lambda V)^{n_{fa}}}{n_{fa}!} \tag{2.2.18}$$

where n_{fa} is the number of false alarms, λ is the spatial density, i.e., the average number of false alarms at each frame.

2.2.5 FIM and PCRLB

The Posterior Cramér-Rao lower bound (PCRLB), which is defined to be the inverse of the Fisher information matrix (FIM), gives a lower bound of the error covariance

matrix of an unbiased estimate. It gives a measure of the achievable optimum performance and can be calculated predictively. Furthermore, the PCRLB is independent of the filtering algorithm, thus it is often used as an effective criterion in optimal sensor resource management problems. For simplicity, the receiver index n is omitted in this subsection. Let $\hat{\mathbf{x}_k}$ be an unbiased estimate of $\mathbf{x}_k$ based on the measurement $\mathbf{z}_k$, $\mathbf{C}_k$ be the error covariance matrix, and $\mathbf{J}(\mathbf{x}_k)$ be the FIM, we have

$$\mathbf{C}_k = \mathbb{E}[(\hat{\mathbf{x}}_k - \mathbf{x}_k)(\hat{\mathbf{x}}_k - \mathbf{x}_k)^T] \geq \mathbf{J}_(\mathbf{x}_k)^{-1} \tag{2.2.19}$$

where $\mathbb{E}$ denotes expectation operator.

A decent recursive formula for the calculation of PCRLB is developed in[86]

$$\mathbf{J}_k = \mathbf{J}_X(\mathbf{x}_k) + \mathbf{J}_Z(\mathbf{x}_k) \tag{2.2.20}$$

where $\mathbf{J}_X(\mathbf{x}_k)$ and $\mathbf{J}_Z(\mathbf{x}_k)$ are the prior knowledge and the information obtained from measurements at time step k respectively.

$$\begin{cases} \mathbf{J}_X(\mathbf{x}_k) = \mathbf{D}_{k-1}^{22} - \mathbf{D}_{k-1}^{21}(\mathbf{J}_k + \mathbf{D}_{k-1}^{11})^{-1}\mathbf{D}_{k-1}^{12} \\ \mathbf{J}_Z(\mathbf{x}_k) = \mathbb{E}\{-\Delta_{\mathbf{x}_k}^{\mathbf{x}_k} \ln p(\mathbf{z}_k|\mathbf{x}_k)\} \end{cases} \tag{2.2.21}$$

where

$$\begin{cases} \mathbf{D}_{k-1}^{11} = \mathbb{E}\{-\Delta_{\mathbf{x}_{k-1}}^{\mathbf{x}_{k-1}} \ln p(\mathbf{x}_k|\mathbf{x}_{k-1}\} \\ \mathbf{D}_{k-1}^{12} = \mathbb{E}\{-\Delta_{\mathbf{x}_k}^{\mathbf{x}_{k-1}} \ln p(\mathbf{x}_k|\mathbf{x}_{k-1}\} = (\mathbf{D}_{k-1}^{21})^T \\ \mathbf{D}_{k-1}^{22} = \mathbb{E}\{-\Delta_{\mathbf{x}_k}^{\mathbf{x}_k} \ln p(\mathbf{x}_k|\mathbf{x}_{k-1}\} \end{cases} \tag{2.2.22}$$

The prior information is given by

$$\mathbf{J}_X(\mathbf{x}_k) = [\mathbf{\Gamma}_{k-1} + \mathbf{F}_k \mathbf{J}(\mathbf{x}_{k-1})^{-1} \mathbf{F}_{k-1}^T]^{-1} \tag{2.2.23}$$

It is assumed that the measurements collected from different bistatic pairs are independent, hence, the total measurement contribution is equal to the summation of measurement contributions obtained by all bistatic pairs.

$$\mathbf{J}_Z(\mathbf{x}_k) = \sum_{n=1}^{N} \mathbf{J}_{Z_n}(\mathbf{x}_k) \tag{2.2.24}$$

The measurement contribution obtained by a single bistatic pair is given by

$$\mathbf{J}_{Z_n}(\mathbf{x}_k) = \mathbb{E}\{q(\mathcal{P}_{n,q,k}, \Sigma_{q,k}) \mathbf{H}_{q,k}^T \Sigma_{q,k}^{-1} \mathbf{H}_{q,k}\} \tag{2.2.25}$$

where $\mathbf{H}_{q,k} = [\Delta_{\mathbf{x}_{q,k}} h_n^T(\mathbf{x}_{q,k})]^T$ is the Jacobian matrix of the measurement function $h_n(\mathbf{x}_{q,k})$ with respect to the target state $\mathbf{x}_{q,k}$ and $\mathbb{E}$ denotes expectation with respect to the target state. The term $q(\mathcal{P}_{n,q,k}, \Sigma_{q,k})$ is the information reduction factor (IRF)[58] which modifies the information obtained from measurements due to MOU. The reader is referred to [82, 25] for details about IRF.

This expected value in equation (2.2.25) can be calculated through Monte Carlo techniques, but it will lead to extra computational costs. To maintain efficiency in real-time applications, the measurement contribution can be approximated using the Jacobian and measurement noise covariance evaluated at the prediction phase.

$$\mathbf{J}_{Z_n}(\mathbf{x}_k) = q(\mathcal{P}_{n,q,k}, \Sigma_{q,k}) \mathbf{H}_{q,k}^T \Sigma_{q,k}^{-1} \mathbf{H}_{q,k} \Big|_{\mathbf{x}_{k|k-1}^q} \tag{2.2.26}$$

where $\mathbf{x}^q_{k|k-1}$ denotes the predicted state of the qth target at time step k. Substituting the prior information and measurement contributions into equation (2.2.20), the predicted FIM is gotten as

$$\begin{aligned}\mathbf{J}|_{\mathbf{x}_k} =&[\mathbf{\Gamma}_{k-1} + \mathbf{F}_k\mathbf{J}(\mathbf{x}_{k-1})^{-1}\mathbf{F}^T_{k-1}]^{-1} \\ &+ \sum_{n=1}^{N}[q(\mathcal{P}_{n,q,k}, \Sigma_{q,k})\mathbf{H}^T_{q,k}\Sigma^{-1}_{q,k}\mathbf{H}_{q,k}]\Big|_{\mathbf{x}^q_{k|k-1}}\end{aligned} \tag{2.2.27}$$

Note the power allocation scheme changes the FIM through $\Sigma_{q,k}$ and the path planning variables change the FIM through $\mathbf{H}_{q,k}$. The predictive PCRLB is defined as the inverse of FIM:

$$\mathbf{C}_{PCRLB} = (\mathbf{J}|_{\mathbf{x}_k})^{-1} \tag{2.2.28}$$

2.3 Optimization Formulation

At every time step k, decisions are made on the power allocation scheme of the transmitter and the maneuver of each receiver, which is controlled by its heading angle and speed. The decision variables are displayed as follows:

$$\begin{cases} \mathbf{P}_k = [P_{1,k}, P_{2,k}, ..., P_{q,k}]^T \\ \mathbf{V}_k = [V_{1,k}, V_{2,k}, ..., V_{n,k}]^T \\ \mathbf{\Theta}_k = [\theta_{1,k}, \theta_{2,k}, ..., \theta_{n,k}]^T \end{cases} \tag{2.3.1}$$

The PCRLB is used as a criterion to be minimized, hence the trace of PCRLB is taken as a scalar metric.

2.3.1 Objective

The diagonal elements of the PCRLB matrix are the lower bounds on the estimation MSE of the target position and velocity. To minimize such lower bounds, the trace of the PCRLB matrix is selected as the objective to minimize. The PCRLB is obtained by taking the inverse of FIM.

$$\min \ \operatorname{tr}(\mathbf{J}|_{\mathbf{x}_{q,k}})^{-1} \tag{2.3.2}$$

Since the information of all targets obtained from all bistatic pairs are independent, the goal of the JPPPA optimization is to minimize the summation of the traces of all PCRLB matrices, i.e., the summation of lower bounds on the estimation MSE of all targets, which is given by

$$U_k(\mathbf{P_k}, \mathbf{V_k}, \mathbf{\Theta_k}) = \sum_{q=1}^{Q} \operatorname{tr}(\mathbf{J}|_{\mathbf{x}_{q,k}})^{-1} \tag{2.3.3}$$

In some works[92], only the position root-mean-square error (RMSE) is considered, which is an alternative objective since the position RMSE is much larger than the velocity RMSE. In that case, the objective function is defined as the summation of the first and the third elements on the diagonal of the PCRLB matrix, which represent the lower bounds on the estimation errors of position in x and y coordinates, respectively.

2.3.2 Constraints

1) *Constraints on UAVs' maneuverability:* The UAVs are constrained by their kinematic capabilities. The path planning variables, which are heading angles and speeds, have upper and lower limits, given by equation (2.2.11).

A minimum and maximum speed of UAVs is also defined to maintain the UAVs' speeds in a reasonable range if a UAV receives consecutive acceleration/deceleration commands.

$$V_{min} < V_{n,k} < V_{max} \tag{2.3.4}$$

where V_{min} and V_{max} are the minimum and maximum speeds.

2) *Constraints on power budget:* The summation of power allocated to all beams must not exceed the total power budget, denoted as:

$$\mathbf{1}^T \mathbf{P}_k = P_{\text{total}} \tag{2.3.5}$$

Each power radiation is constrained by a minimum value P_{min} to ensure sufficient signal intensity for detection, and a maximum value P_{max} to ensure reasonable allocation to other beams.

$$P_{min} \leq P_{q,k} \leq P_{max} \tag{2.3.6}$$

Mathematically, a beam with very weak power radiation will make the corresponding covariance of measurement noise in equation (2.2.15) close to singular. This will be avoided by the power constraint.

Since the power radiations and speeds of UAVs are not direct decision variables, constraints in equations (2.3.4) and (2.3.6) may be violated during the optimization process. Penalty functions are defined to restrain these variables within their constrained ranges.

The penalty function for constraint in equation (2.3.4) is expressed as

$$\begin{aligned}\mathcal{F}_1(k) = \mathcal{U} \sum_{n=1}^{N} [&\max\ (|V_{max} - V_{n,k}|, 0) + \\ &\max\ (|V_{min} - V_{n,k}|, 0)]\end{aligned} \tag{2.3.7}$$

where $\mathcal{U}$ is a large positive constant.

Similarly, the penalty function for constraint in equation (2.3.6) is expressed as

$$\begin{aligned}\mathcal{F}_2(k) = \mathcal{U} \sum_{q=1}^{Q} [&\max\ (|P_{max} - P_{q,k}|, 0) + \\ &\max\ (|P_{min} - P_{q,k}|, 0)]\end{aligned} \tag{2.3.8}$$

2.3.3 Receding Horizon Control

Receding horizon control (RHC) frameworks are popular for the control of UAVs. By extending a one-step optimization to a control sequence, these approaches offer the potential of responding to a dynamic environment[20] with an increase in computational cost. Since the UAVs are constrained by their kinematic capabilities, the controlling decision made on UAVs at time step k ($\mathbf{V}_k, \mathbf{\Theta}_k$) will affect the future moves. Therefore, it is practical and technically useful to consider future steps instead of performing only a greedy one-step optimization. The weighted sum of predicted PCRLB in the next H steps is given below.

$$\sum_{h=1}^{H} w_{k+h} U_{k+h} = \mathbf{W}_k^T \mathbf{U}_k \tag{2.3.9}$$

where $\mathbf{W}_k = [w_{k+1}, w_{k+2}, ..., w_{k+H}]^T$ is the vector of weights on predicted worst-case PCRLBs, also referred to as receding horizon decay factors.

Remark 1: Since the hard constraints in equations (2.3.4) and (2.3.6) are transformed into penalty functions and added to the objective function, it is possible that these constraints might be violated due to the long-term multi-step planning of RHC. This can be avoided by increasing the penalty factor $\mathcal{F}$.

When the fitness value is being evaluated, the updated tracks from previous time steps are required to predict the current states of targets, which are needed in the predictive PCRLB. When planning for future steps in the RHC sequence, such updated tracks will not be available. To handle this, predicted tracks from previous time steps are used as if no valid measurements were obtained.

Remark 2: While RHC introduces extra computational load without being able to significantly improve the optimization result, it is still meaningful to apply RHC in this case as it is most suitable in obstacle avoidance[20] where the environment is dynamic. Sending sequenced commands to UAVs is advantageous over continuously sending one-step commands due to possible communication failure or other unexpected situations.

2.3.4 Problem Formulation

By adding the weighted sum of PCRLB at all time steps in the RHC sequence with the penalty functions, the objective function of the JPPPA optimization is obtained.

$$\mathbb{F}(\mathbf{P_k}, \mathbf{V_k}, \mathbf{\Theta_k}) = \mathbf{W}_k^T \mathbf{U}_k + \mathcal{F}_1 + \mathcal{F}_2 \tag{2.3.10}$$

The optimization problem is summarized as

$$
\begin{aligned}
\min \quad & \mathbb{F}(\mathbf{P_k}, \mathbf{V_k}, \mathbf{\Theta_k}) \\
\text{s.t.} \quad & \mathbf{1}^T \mathbf{P}_k = P_{\text{total}} \\
& P_{min} \leq P_{k,m}^q \leq P_{max} \\
& |V_{n,k} - V_{n,k-1}| \leq a_{max} \\
& |\theta_{n,k} - \theta_{n,k-1}| \leq \theta_{max} \\
& V_{min} < V_{n,k} < V_{max}.
\end{aligned} \tag{2.3.11}
$$

2.4 Joint Path Planning and Power Allocation Strategy

2.4.1 Solution Technique Based on Genetic Algorithm

In problem (2.3.11), the mappings from the decision variables to the objective are not primary functions, making it hard to solve the problem with gradient-based methods. Hence, a genetic algorithm (GA) with a custom operator was developed.

Genetic algorithm is an evolutionary searching technique inspired by natural selection [64]. The parallel searches are called generations. The decision variables in the solution space are represented as individuals (also referred to as chromosomes). The basic idea of GA is to evaluate each individual's fitness value and eliminate those with low values. GA is capable of finding sub-optimal solutions quickly, but a global optimum is not guaranteed. In the scenario where the receivers await their moving commands at each time step, the decision variables must be determined online in a

limited time and sent to receivers. Therefore, it is more desirable to quickly obtain a sub-optimal solution than to spend extra time searching for the global optimum.

The individuals are structured as follows: for each time step, the first Q genes represent the power radiations that are allocated to Q targets, and the rest of the genes represent the path planning variables (speeds and heading angles). The same structure repeats for every time step that is in the RHC sequence. The total length of a single individual is $H(Q+2N)$. The power radiations are random numbers from 0 to 1 that satisfy constraint in equation (2.3.5) when generated. For simplicity, the speeds and heading angles are mapped to continuous values from 0 to 1. The mapping functions are given by

$$\bar{V}_{n,k} = \frac{V_{n,k} + a_{max}}{2a_{max}},\ \bar{\theta}_{n,k} = \frac{\theta_{n,k} + \theta_{max}}{2\theta_{max}} \tag{2.4.1}$$

When evaluating the fitness value of an individual, these intermediate values are converted back to real ones.

Remark 3: A proper encoding method is vital to the performance of GA. In this work, real number encoding, where each decision variable is represented by one gene, is adopted. Gray encoding is more suitable for local search because the randomness introduced in crossover and mutation operations is smaller. However, its encoding efficiency is low since a decision variable is represented by multiple binary genes. Therefore, the computational cost is increased due to the large chromosome length. Numerical experiments showed that gray encoding offered worse integral performance.

Individuals are evaluated and updated through the selection operation, where the traits of two parent chromosomes are exchanged to breed new offspring. Those with high fitness values are more likely to be selected and copied to the next generation,

while those with low fitness values will be eliminated. Roulette wheel and tournament schemes are the most used strategies for selection [64, 56]. To protect the elite individuals, a binary tournament selection is adopted in this paper.

The information of the population is shared and exchanged in the crossover operation where a random locus is selected, and then the genes before and after that locus are exchanged between two chromosomes.

To maintain the diversity of the population, a mutation operation is performed. Each gene has a small probability P_m to mutate. Binary variables are flipped, and continuous variables are replaced by a random value. In this case, where all the genes are continuous variables, they will mutate to a random value between 0 and 1.

In the crossover and mutation operations, the power constraint in equation (2.3.5) may be violated, hence, a repair operation is provided to rectify infeasible individuals. If the summation of power radiations is not equal to 1, the whole power scheme will be scaled so that the power constraint is met.

Elitism is adopted to protect highly fitted individuals. A few individuals with high fitness values are preserved after the selection operation and are directly copied to the next generation without participating in the crossover and mutation operations. Elitism prevents the loss of top-ranked individuals and preserves fitted genes, which might improve the performance of the algorithm[1]. The population keeps evolving until some termination conditions are met, e.g., the maximum number of iterations is reached, or there is no improvement found in the population for a certain number of generations.

From the second step, the JPPPA decision is based on the previous RHC sequence,

and it will become available under the RHC framework. The previously obtained decision will be referred to as a *prior*. Since the prior was already a near-optimal solution, taking advantage of it will significantly improve the structure of the population and reduce the computational cost. Based on the prior information, a pre-selection operator that will replace the normal population generation is developed.

The pre-selection operation includes the following steps:

1) *Generate the elite individual:* Generate random sets of genes that represent the decision variables at the last time step in the current RHC sequence (where there is no prior available). Combine the random genes with the prior information to generate new individuals. Find the fittest one among those individuals and preserve it as an elite.

2) *Generate population:* Randomly generate individuals and put them together with the elite to establish a population.

3) *Small-scale crossover:* Choose the elite individual as a parent and crossover with other individuals.

4) *Small-scale mutation:* Mutate the elite individual. In this phase, genes to be mutated are not replaced by a random value, but an increment that satisfies a zero-mean Gaussian distribution will be added. i.e., the mutated individuals are more likely to be around the elite in the solution space.

5) *Repair and replace:* Repair the individuals generated from previous crossover and mutation. Use them to replace random individuals.

By essentially changing the structure of the population, the pre-selection operator achieves the aim of providing guidance to the randomly generated population and searching the space around the prior information. This operation is equivalent to

giving more weight to the prior information and can be seen as an extra generation of evolution. Note that the pre-selection is performed only once at each time step. Limited time is spent to crossover and mutate the elite individual that could breed better offspring. To preserve the population's diversity that may be reduced by the pre-selection operation, only a limited portion of individuals will be replaced.

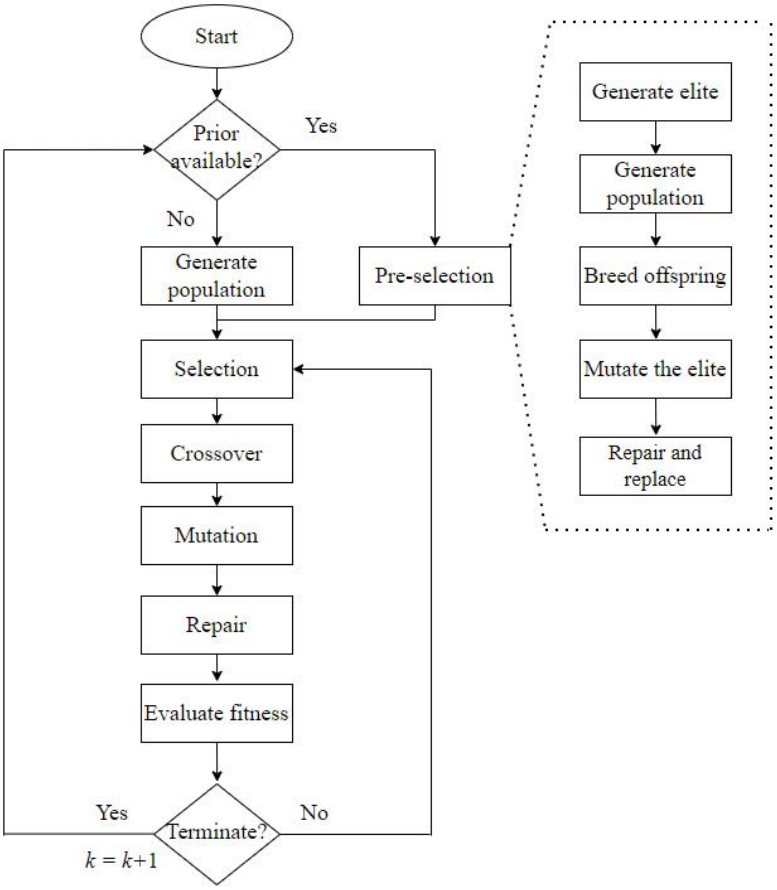

Figure 2.2: Flow chart of the modified genetic algorithm with custom pre-selection operator

2.4.2 Multiple Target Tracking

It is assumed that the targets are widely separated in the surveillance area. Therefore, after the decisions are made by the JPPPA strategy, the multitarget tracking problem becomes several single target tracking problems that can be handled independently.

In this work, the measurements in equation (2.2.13) are highly nonlinear, hence a particle filter (PF), which has a strong potential when dealing with nonlinear measurements [5], is an ideal choice.

The particle filter is a Monte Carlo technique that represents the density $p(\mathbf{x_k}|\mathbf{z_k})$ as a random set of samples (particles) $\{\mathbf{x}_k^p : p = 1, ..., P\}$ with corresponding weights $\{w_k^p : p = 1, ..., P\}$. At each time step, particles are generated by sampling from the prior. Then, they are predicted and updated under the Bayesian filtering framework. The weight of each particle is updated correspondingly after measurements are collected. Finally, resampling is performed to eliminate particles with low weights. In this paper, a Sampling Importance Resampling (SIR) is used as the resampling strategy. A brief summary of SIR-PF is given in Algorithm 1. Note that other nonlinear filters can also be used, for example, the extended Kalman filter (EKF)[8].

The entire signal processing framework that incorporates a JPPPA optimization module and a particle filter is structured as follows. First, the estimated state of each target is obtained by PF. Then, based on the estimated tracks, the predictive PCRLB is evaluated by JPPPA, and optimal resource management deployment is obtained. Finally, the resource management decisions are sent back to the transmitter and receivers to guide their behaviors in the next few steps.

Algorithm 1 Multi-target Tracking with JPPPA

1: Let $k = 1$; assume initial JPPPA decisions; assume initial density $p(\mathbf{x}_{k-1})$
2: Sample N_p particles from the prior $p(\mathbf{x}_{k|k-1})$ and define corresponding weights.
3: **for** each $q \in [1, Q]$ **do**
4: Obtain measurements in the environment that are determined by the JPPPA decisions.
5: Update particles' weight based on the posterior $p(\mathbf{x}_k|\mathbf{z}_k)$.
6: Resample with SIR strategy and perform weight normalization.
7: Calculate the estimation based on particles and weights.
8: **end for**
9: Formulate the JPPPA optimization problem (2.3.11) and solve it with the proposed GA.
10: Let $k = k + 1$, and go to step 3.

2.4.3 Analysis of Computational Complexity

The computational complexity of GA depends on the size of individuals, the population size, and the number of generations, while the size of individuals is determined by the size of the problem, i.e., the number of transmitters, receivers and targets, and the length of the RHC sequence. The complexity is on the order of $\mathcal{O}(gpL(MQ + 2N))$, where g is the number of generations, p is the population size and L is the length of the RHC sequence. The size of the problem increases the complexity by the order of 3 at most. The complexity arises from the enlarged size of individuals. Note that in this paper, the number of transmitters $M = 1$.

However, the complexity given above is the maximum one where the generation of the population reaches its maximum limit. The population will quit evolving if no improvement is found for a certain value of generations. Therefore, the performance of GA cannot be evaluated simply by its complexity. The custom pre-selection operator, which improves the distribution of individuals, can make the population converge faster, although it does not change the maximum complexity. The evaluation of the

pre-selection operator is presented in the next section.

2.5 Simulation Result and Discussion

A multistatic radar with one transmitter and $N = 5$ movable receivers is considered. The area is surveilled for 30 frames with the time interval $\Delta T = 1$s. The signal effective bandwidth and effective time duration are set to $\beta_n = 1$ MHz and $T_n = 1$ ms, respectively. The carrier wavelength $\lambda = 0.2$ m and the detection probability $\mathcal{P}_{n,q,k}$ is modeled as a function of bistatic range[74]. The lower and upper bounds for power constraints are $P_{min} = 0.1P_{total}$ and $P_{max} = 0.8P_{total}$, respectively. The maximum linear and angular accelerations per frame are set to $a_{max} = 300$ m/s^2 and $\theta_{max} = 15°$/s, respectively. The lower and upper bounds for UAVs' speed are $V_{min} = 200$ m/s and $V_{max} = 400$ m/s. $Q = 5$ targets are widely separated in the surveillance region with $\kappa = 50$m^2/s^3 for all targets. The initial states of targets and receivers are given respectively in Table 2.1 and Table 2.2. The transmitter is located at the origin. Fig.2.3. illustrates the trajectories of targets and the initial radar deployment.

Table 2.1: Initial Target States

Target Index	Position (km)	Velocity (m/s)
1	(40,45)	(-200,-250)
2	(-50,35)	(300,0)
3	(-45,-40)	(100,250)
4	(35,-30)	(-150,200)
5	(0,-55)	(250,50)

It is assumed that the probability of detection decreases with the bistatic range, shown in Fig.2.4.

Table 2.2: Initial Receiver States

Receiver Index	Position (km)	Speed (m/s)	Heading Angle (°)
1	(20,20)	300	90
2	(-25,15)	300	120
3	(-5,-20)	300	270
4	(55,5)	300	120
5	(-55,-5)	300	240

The population of GA is 101. The probabilities of crossover and mutation are set to $P_c = 0.6$ and $P_m = 0.1$ respectively. The maximum generation is 30. The GA terminates when the maximum generation is reached or when there is no improvement in the population for five generations. All the results are averaged over 100 Monte Carlo runs.

2.5.1 Demonstration of the JPPPA Strategy

The JPPPA strategy is compared to a two-step algorithm that incorporates typical algorithms in path planning[26] and power allocation[95], respectively.

In the first step, it is assumed that the power scheme remains the same as the last time step. Then, the solution space is discretized, and a dynamic programming (DP) is used to find the optimal path planning decisions. Due to the high complexity of DP, the searching technique proposed in [26] is used. Note that DP is applied in dynamic environments under the RHC framework, it reduces to a greedy search if the problem is a one-step planning.

After the optimal sensor deployment is obtained, the succeeding power allocation problem is convex[10] and thus can be solved with basic optimization techniques. In this simulation, a pattern search technique[42] is used to find the optimal solution.

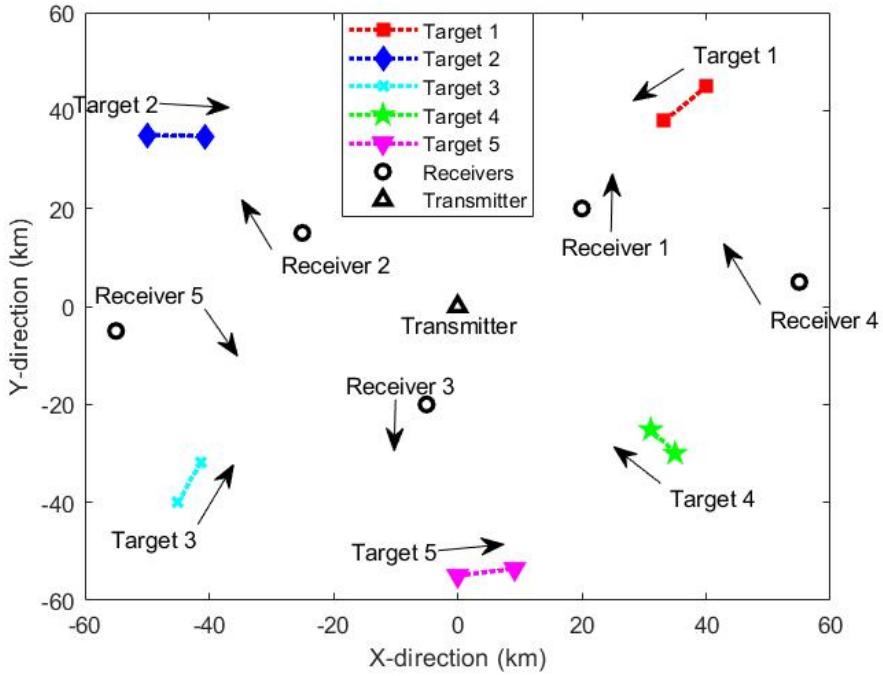

Figure 2.3: Target trajectories and initial radar deployment

Pattern search searches the solution space in pre-defined directions. Since it is not required to determine the gradient or the step length, pattern search is suitable in this scenario. This two-step algorithm is referred to as dynamic programming-linear search (DP-LS).

Remark 4: Since the power allocation problem with a fixed receiver deployment is convex, it can be solved easily, e.g., with the CVX toolbox, and no advanced algorithm is required. The gradient projection (GP) used in [95] is a favorable solution due to the existence of equality constraints. However, in the proposed scenario, the gradient is hard to determine due to the large scale of the problem. Several similar works [92, 47] have made contributions to transforming or relaxing their original problems into convex ones that are easy to solve. This approach, however, is infeasible in our

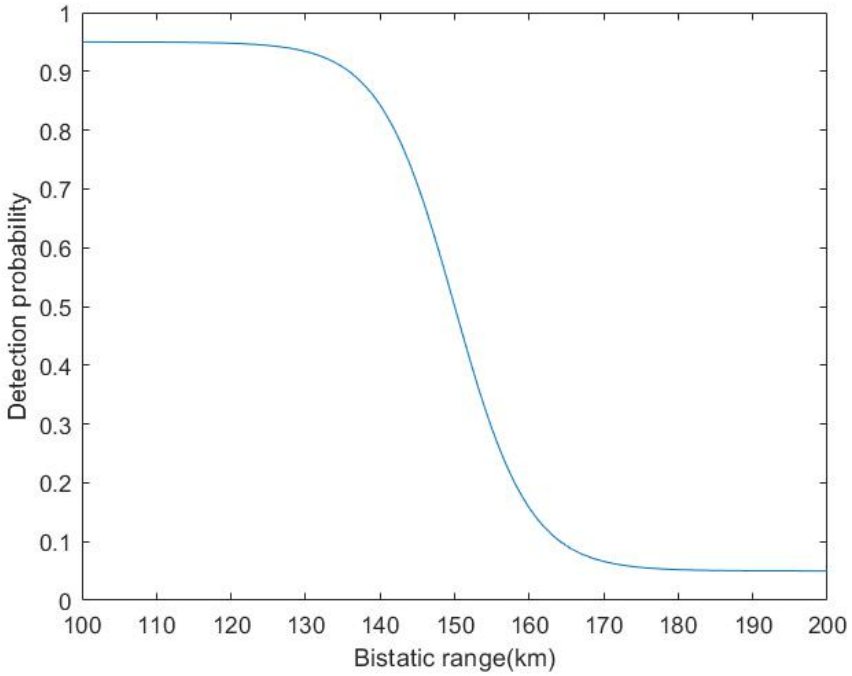

Figure 2.4: Detection probability with respect to bistatic range

scenario due to the complexity of the objective function introduced by sensor mobility.

The proposed JPPPA strategy is also compared with the following strategies:

1) *One-step JPPPA* (1-JPPPA): The same algorithm is adopted, except that RHC is not considered. At each time step, the solver only seeks the decision variables for the next frame without considering the future.

2) *Uniform Power Allocation* (UPA): By assuming the power is uniformly allocated to all targets, the joint optimization degrades into a pure path planning, which is also nonconvex.

Fig.2.5 displays the real PCRLB values after the optimization result is obtained. Concerning resource management strategies, the UPA strategy demonstrates a higher PCRLB than JPPPA because power allocation, as an important issue to address in

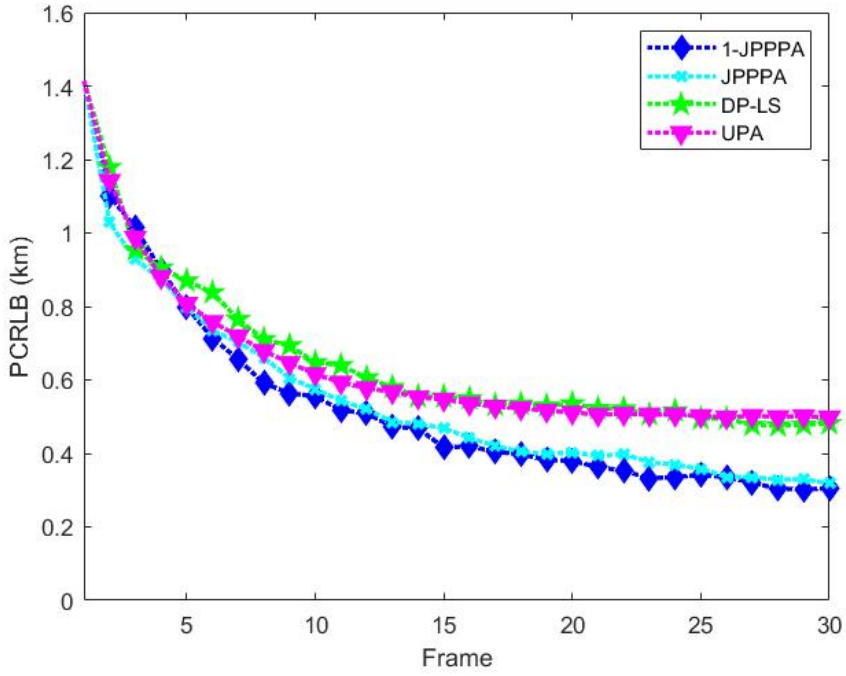

Figure 2.5: Optimized PCRLB results of different algorithms

any resource-aware system, is ignored. The inefficient utilization of power resources causes the unsatisfactory performance of the radar system. With respect to algorithms, GA-based JPPPA offers better performance than dynamic programming because of the following: first, DP-LS is a two-step algorithm where path planning and power allocation are considered separately, so the result obtained by path planning may not remain optimal when power allocation is considered. Second, the dynamic programming based on space discretization may be inaccurate due to the nonconvexity of the objective function.

It is important to note that 1-JPPPA and JPPPA have similar performance, and 1-JPPPA achieves slightly better results than JPPPA. The explanations for the slightly better results are: First, under the RHC framework, with the chromosomes becoming

$$\mathrm{RMSE}_k = \frac{1}{N_{MC}} \sqrt{\sum_{j=1}^{N_{MC}} \left[\left(x_{q,k} - \hat{x}_{q,k}^{j} \right)^2 + \left(y_{q,k} - \hat{y}_{q,k}^{j} \right)^2 \right]} \tag{2.5.1}$$

longer and more complex, it is generally more difficult for the JPPPA strategy to find the optimal combination of genes. Second, the performance of RHC used in the JPPPA depends not only on the trackers but also on the accuracy of the state model. When the solver makes decisions on future steps in the RHC sequence, future states are predicted with the current predicted state using the state model. Therefore, the errors introduced by the state model will be accumulated in RHC, which may cause the solver to make inaccurate decisions on future steps. Since future steps and the current step are constrained, some sacrifice on the performance in the current step may be made to compensate for future steps. However, this does not indicate that the 1-JPPPA is a better strategy than the long-term JPPPA under the RHC framework. As previously stated in Section IV, RHC provides the system with time to deal with a dynamic environment, which is more meaningful in practice. More discussions about RHC and our proposed custom pre-selection operator will be provided in the following subsections.

2.5.2 Performance of the Multitarget Tracker

A SIR particle filter with $N_p = 500$ particles is used in the system. The root mean squared error (RMSE) of the position is used to evaluate its performance.

Fig.2.6 presents the position RMSE of target 1 with the four resource management strategies. Table 2.3 gives the position RMSE of all targets in the last surveillance

epoch.

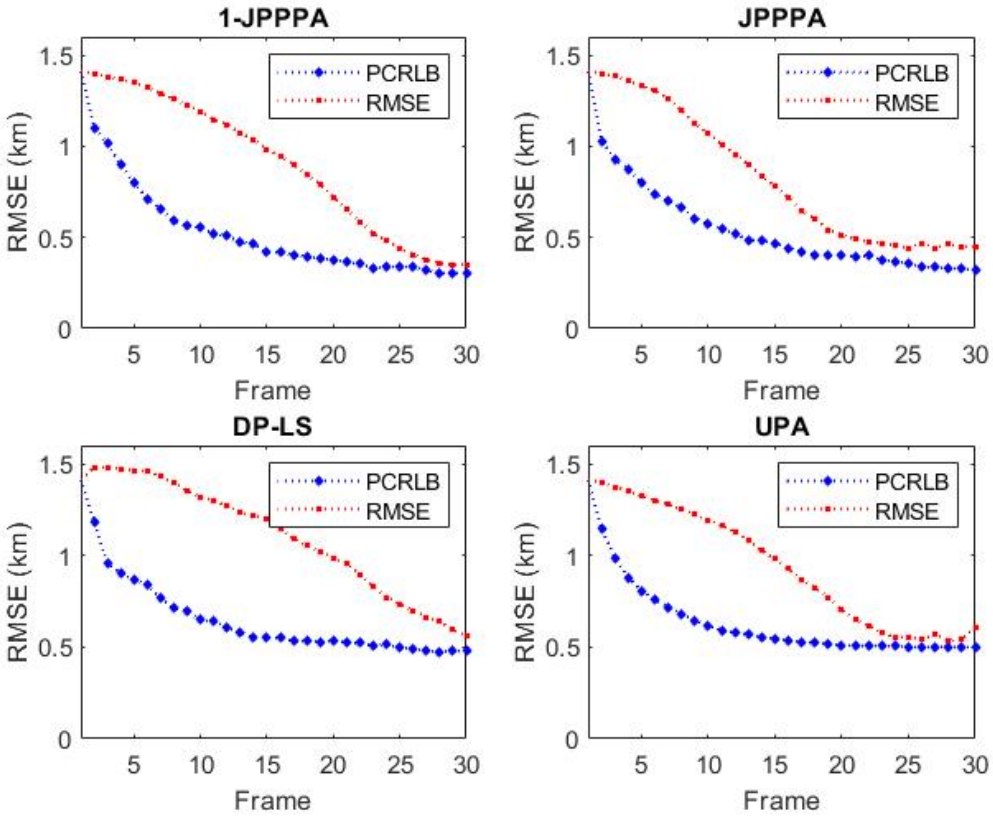

Figure 2.6: Comparison of position MSE of Target 1 between different resource management strategies

Fig.2.6 shows that trackers achieve better tracking performance in environments where the targets have lower PCRLB. The result of the JPPPA optimization is nearly consistent with the tracking accuracy. The lower PCRLB the target has in the environment, the better performance the trackers will achieve. The proposed algorithm outperforms the DP-LS algorithm, which handles the joint optimization in a decoupled manner. Fig.2.6 shows that when the filter starts to converge, the estimation error approaches the PCRLB value, which verifies the previous statement that PCRLB

is a good choice for objective functions in optimization problems that are related to tracking.

Remark 5: The true PCRLB depends only on the estimator and is irrelevant to the trackers employed. However, the predictive PCRLB evaluated by the solver, as approximated in equation (2.2.27), is dependent on the targets' predicted states, thus it is affected by the performance of the tracker. Therefore, the choice of trackers will in return affect the JPPPA solver. It is reasonable to use trackers that offer better nonlinear tracking performances, such as unscented Kalman filter (UKF) or PF that is adopted in this work.

Table 2.3: Comparison of Position PCRLB between Different Resource Management Strategies

Strategy	PCRLB (m)				
	Target 1	Target 2	Target 3	Target 4	Target 5
1-JPPPA	305.4	461.6	489.1	317.2	563.2
JPPPA	318.1	471.2	478.3	388.6	621.1
DP-LS	481.5	492.7	488.7	547.0	794.7
UPA	497.9	492.3	477.7	553.8	822.6

Table 2.4: Comparison of Position RMSE between Different Resource Management Strategies

Strategy	RMSE (m)				
	Target 1	Target 2	Target 3	Target 4	Target 5
1-JPPPA	354.2	546.1	538.6	436.2	912.6
JPPPA	446.7	538.1	472.2	489.4	870.9
DP-LS	559.3	876.6	666.9	797.7	1248.6
UPA	604.0	598.4	592.1	654.8	1472.3

2.5.3 Evaluation of the Custom Pre-selection Operator

In this subsection, three simulations are conducted to evaluate the performance of the pre-selection operator. Simulations I and II are identical to the previous simulations on 1-JPPPA and JPPPA, respectively. In the population generated by the pre-selection operator, 10% of individuals are offsprings of the elite and another random individual; 10% of the individuals are mutated from the elite. Note that the mutation in the pre-selection operator is different from the normal mutation. In simulation III, the pre-selection operator is not used, and the initial population at each time step is generated randomly. All simulations are conducted using MATLAB R2019a on a laptop with a Core™ i5 2.6 GHz CPU and 8 GB RAM.

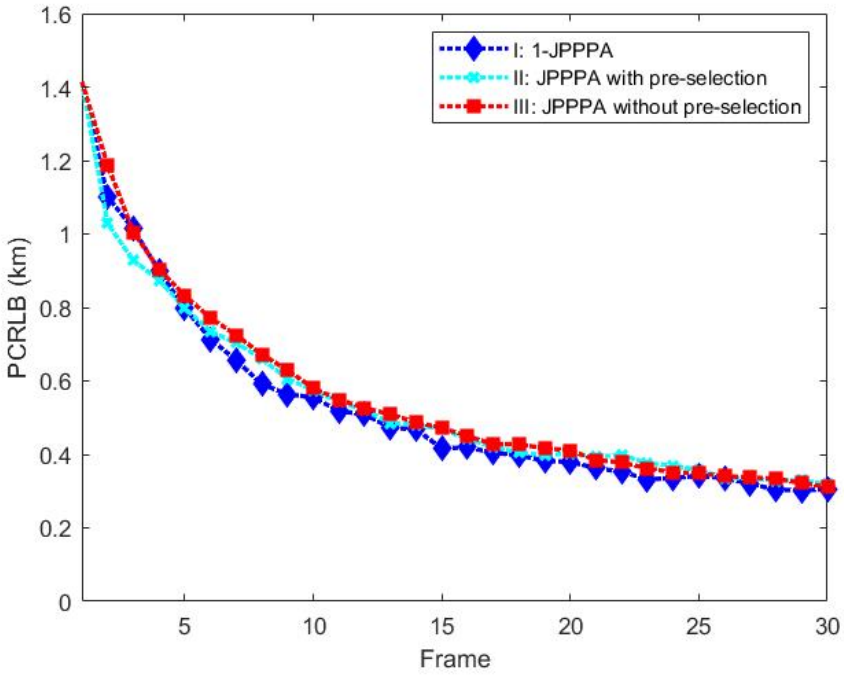

Figure 2.7: Comparison between algorithms with and without the pre-selection operator

Table 2.5: Comparison of Speed between Different Algorithms

Simulation	Generations	Time per Frame (s)	Total Time (s)
I	24.28	1.451	60.85
II	15.74	2.732	95.64
III	22.19	3.827	131.40

The true PCRLB values calculated with the optimization results that are obtained by three algorithms are presented in Fig.2.7. The three algorithms have similar performance. Table 2.5 demonstrates the speed of three algorithms. The average number of generations when the GA terminates is recorded in column 2. Columns 3 and 4 give the average processing time of one frame and of the whole surveillance period, respectively. Note that the particle filter requires a certain amount of time due to a large number of particles.

It can be seen in Table 2.5 that Simulation II takes less time while it achieves nearly the same result as Simulation III in Fig.2.7, which verifies the efficiency of the proposed pre-selection operator under the RHC framework. The population spends fewer generations evolving due to the existence of the prior information. From Table 2.5, it can be seen that Simulation II takes about one second less to make decisions at each epoch compared to Simulation III, which is vital in practice. Moreover, in a radar system that adopts RHC, the receivers will get commands on speed and heading angle in future steps, which makes the system less vulnerable to emergency situations such as communication failure.

Note that the average generation in Simulation III is less than in Simulation I, which means the solver terminates in Simulation I when the maximum generation is reached, while in Simulation III, no improvement can be found in the past five generations. It can be inferred that the solver in Simulation III is stuck at a local

minimum, and the crossover and mutation operators cannot get it out of the local minimum. This is consistent with the previous statement that it is more difficult to find the best combination of genes when chromosomes become longer. Further research can be done on the modification of crossover and mutation operators to reduce the probability of the solver being stuck in the local minimum.

GA is characterized as an *unguided* heuristic algorithm, which is both an advantage and a disadvantage. GA is advantageous because the user does not need to know how the population evolves, only discarding unfitted individuals is required. On the other hand, it also causes inefficiency when the algorithm starts to converge since improvement is generally achieved by randomness.

With the pre-selection operator, a small proportion of individuals are more likely to be generated around the prior information, and the solver is more likely to search for candidates in that area. As previously stated in Section IV, the pre-selection operator is similar to giving more weight to an individual in a particle swarm optimization (PSO), i.e., advantages of PSO are incorporated into the solver through the custom pre-selection operator. When applying GA, there might exist useful information to provide guidance for the evolution of the population, depending on the specific problem formulation. Modifying the algorithm by making use of such information will improve the performance.

2.5.4 Factors that Affect JPPPA Results

To demonstrate other factors that affect the JPPPA result, another set of simulations is presented in this subsection. The simulations are conducted to reveal the effect of target RCS and bistatic ranges on the JPPPA optimization results. To enhance the

effect of these factors, the simulation case is simplified by removing target 5, receiver 4, and receiver 5. The original target state and sensor deployment are displayed in Table 2.1 and Table 2.2, respectively.

Two different RCS models $\mathbf{H_1}$ and $\mathbf{H_2}$ are provided. In $\mathbf{H_1}$, all targets' RCS are modeled by the Swerling I model, i.e., the RCS is a random number that satisfies a chi-squared distribution with two degrees of freedom but remains constant over the measurement scan. In $\mathbf{H_2}$, the RCS model of targets 3, and 4 remain unchanged, while targets 1 and 2 are assumed to have larger RCS. Fig.2.8 shows the RCS of all targets in this scenario.

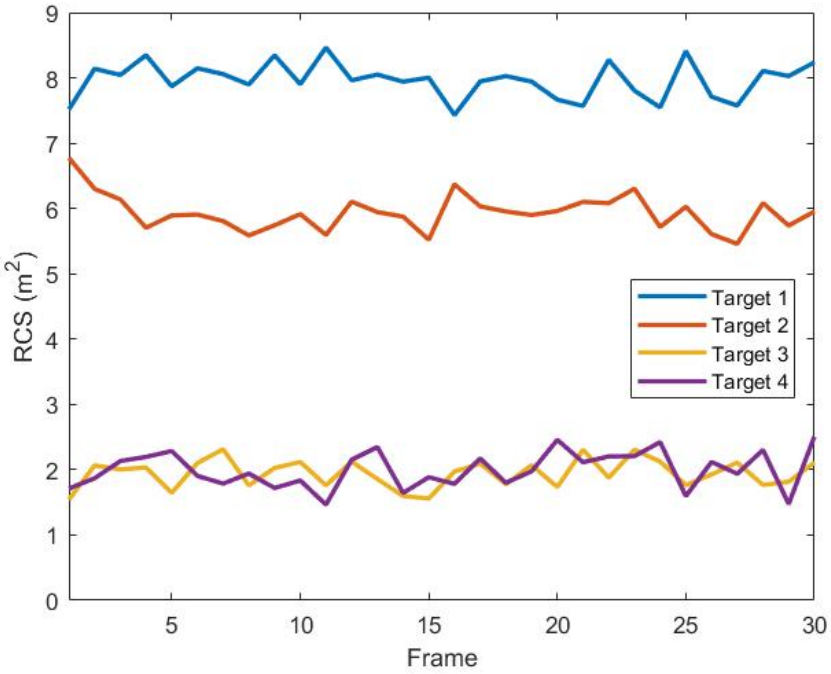

Figure 2.8: RCS of different targets in scenario $\mathbf{H_2}$

There are also two different transmitter locations, $\mathbf{Tx_1}$: $(0, 0)$ and $\mathbf{Tx_2}$: $(40, 10)$ available. In case $\mathbf{Tx_1}$, all targets have similar overall bistatic ranges with respect

to all bistatic pairs while in $\mathbf{Tx_2}$, with the transmitter located in the first quadrant, some targets will have significantly increased bistatic ranges, as shown in Fig.2.9.

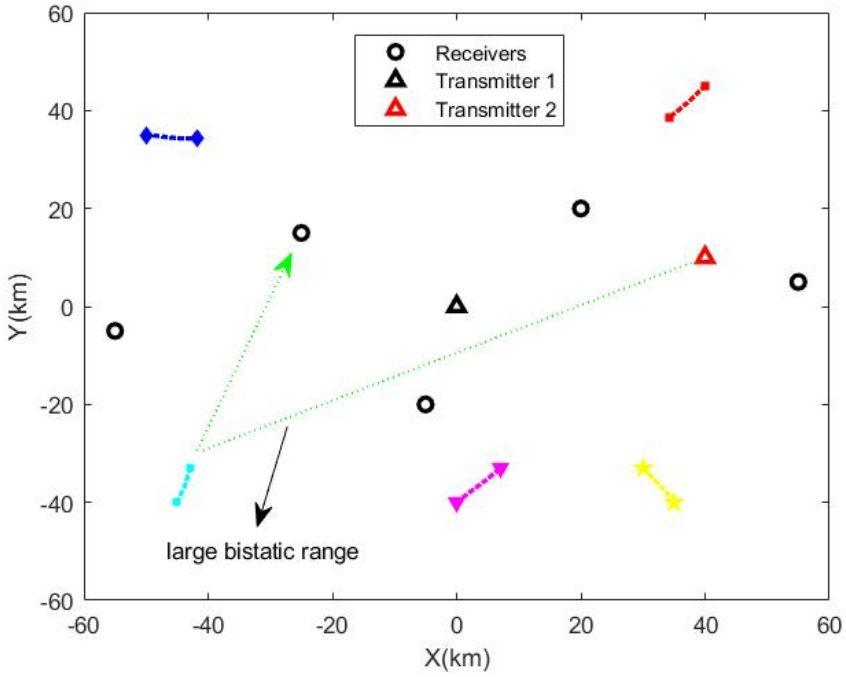

Figure 2.9: Different transmitter locations $\mathbf{Tx_1}$ and $\mathbf{Tx_2}$

Simulations are conducted on three different scenarios:

(1) case 1: $\mathbf{H_1}$ and $\mathbf{Tx_1}$;

(2) case 2: $\mathbf{H_2}$ and $\mathbf{Tx_1}$;

(3) case 3: $\mathbf{H_1}$ and $\mathbf{Tx_2}$.

The power allocation results are presented in Fig.2.10. It can be intuitively seen that in case 1, targets 1 and 2 are allocated with more power while in case 2, with their RCS becoming larger, they are allocated with less power. The power radiation values at time step 30 are given in Table 2.6. It can be concluded that the transmitter tends to illuminate the target with relatively low RCS.

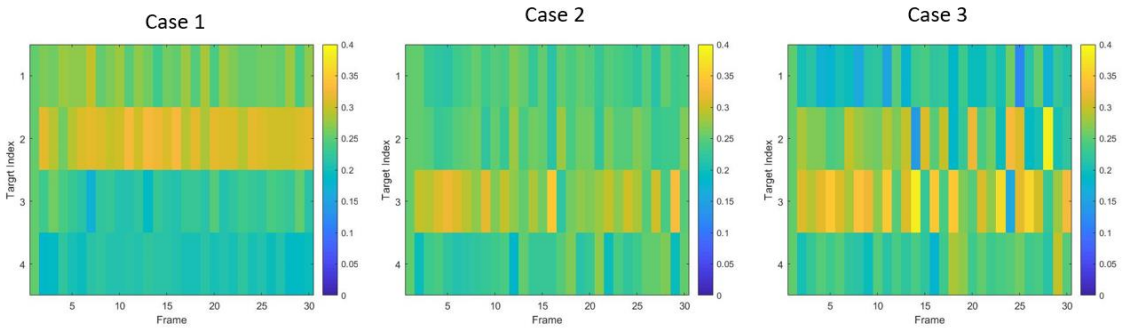

Figure 2.10: Power allocation result of 3 cases

Table 2.6: Comparison of the Power Allocated in Case 1 and 2

Target Index	Case 1		Case 2	
	RCS (m^2)	Power Allocated	RCS (m^2)	Power Allocated
1	2.11	0.2641	8.71	0.2438
2	1.58	0.3045	7.74	0.2652
3	1.71	0.2280	2.06	0.2587
4	2.19	0.2034	1.60	0.2323

Table 2.7: Power Allocation Result and Bistatic Range

Target Index	Bistatic Range (km)			Power Allocated
	R1	R2	R3	
1	98.34	138.32	145.89	0.2641
2	131.35	91.52	131.16	0.3045
3	141.40	111.31	97.33	0.2280
4	99.19	122.02	87.91	0.2034

From the result of case 3 shown in Fig.2.10, it can easily be seen that after the transmitter is moved from the origin to (40,10), there is a significant increase in the power radiation that is allocated to track target 3, which is located in the third quadrant and thus has the largest overall bistatic ranges. Meanwhile, target 1 located in the first quadrant, since it's closer to the transmitter, is now assigned with less power. Table 2.7 gives the power allocation result and the bistatic ranges with respect to three receivers at time step 30. Although the exact mathematical relationship between the bistatic range and the allocated power is hard to determine with the simulation results presented since the system is configured with more than one receiver, it can be concluded that the transmitter tends to assign more power to targets with large bistatic ranges under the objective of optimizing overall tracking performance.

Remark 6: When tracking multiple targets, the transmitter will allocate more power to illuminate targets with low SNR (small RCS, large bistatic range, etc.). Therefore, the tracking performance of targets with high SNR will be degraded. Such compromise may not be a wise resource management strategy if these factors that affect the optimization result have a significant difference among targets. For example, if target 1 and target 2 have a RCS of 1 unit and 100 units, respectively, and other parameters are identical, the transmitter would allocate 100 units of power to target 1 and 1 unit to target 2, which might waste limited resources on targets that are already hard enough to track. However, in a multistatic radar system with multiple transmitters, a clever approach for a transmitter is to discard such targets and let other transmitters with better bistatic geometries illuminate them. These problems are addressed in the literature as beam selection[95], base station selection[78], etc. Future research will investigate multistatic radar systems with multiple transmitters.

2.6 Conclusion

In this paper, a JPPPA strategy for multitarget tracking in a multistatic radar system was proposed. The radar adopts a multibeam mode that tracks multiple targets simultaneously, and the receivers are mounted on UAVs whose trajectories are to be optimized for better tracking performance. The basis of the proposed strategy is the cooperative receding horizon control of both power allocation patterns and UAV trajectories based on PCRLB. The formulated problem is a three-variable nonconvex problem, and a modified GA with a custom pre-selection operator was proposed to solve the problem. It was shown that our method does not depend on the convexity of the objective function, and can be applied to more complicated scenarios. Numerical simulations were performed to demonstrate the effectiveness of the proposed JPPPA strategy and its advantage over methods that consider path planning and power allocation, respectively.

This work can be extended by considering the following issues. First, the JPPPA problem can be tackled jointly with beamforming, beam selection, and radar mode selection in more complex radar configurations. Second, the number of targets is assumed to be known and fixed in this work. Future research will explore scenarios where the number of targets is unknown by applying optimal resource management strategies to tracking problems based on a random finite set (RFS).

Chapter 3

Adaptive Beam Scheduling for Cooperative Phased Array Radars with High-Precision Pencil-Beam

3.1 Introduction

3.1.1 Background and Motivation

Recent advancement in phased array technology enables the control and adaptation of a radar's beam instantaneously [19, 87, 59]. The use of phased array antennas or electronically steered antennas (ESA) has enhanced the flexibility and effectiveness of radars by allowing them to swiftly switch tasks when necessary. These advantages of phased array radars provide them with the capability to carry out multiple functions simultaneously, which typically include surveillance, tracking, and weapon engagement. This, however, leads to issues with radar resource management.

The problem of resource management[15, 51, 62, 82, 27, 66] arises when a radar does not have sufficient resources to handle all tasks. An effective resource management algorithm is required to properly allocate limited radar resources to different tasks and to maintain the tracking error under a certain threshold. The three major resources in a radar system are time, power, and processing budget. Time is the most constraining resource that determines whether a task or function should be executed or delayed. Correspondingly, several typical resource management problems involve time allocation, such as task prioritization[43] and sensor scheduling[53]. The performance of a certain task is dependent on the power allocated to it, thus power allocation problems arise to maximize the overall performance by efficiently allocating limited power to all tasks [71, 94]. The processing budget is consumed by signal processing operations such as confirming or updating tracks, and it is limited by the capacity of computer processors[81]. These issues often appear as constraints (e.g., battery life) in resource management problems. In a more generalized sense, certain radar parameters that affect radar performances such as waveform or bandwidth, are also considered as special resources and need to be optimized during task execution. Considerable efforts have been dedicated to investigating waveform design[39], bandwidth allocation[60], and tracking update scheduling[29], in terms of radar resource management.

Due to the broad definition of resource management problems, detailed mathematical modeling varies. Generally, radar resource management is treated either as an optimization problem with a predefined criterion or an objective function with several operational constraints. One typical criterion for resource management problems is quality of service (QoS)[21]. QoS-based radar allocation model (Q-RAM)

algorithms are defined to optimize the radar system and maintain an acceptable level of QoS. Q-RAM allows multiple QoS requirements such as timeliness, cryptography, and reliable data delivery to be addressed and traded off against each other. In [33], Q-RAM for single and multiple resource types was comprehensively studied and a gradient projection algorithm was developed.

Solution techniques for resource management optimization can be categorized into AI approaches and non-AI approaches[15]. A recent research[69] proposed a machine learning-based branch-and-bound (B&B) method to solve the non-deterministic polynomial-time hard (NP-hard) problem while maintaining a modest computational cost. In [34], a neural network approach was adopted to solve the time scheduling problem of transmitting and receiving pulses. In [50, 49], a fuzzy logic method was developed to determine the priority of tasks, and thereafter allocate power to them. Rule-based heuristic searches, such as genetic algorithm (GA)[98] or particle swarm optimization (PSO)[100] are also in this category. Non-AI approaches include dynamic programming [79, 12, 88] and convex optimization techniques [10, 45, 96]. Due to the complexity of radar models, either the objectives or the constraints are significantly nonlinear. Therefore, it's hard to model or solve radar resource management problems from the view of pure mathematical optimization. Usually, different techniques are combined into the solution. [68] incorporated a graph theory-based approach with simulated annealing (SA).

Another radar resource management constraint is beam scheduling, where the radar beams are scheduled to determine the steering direction and operation time to perform certain tasks. Additionally, power allocated to each beam and beam parameters, e.g., beamwidth, may also be considered as variables to be optimized. Recently,

a task scheduling problem has been studied in [98] and a hybrid adaptively genetic algorithm utilizing chaotic sequence was proposed that outperforms both adaptive GA and high priority and earliest deadline first (HPEDF) algorithm.

Radars have flexible beam generation modes to satisfy different requirements. They can generate pencil beams with narrow beamwidth to provide measurements with high angle resolution which are preferred in high-precision tracking, and also fan-beams with wide beamwidth to search for potential targets. Fig 3.1 shows the different types of beams that can be generated by PAR. Recent works have studied resource management problems in multi-functional radars[49, 96, 68]. [96] provides a good trend of compound resource management problems by jointly considering tracking and detecting missions and formulating a bi-objective problem. Existing works don't make special assumptions on the size of beams. It is often assumed a beam can cover the whole area of interest once a mission is assigned to it. In fact, a beam can be generated to be extremely thin for accurate tracking and the saving of energy.

In the literature, it is assumed that the radar's scan resolution cell size is large enough to cover the potential location of the targets[25, 8, 96]. Hence, the beam steering problem coincides with the task scheduling problem where steering a beam to point at a certain target is equivalent to assigning the beam to that tracking task. However, for tracking highly maneuvering targets with pencil-beams, the previously stated assumption may not hold and it is not guaranteed that the target can be detected within one scan due to the small coverage size of the pencil-beams. Thus, our interest is to develop an adaptive scheduling algorithm for pencil-beams to make best

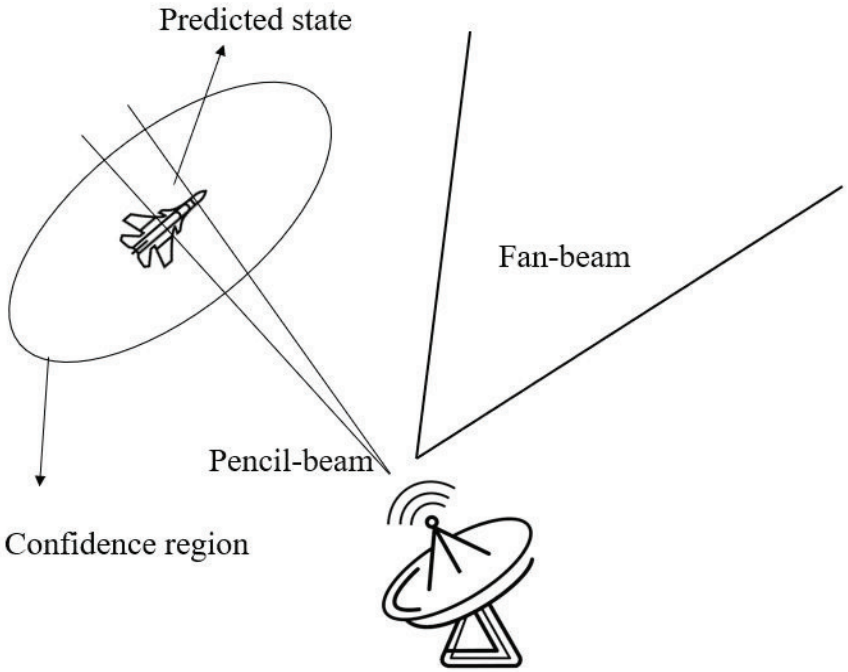

Figure 3.1: Illustration of Pencil-beam and Fan-beam PAR beam modes

use of limited resources and produce the best tracking performance. At each scheduling interval, the scheduler controls the radar's beams and uses the measurement data to maximize tracking performance. Searching functions can be fulfilled using the gap time[38].

Existing research on beam scheduling in terms of resource management mainly focuses on normal-size beams to increase tracking accuracy, but pencil-beams are barely considered. In practice, however, the adoption of pencil-beams is necessary when high-resolution tracking is required. Furthermore, launching narrow beams is an effective and efficient method of resource allocation since it concentrates the power for beam generation. Pencil beams have great prospects in large-volume surveillance and highly maneuvering target tracking applications, hence the pencil beam scheduling problem needs to be addressed. Our work models the tracking problem and the beam scheduling optimization, with the objective of more tracking accuracy.

The Posterior Cramér-Rao lower bound (PCRLB), given by the inverse of the Fisher Information Matrix, provides a lower achievable minimum estimation of the mean squared error (MSE) for any unbiased estimator[86]. [57] states that the estimation error asymptotically approaches the PCRLB in areas with a high signal-to-noise ratio (SNR) if the measurement noise is Gaussian. Hence, PCRLB is often used as a criterion to minimize[94, 96, 82, 62]. However, In the case of high-accuracy tracking with pencil-beams, partial observations occur due to the small width of the beams. In these scenarios, PCRLB cannot accurately give the accuracy of the estimator. Furthermore, PCRLB cannot be obtained analytically[86]. In our paper, we propose a new concept of expected PCRLB (EPCRLB) that uses the Monte Carlo technique to handle the issue of partial observations.

3.1.2 Main Contributions

In this paper, the problem of pencil-beam scheduling for cooperative phased array radars is addressed. All radar nodes in the system work in a cooperative fashion sharing measured data and making decisions on beam control. The information exchange among radar nodes will be realized via wireless communication.

This paper makes the following contributions:

1) *The pencil-beam scheduling problem is addressed and formulated as an optimization problem.* Pencil beams are suitable for high-accuracy tracking with the cost of moderate energy consumption. However, they cannot cover the entire area of interest and lead to partial observations in tracking missions. This paper addresses this novel problem of tracking with pencil-beams and formulated a corresponding beam scheduling problem as to where to steer the beams to obtain better tracking accuracy.

2) *The concept of expected posterior Cramér-Rao lower bound (EPCRLB) is proposed and utilized as the criterion to minimize.* The PCRLB, which gives an achievable lower bound for any unbiased estimator, is utilized as the metric that needs to be optimized. However, due to partial observations obtained by pencil-beams, PCRLB cannot be obtained analytically. Hence, we propose a new concept of expected PCRLB that applies the idea of the Monte Carlo trial. EPCRLB is also used as a criterion to guide real-time optimization. Our results show that it offers superior performance over those strategies that don't involve the concept of EPCRLB.

3) *An alternative linear wipe solution is proposed.* A target-driven solution that utilizes a linear wipe strategy is proposed. It has less computational complexity and is shown to be effective while the maneuvering level of targets is low.

4) *An ABS-based framework for multitarget tracking is developed.* An interacting

multiple model (IMM) algorithm is employed to handle maneuvering target tracking. The nonlinear filtering is dealt with by a local unscented Kalman filter (UKF). A closed-loop signal processing framework based on adaptive beam scheduling (ABS) is established for the radar system. Details of the framework are illustrated in Fig.3.2.

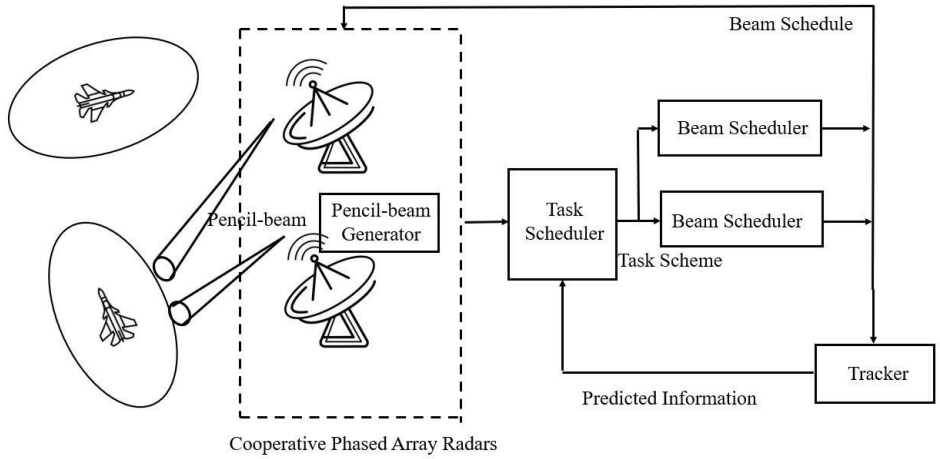

Figure 3.2: ABS-based multitarget tracking framework in a cooperative radar system

5) *A starter of hybrid beam scheduling in PAR systems is given through this paper.* PARs launch different types of beams to perform different tasks. This work provides a perspective on hybrid beam scheduling and resource allocation research in PARs. It's promising to extend our work by considering target detection applications with fan-beams.

The remainder of the paper is organized as follows. Section II describes the problem and introduces preliminary knowledge. Problems formulations and corresponding solution techniques are presented in Section III. Numerical simulations are demonstrated in Section IV and conclusions are given in Section V.

3.2 Problem Description

For simplicity, a 2-D surveillance area is assumed where a radar system with N cooperative phased array radar nodes is deployed. The position of the nth node is denoted by (x_n, y_n). There are Q airborne targets to be tracked. The qth target is initially located at $(x_{q,1}, y_{q,1})$ with an initial velocity $(\dot{x}_{q,1}, \dot{y}_{q,1})$. At time step k, the qth target is located at $(x_{q,k}, y_{q,k})$ with velocity $(\dot{x}_{q,k}, \dot{y}_{q,k})$.

The assumptions used to define the problem are as follows:

1. The radars can provide a pencil-beam mode for high-accuracy target tracking. Such pencil-beam cannot cover the entire confidence region of the target location.

2. Each radar can only launch a single beam for target tracking.

3. The number of radar nodes N is less than the number of targets Q, i.e., there will always be targets that are not illuminated by any radar in each time step.

4. The radars can switch the direction of their beams instantaneously.

5. The number of targets is known and remains constant. All tracks are already confirmed.

3.2.1 Target Dynamics

Let $\mathbf{x}_q^k = [x_{q,k}, \dot{x}_{q,k}, y_{q,k}, \dot{y}_{q,k}]^T$ denote the state vector of the qth target, where $[x_{q,k}, y_{q,k}]$ and $[\dot{x}_{q,k}, \dot{y}_{q,k}]$ denote the position and velocity of the target respectively.

The state space model that describes the qth target's motion is given by

$$\mathbf{x}_{q,k+1} = \mathbf{F}_k \mathbf{x}_{q,k} + \mathbf{w}_{q,k} \tag{3.2.1}$$

$\mathbf{F}_k$ denotes the state transition matrix, and $\mathbf{w}_{q,k}$ is the process noise that describes the inaccuracy of the motion model. It is assumed to be zero-mean Gaussian distributed with a known covariance $\mathbf{\Gamma}_k$.

$$\mathbf{\Gamma}_k = \kappa \mathbf{I}_2 \otimes \begin{bmatrix} \frac{1}{3}T^3 & \frac{1}{2}T^2 \\ \frac{1}{2}T^2 & T \end{bmatrix} \tag{3.2.2}$$

where κ is the intensity of process noise. In this paper, two target dynamic models are considered which are constant velocity (CV) and constant turn (CT) with a known turn rate.

For the CV model, the transition matrix is given by

$$\mathbf{F}_k = \mathbf{I}_2 \otimes \begin{bmatrix} 1 & T \\ 0 & 1 \end{bmatrix} \tag{3.2.3}$$

where $\otimes$ is the Kronecker operator, and $\mathbf{I}_2$ denotes the 2×2 identity matrix.

For the CT model, the transition matrix is given by

$$\mathbf{F}_k = \begin{bmatrix} 1 & \frac{\sin \omega T}{\omega} & 0 & -\frac{1-\cos \omega T}{\omega} \\ 0 & \cos \omega T & 0 & -\sin \omega T \\ 0 & \frac{1-\cos \omega T}{\omega} & 1 & \frac{\sin \omega T}{\omega} \\ 0 & \sin \omega T & 0 & \cos \omega T \end{bmatrix} \tag{3.2.4}$$

3.2.2 Measurement Model

A binary variable $o^k_{m,n,q}$ is defined to indicate whether the qth target is illuminated by the mth scan of the nth radar node at time step k. Failure to illuminate a certain target may be caused by task assignment schemes (as previously mentioned, there are always targets that are not tracked) or missed detection due to partial observation. The measurement is given by:

$$\mathbf{z}_{n,q,k} = \begin{cases} h_n(\mathbf{x}_{q,k}) + \mathbf{w}_{n,q,k} & \text{if } o_{n,q,k} = 1 \\ \mathbf{0} & \text{if } o_{n,q,k} = 0 \end{cases} \tag{3.2.5}$$

where $\mathbf{z}_{n,q,k}$ is the measurement of target q at time step k that is obtained by the nth radar, h_n is the nonlinear observation function. Generally the measurements include range $R_{n,q,k}$ and bearing $\theta_{n,q,k}$:

$$h_n(\mathbf{x}_{q,k}) = [R_{n,q,k}, \theta_{n,q,k}]^T \tag{3.2.6}$$

which are given by:

$$\begin{cases} R_{n,q,k} = \sqrt{(x_{n,q,k} - x_{n,k})^2 + (y_{n,q,k} - y_{n,k})^2} \\ \theta_{n,q,k} = \arctan\left(\frac{y_{n,q,k} - y_{n,k}}{x_{n,q,k} - x_{n,k}}\right) \end{cases} \tag{3.2.7}$$

$\mathbf{v}_{n,q,k}$ is the measurement noise, which is assumed to be a zero-mean Gaussian random variable with covariance $\mathbf{\Sigma}_{n,q,k}$.

$$\mathbf{\Sigma}_{n,q,k} = \text{diag}\left(\sigma^2_{R_{n,q,k}}, \sigma^2_{\theta_{n,q,k}}\right) \tag{3.2.8}$$

In practical scenarios, the probability of detection P_d of each target is always less

than unity due to imperfect interference. Besides, there exist false alarms over the surveillance area due to inevitable clutters. They are assumed to be a zero-mean Gaussian random variable uniformly distributed in the measurement space (within the observation volume V) with their number being a Poisson-distributed variable, given by

$$p(n_{fa}) = \frac{e^{-\lambda V}(\lambda V)^{n_{fa}}}{n_{fa}!} \tag{3.2.9}$$

where n_{fa} is the number of false alarms, λ is the spatial density, i.e., the average number of false alarms at each frame.

3.2.3 PCRLB and EPCRLB

The Cramér-Rao lower bound (CRLB), given by the inverse of the Fisher information matrix (FIM), provides a lower bound of the error covariance matrix of any unbiased estimator for a certain parameter. The Posterior Cramér-Rao lower bound (PCRLB) gives a measure of the achievable accuracy for dynamic state estimation. Since the PCRLB is irrelevant to the tracker, it is often adopted as a criterion to minimize resource management problems. Let $\hat{\mathbf{x}_k}$ be an unbiased estimate of $\mathbf{x}_k$ based on the measurement $\mathbf{z}_k$, $\mathbf{C}_k$ be the error covariance matrix, and $\mathbf{J}(\mathbf{x}_k)$ be the FIM, then

$$\mathbf{C}_k = \mathbb{E}[(\hat{\mathbf{x}}_k - \mathbf{x}_k)(\hat{\mathbf{x}}_k - \mathbf{x}_k)^T] \geq \mathbf{J}_(\mathbf{x}_k)^{-1} \tag{3.2.10}$$

where $\mathbb{E}$ denotes expectation operator.

The FIM can be calculated with the following recursion[86]:

$$\mathbf{J}_k = \mathbf{J}_X(\mathbf{x}_k) + \mathbf{J}_Z(\mathbf{x}_k) \tag{3.2.11}$$

$\mathbf{J}_X(\mathbf{x}_k)$ and $\mathbf{J}_Z(\mathbf{x}_k)$ are referred to as the prior knowledge and the measurement contribution at time step k respectively.

$$\begin{cases} \mathbf{J}_X(\mathbf{x}_k) = \mathbf{D}_{k-1}^{22} - \mathbf{D}_{k-1}^{21}(\mathbf{J}_k + \mathbf{D}_{k-1}^{11})^{-1}\mathbf{D}_{k-1}^{12} \\ \mathbf{J}_Z(\mathbf{x}_k) = \mathbb{E}\{-\Delta_{\mathbf{x}_k}^{\mathbf{x}_k} \ln p(\mathbf{z}_k|\mathbf{x}_k)\} \end{cases} \tag{3.2.12}$$

where

$$\begin{cases} \mathbf{D}_{k-1}^{11} = \mathbb{E}\{-\Delta_{\mathbf{x}_{k-1}}^{\mathbf{x}_{k-1}} \ln p(\mathbf{x}_k|\mathbf{x}_{k-1})\} \\ \mathbf{D}_{k-1}^{12} = \mathbb{E}\{-\Delta_{\mathbf{x}_k}^{\mathbf{x}_{k-1}} \ln p(\mathbf{x}_k|\mathbf{x}_{k-1})\} = (\mathbf{D}_{k-1}^{21})^T \\ \mathbf{D}_{k-1}^{22} = \mathbb{E}\{-\Delta_{\mathbf{x}_k}^{\mathbf{x}_k} \ln p(\mathbf{x}_k|\mathbf{x}_{k-1})\} \end{cases} \tag{3.2.13}$$

and Δ_x^y is the second-order partial derivative operator, given by

$$\Delta_x^y = \frac{\partial^2}{\partial x \partial y} \tag{3.2.14}$$

and x, y are vectors.

The prior information $\mathbf{J}_X(\mathbf{x}_k)$ is the knowledge we already know once the estimation of the previous step is acquired. It can be calculated by:

$$\mathbf{J}_X(\mathbf{x}_k) = [\mathbf{\Gamma}_{k-1} + \mathbf{F}_k \mathbf{J}(\mathbf{x}_{k-1})^{-1} \mathbf{F}_{k-1}^T]^{-1} \tag{3.2.15}$$

The measurement contribution calculates how much information we can get from the

current measurement, which is given by

$$\mathbf{J}_{Z_n}(\mathbf{x}_k) = \mathbb{E}\{\mathbf{H}_{q,k}^T \Sigma_{q,k}^{-1} \mathbf{H}_{q,k}\} \tag{3.2.16}$$

where $\mathbf{H}_{q,k} = [\Delta_{\mathbf{x}_q^k} h_n^T(\mathbf{x}_q^k)]^T$ is the Jacobian matrix of the measurement function $h_n(\mathbf{x}_q^k)$ with respect to the target state $\mathbf{x}_q^k$ and $\mathbb{E}$ denotes expectation with respect to the target state.

This expected value in equation (3.2.16) cannot be obtained analytically. The approximation is usually made by using the Jacobian and measurement noise covariance evaluated at the prediction phase to avoid extra computational costs.

$$\mathbf{J}_{Z_n}(\mathbf{x}_k) = \mathbf{H}_{q,k}^T \Sigma_{q,k}^{-1} \mathbf{H}_{q,k} \Big|_{\mathbf{x}_{k|k-1}^q} \tag{3.2.17}$$

where $\mathbf{x}_{k|k-1}^q$ denotes the predicted state of the qth target at time step k.

Note that in the calculation of $\mathbf{J}_{Z_n}(\mathbf{x}_k)$, an important assumption is that the target is scanned by the radar beam at time k with a known target detection probability, false alarm rate, and gating sizes. However, in the cases with pencil-beam radar and a target (i.e., drone) with high motion uncertainty, one beam scan will not be able to provide a full observation of the target, which makes the traditional PCRLB calculation inapplicable. Hence, an expected PCRLB (EPCRLB) is introduced to handle the partial observation problem as the calculation of $\mathrm{J}_X(k)$ in E-PCRLB is the same as that in traditional PCRLB. Thus, only the new measurement contribution part denoted as $\mathrm{EJ}_Z(k+1)$ is detailed. $\mathrm{EJ}_X(k)$ is calculated based on the target existence density $\mathcal{D}_t$ (i.e., tracker outputs) and the angle coverage capability $\mathcal{C}_p$ of

radar. Thus, one arrives at

$$\mathrm{E}\mathbf{J}_{Z_n}(\mathbf{x}_k) = \int\limits_{\mathbf{x}_k \in \mathcal{C}_p} \mathcal{D}_t(\mathbf{x}_k) \mathbb{E}\left\{-\Delta_{\mathbf{x}_k}^{\mathbf{x}_k} \ln p(\mathbf{z}_k|\mathbf{x}_k)\right\} d\mathbf{x}_k \tag{3.2.18}$$

Note that the intersection of target existence density (TED) $\mathcal{D}_t$ and beam coverage $\mathcal{C}_p$ cannot be obtained analytically, hence the Monte-Carlo approach can be implemented. An artificial dataset $\mathcal{S}$ of $\{\mathrm{X}_k\}_1^{N_p}$is obtained from the TED. Next, an averaged PCRLB over the whole dataset $\mathcal{S}$ is calculated with

$$\mathrm{E}\mathbf{J}_{Z_n} \approx \frac{1}{N_p} \sum_{\substack{\mathbf{x}_k \in \mathcal{C}_p \\ \mathbf{x}_k \in \mathcal{S}}} \mathbb{E}\left\{-\Delta_{\mathbf{x}_k}^{\mathbf{x}_k} \ln p(\mathbf{z}_k|\mathbf{x}_k)\right\} \tag{3.2.19}$$

where N_p is the total number of points covered under one beam.

When the coverage of a single beam is larger than the target existence area and can provide a full observation of the target, the EPCRLB reduces to PCRLB. This is the first time an expression for EPCRLB has been derived. The EPCRLB is one of the critical formulations needed to address the measurement realization in CRLB and verify the accuracy of target state estimates obtained from actual measurement realizations. Starting with the concepts in[76], the predictive EPCRLB (PE-PCRLB) is used by introducing the latest available measurement information to refine EPCRLB and formulate the ABS strategy for multitarget tracking in a multiple-function phased array radar.

3.2.4 Cooperative multitarget tracking

In this paper, cooperative tracking is considered as opposed to independent tracking where tracks of a target are initialized and maintained separately by different radars.

In a cooperative tracking framework, there is only one track for a single target. If there is more than one detection from multiple radars (or from false alarms), a detection-to-track data association is conducted[52].

Since there are multiple models for target motion (Section 3.2.1) and the measurement equations are nonlinear (Section 3.2.2), Interacting Multiple Model Unscented Kalman Filter (IMM-UKF) is used to handle the multitarget tracking. The IMM algorithm blends various motion models to offer better tracking accuracy against maneuvering targets. In brief, IMM runs local filters for each model in the library and then evaluates the model probability μ_k^{j-} at each time step. By combining all tracking outputs of different motion models, IMM can achieve better tracking performance, as opposed to a single filter.

The updated state estimation is given by

$$\hat{\mathbf{x}}_k = \sum_{j=1}^{J} \mu_k^{j-} \hat{\mathbf{x}}_k^j \tag{3.2.20}$$

The updated covariance matrix is given by

$$\hat{P}_k = \sum_{j=1}^{J} \mu_k^{j-} \{\hat{P}_k^j + [\hat{\mathbf{x}}_k - \hat{\mathbf{x}}_k^j] \cdot [\hat{\mathbf{x}}_k - \hat{\mathbf{x}}_k^j]^T\} \tag{3.2.21}$$

where J is the number of motion models and j is the model index, and $\hat{\mathbf{x}}_k^j$ and $\hat{P}_k^j$ are the estimated state and covariance of the filter that adopts the jth motion model.

Due to the nonlinearity of the measurement function in equation (3.2.5), the unscented Kalman filter (UKF) is used to perform the local filtering with one single motion model. A brief introduction to UKF is given below. For more information, the reader is referred to [8]. Note each single filter can only assume one motion model,

so the model index j is omitted below.

Unscented transform (UT) is the core to approximate nonlinear evolution. We generate a set of samples, referred to as sigma points σ_k^i, with corresponding weights w^i, to represent the state distribution $\mathbf{x}_k$.

The prediction is completed by predicting all sigma points and adding them up by weight.

$$\mathbf{x}_{k+1}^- = \sum_i w^i \cdot \mathbf{F}_k \sigma_k^i \tag{3.2.22}$$

$$P_{k+1}^- = \sum_i w^i \cdot [\mathbf{x}_{k+1}^- - \sigma_k^i] \cdot [\mathbf{x}_{k+1}^- - \sigma_k^i]^T + \mathbf{\Gamma}_k \tag{3.2.23}$$

where the superscript $-$ denotes prediction.

Similarly, the prediction of measurements is given by

$$\mathbf{z}_{k+1}^- = \sum_i w^i \cdot h(\sigma_k^i) \tag{3.2.24}$$

In the update step, firstly, the innovation is obtained by

$$S_{k+1} = \sum_i w^i \cdot [\mathbf{z}_{k+1}^- - \mathbf{z}_{k+1}] \cdot [\mathbf{z}_{k+1}^- - \mathbf{z}_{k+1}]^T + \mathbf{\Sigma}_{k+1} \tag{3.2.25}$$

The Kalman filter gain is given by

$$K_{k+1} = (\sum_i w^i \cdot [\mathbf{x}_{k+1}^- - \sigma_k^i] \cdot [\mathbf{z}_{k+1}^- - \mathbf{z}_{k+1}]^T) \cdot S_{k+1}^{-1} \tag{3.2.26}$$

Finally, filter gain is used to update the predicted state and covariance.

$$\hat{\mathbf{x}}_{k+1} = \mathbf{x}_{k+1}^{-} + K_{k+1} \cdot [\mathbf{z}_{k+1}^{-} - \mathbf{z}_{k+1}] \tag{3.2.27}$$

$$\hat{P}_{k+1} = P_{k+1}^{-} - K_{k+1} \cdot S_{k+1} \cdot K_{k+1}^{T} \tag{3.2.28}$$

Probabilistic data association (PDA)[8] is used to handle measurement origin uncertainty that rises from missed detection and false alarms. If a missed detection occurs when tracking a target, whether due to the partial observation or because this target was not assigned to any radar node, the tracker will simply predict the target's state and covariance and use them as the filter output.

3.3 Beam Scheduler for Cooperative Phased Array Radar

In this section, detailed mathematical formulations of the beam scheduling problem are presented. Sections 3.3.1 to 3.3.3 present three mathematical modeling and corresponding solution techniques. Section 3.3.4 gives the complexity analysis of these schedulers.

3.3.1 Beam Scheduler 1: Fixed Linear Wipe

Since pencil-beams with small beamwidth cannot cover the entire area of interest, a straightforward solution is to rapidly scan a position of potential target existence and its adjacent cells[40]. If the radar scans the area in a linear fashion, such a technique

is referred to as linear wipe.

Before scheduling precise beam steering directions, the radar system will roughly assign tracking tasks to each node with the task scheduler.

Let A be the radar-to-target assignment matrix, such that

$$A = \begin{bmatrix} a_{11} & & a_{1Q} \\ & \ddots & \\ a_{N1} & & a_{NQ} \end{bmatrix}_{N \times Q} \tag{3.3.1}$$

where $a_{n,q}$ takes value 1 if the qth target is assigned to the nth radar and 0 otherwise. Since every radar will be assigned to a tracking task, A satisfies $\sum_{n \in R} a_{n,q} = 1$.

To meet the requirement of tracking accuracy, the radar-to-target task assignment is completed by maximizing the worst-case PCRLB.

$$\min \ \max_{q} \ \{\text{PCRLB}_q\}, q = 1, \cdots, Q \tag{3.3.2}$$

where PCRLB_q is the PCRLB of the qth target. Since it depends on the Jacobian matrix, which is relevant to the target's state, the PCRLB is evaluated with the predicted state $\mathbf{x}_k^-$ at time k.

Remark 1: The diagonal elements of the PCRLB matrix directly give the lower bounds of the squared estimation errors. Therefore, the trace of the PCRLB matrix is often used as a scalar characteristic while evaluating PCRLB. As an alternative, the sum of the first and the third diagonal elements, which represent the lower achievable squared errors of target position estimation, can be used for evaluation.

The PCRLB is calculated as

$$\text{PCRLB}_q = \mathbf{J}_X^q + \sum_{n \in \mathcal{N}} \mathbf{J}_{Z_n}^q \tag{3.3.3}$$

where $\mathcal{N}$ is the set of radars that are assigned to target q. Note that during the task scheduling phase, multiple radars may be assigned with the same tracking task. $\sum_{n \in \mathcal{N}} \mathbf{J}_{Z_n}^q$ is the sum of measurement contributions obtained from all the radars tracking target q. A coordinated tracking framework is used where there exists one single track for each target. If there are multiple detections from different radars, a detection-to-track data association is performed.

Remark 2: Although it is possible that a single tracking task is assigned to multiple radar nodes, this situation does not commonly happen unless one target's motion uncertainty is significantly greater than the others. Besides the data association technique, the issue of overlapped tasks can be handled by giving the current task only to the radar that provides the most measurement contribution $\mathbf{J}_Z^q$ and assigning other radars with different tasks. In this case, the overall estimation errors for multitarget tracking will be reduced.

It is assumed that the target does not move too much during N_s successive tracking scans. Typically, a scan takes 0.05 s while a complete dwell for a tracking task is 2 s. During a tracking task, N_s scans will be used on a target with predicted state $\mathbf{x}_k^-$ and predicted covariance P_k^-. The mean m_k and covariance R_k in the polar measurement space with unscented transform (UT) will be computed as shown in Fig.3.3. UT handles the nonlinear mapping from target state to sensor measurement[8].

Using a gating technique, the range of bearing around m_k can be determined. For simplicity, the range information is ignored here. Fig.3.4 shows an illustration of the

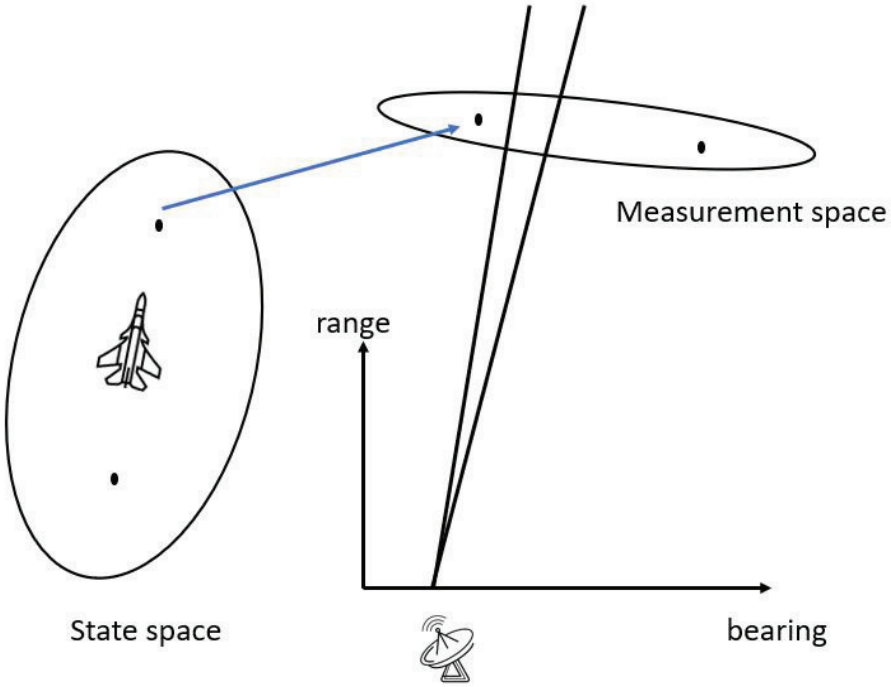

Figure 3.3: Illustration of Unscented Transform for nonlinear mapping of target state to measurement

fixed linear wipe beam scheduling approach. $c0$ is the value of bearing from the m_k, where the target exists with the highest possibility. cl_i, cr_j are the bearing cells on the left and right sides of the mean bearing value. Note that the cell size here is θ_{track}. Let $N_s = 18$, then we have a sequence of scans as the pattern below

$$c0, cl_1, cr_1, cl_2, cr_2, cl_3, cr_3, cl_4, cr_4, cr_5, c0,$$
$$cl_1, cr_1, cl_2, cr_2, cl_3, cr_3, cl_4$$

The effective probability of detection can be computed using $\bar{p}_d = 1 - \prod_{s=1}^{S}(1 - p_g^s p_d)$[8], where S denotes the number of times the radar covers the covariance area,

which is $S = 2$ in this case. The probability of gate, i.e., p_g, is the modifier due to a single scan. For example, the first scan covers the entire target existence region, so we have $p_g = 1$. It can be seen that for the second scan, the radar cannot guarantee a full p_g.

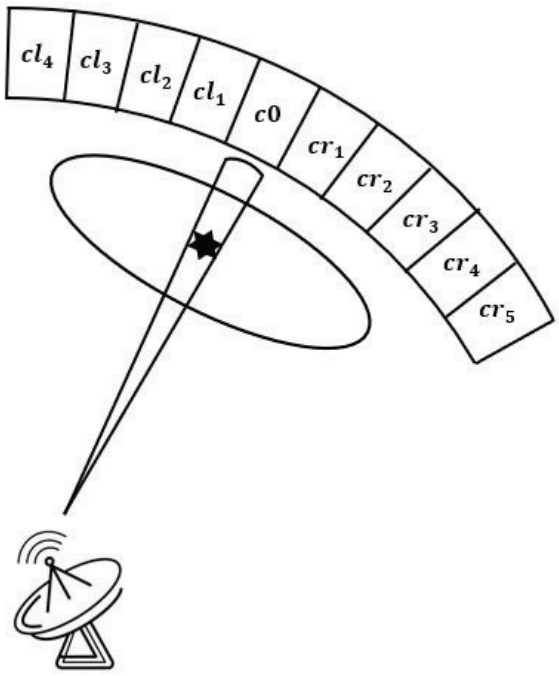

Figure 3.4: Illustration of the linear wipe beam scheduler approach

Remark 3: The number of scans N_S is determined by the total time of the mission interval. The total scan width for a batch scan (in the previous example, 10 cells) is determined by both the width of the target distribution (along the bearing direction) and the beamwidth. The radar will continue scanning linearly until the beam reaches the edge of the gate or until all scans have been used.

3.3.2 Beam Scheduler 2: Open-loop Linear Wipe

With the fixed scanning pattern, a linear wipe can be used to perform tracking tasks. However, the size of the target spatial existence area changes during the surveillance period and its shape is dependent on the target-sensor geometry. Therefore, the fixed linear wipe will not be suitable in this scenario. Fig.3.5 shows a scenario where the target's existence area is small and only limited scans are required to track this target. With the fixed linear wipe strategy, the radar will continue to scan the area repeatedly while these scans could be allocated to other targets. Hence, an open-loop linear wipe beam schedule solution that allocates tracking scans based on the specific target distribution P_k^- is developed. Note that there is no task scheduling module before the beam scheduler. The evaluation of PCRLB, which is accomplished by the task scheduler, is incorporated into the beam scheduling process here.

Assume that N_s scans are allocated for the tracking mission at time k, then the radar will scan the area of interest from the centroid to the edge successively. Assume there are M_S batch scans in total. The solver will determine, for each series of batch scans, which target to scan and the length of the scan sequence. Note that M_S determines the size of the sequence and $N_S = \sum_{m=1}^{M_S} N_{s,m}$, denoting the total number of tracking scans cost in this mission interval. The total number of scans should be less than the restricted value from the duty cycle. $0 \leq N_{s,m} \leq N_S$, $t_{\text{start}} \leq t_m \leq t_{\text{start}} + t_{\text{plan}}$. $\sum_{m=1}^{M_S} N_{s,m} = N_S$. t_{start} is the time point the batch scan starts and t_{plan} is the duration of the planned batch scan. The scanning pattern is denoted as S, which is a sequential order of beam schedules. Each beam schedule

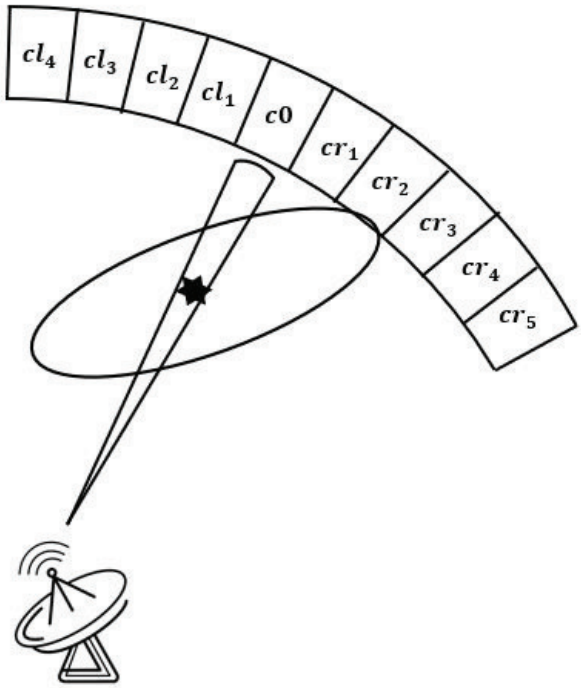

Figure 3.5: Illustration of open-loop linear wipe with a target with a small existence area

consists of the angle of the beam and the time when the beam is steered.

$$S = \{(t_1, \theta_1), (t_2, \theta_2), ..., (t_{N_S}, \theta_{N_S})\} \tag{3.3.4}$$

where t_i is the time when the ith scan is made and θ_i is the angle of the steered beam, $i = 1, 2, ..., N_S$.

Objective functions To achieve a feasible beam scheduler that can aid the tracker with minimum track drops, errors, and resources (time), multiple objective functions are adopted.

1. Accuracy:

$$\begin{aligned} &\min_{S} \ \max_{q} \ \{\mathrm{tr}(\mathrm{PCRLB}_{q,t_{\mathrm{scan}}^{-}})\} \\ &\text{s.t.} \quad t_{\mathrm{scan}}^{-} \in (t_{\mathrm{start}}, t_{\mathrm{start}} + t_{\mathrm{plan}}) \end{aligned} \tag{3.3.5}$$

where $\mathrm{PCRLB}_{q,t_{\mathrm{scan}}^{-}}$ is the PCRLB matrix of target q at time t_{scan} without update.

2. Maximum average probability detection

$$\max_{S} \ \min_{q} \ \{\frac{1}{\bar{N}_i} \sum_{m=1}^{M_S} O(m,q) \bar{p}_d^m\} \tag{3.3.6}$$

where $\bar{N}_q$ is the total number of batch scans over a single target, i.e.,

$$\bar{N}_q = \sum_{m=1}^{M_s} O(m,q) N_{s,m}, q = 1, \cdots, Q \tag{3.3.7}$$

and $O(m,q)$ equals one or zero depending whether or not the target q is illuminated by mth batch scan.

Using this objective function, a good probability of detection (maximum p_d) could be guaranteed.

$$\bar{p}_d^m = 1 - \prod_{i=1}^{I_m} (1 - p_g^i p_d) \tag{3.3.8}$$

Where $I_m = \mathrm{ceil}(N_{s,m}/\hat{N}_{g,m})$, $\mathrm{ceil}(\gamma)$ returns the smallest integer value that is bigger than or equal to a number γ, and $\hat{N}_{g,m}$ is minimum number of scans

that one needs to get a full p_g at mth batch scan. $\hat{N}_g$ varies with the state of the target and size of covariance (mainly on bearing and elevation directions). From equation (3.3.8), the practical $\bar{p}_d$ can increase infinitely close to 1 when $\hat{N}_g << N_{s,m}$. As mentioned above, the value of p_g^i is determined by the size of the area of interest scanned within mth batch scan. For the case in Figure 3.4, with a full $p_g = 0.95$, one has $S = 2$, $p_g^1 = 0.95$ and $p_g^2 = 0.8 * 0.95$

3. Measurement contribution (Reward):

$$\max_{S} \min_{q} \{\sum_{m=1}^{M_S} O(s,q)\mathbf{J}_Z^{m,q}\} \tag{3.3.9}$$

where the measurement contribution from the mth batch scan $\mathbf{J}_Z^{m,q}$ is given by

$$\mathbf{J}_Z^{m,q} = \bar{p}_d^m * \mathbf{J}_Z^q \tag{3.3.10}$$

Optimization method The optimization problem is a mixed-integer nonlinear programming (MINLP). It combines both mixed-integer programming and nonlinear programming, which is generally hard to solve within polynomial time. To meet the real-time requirements, a fast method is needed. Hence, a hierarchical genetic algorithm is used.

Genetic algorithm (GA) is a heuristic searching technique that imitates the process of natural selection. Feasible solutions to the optimization problem are represented as individuals (also referred to as chromosomes) and are searched in a parallel manner that is called generations. In each generation, the fitness value of each individual is evaluated, and then a selection operation is conducted. Individuals with high fitness

values are more likely to be reproduced into the next generation, while those with low fitness will be eliminated. Common selection techniques include roulette wheel and tournament selection. A binary tournament selection strategy is adopted in this work.

To maintain the diversity and prevent early maturing, crossover and mutation operations are performed. In a crossover operation, a locus is randomly chosen and the genes before and after this locus between two parent chromosomes are exchanged. In a mutation operation, each gene has a probability P_m to be replaced by a random value.

Elitism is adopted in this paper to prevent the loss of highly fitted individuals. After each selection, a few individuals with the highest fitness values will be directly copied into the next generation without participating in the crossover and mutation operation.

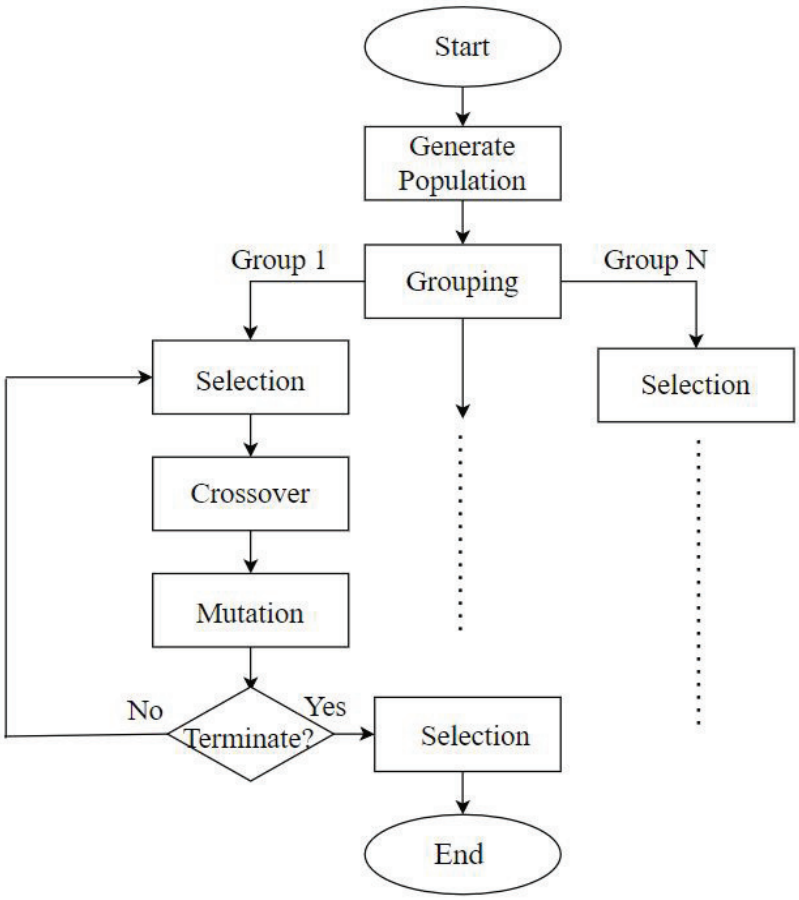

Figure 3.6: Hierarchical representation of the genetic algorithm.

In the optimization problem, the length of chromosomes is determined by the number of batch scans M_S, thus individuals that represent diverse M_S values will have different chromosome lengths. Chromosomes with different lengths cannot crossover with each other. Therefore, a hierarchical genetic algorithm (HGA) is applied. Hierarchy refers to the presence of modules at multiple levels. Its basic idea is to group individuals with similar characteristics and have them evolve independently within

their own group. In the MINLP, the structure of chromosomes is hierarchically divided into two different gene sequences that control M_S and n_S, respectively. The entire population is split into several groups based on their M_S value. Within each group, the individuals evolve independently, and the best one is found. Then, a global optimum is found among all groups by comparing their local optimum. The flow chart of HGA is presented in Fig.3.6, and a brief pseudo-code is given below.

Algorithm 2 Hierarchical Genetic Algorithm

Input:

Estimates of all targets $\hat{\mathbf{x}}_{k,q}$, $\hat{P}_{k,q}$. System configuration parameters. Maximum iteration i_{max}

Output:

The beam steering sequence $\mathbf{S}$

```
Generate a random number of groups N;
for Each group n in N do
    Generate random population
    Evaluate individual fitness and selection
    while i < i_max do
        Crossover
        Mutation
        Selection by fitness value
    end while
    Selection by fitness value
end for
```

3.3.3 Beam Scheduler 3: EPCRLB-based optimal solution

In previous sections, it is assumed that the mobility of one target is low compared with the speed of tracking scans. This assumption might hold in some cases, but it is clearly not an optimal solution for the narrow beam scheduling problem. Therefore, an optimal open-loop beam scheduler, which considers the target motion characteristics in the formulation, is proposed.

Objective functions Based on [82, 62, 25], the method proposed in Section 3.2.3 utilizes the predictive PCRLB where the $\mathbf{J}_Z$ can be computed as in equation (3.2.17).

Note that $\mathbf{J}_Z$ is determined by the predictive target state $\mathbf{x}_k$ with a fixed state of sensor x_n, which is valid as it is assumed that the area where the target potentially exists can be covered with one scan or multiple combined scans[76]. However, in practical cases with narrow beam scans, this assumption no longer holds due to the smaller coverage area of the beam compared with the target localization uncertainty, as discussed in Section 3.2.3. Thus, an EPCRLB is proposed and adopted for the objective formulation. EPCRLB is calculated based on the target localization distribution and the scan capability of the radar. With a set of state vectors $\mathbf{x}_k^m$, covariance matrices P_k^m and corresponding weight values w_k^m, $m = 1, \cdots, M$, a target localization distribution can be formulated. However, it is hard to analytically calculate the possible states covered by one beam scan. Several particles extracted from the distribution are used to represent all the potential target states, which can be used to calculate the EPCRLB. As shown in Fig.3.7, a set of particles $\xi_{p,i}, i = 1, \cdots, N_p$(points) are extracted from two Gaussian distributions with known mean, covariance and weights.

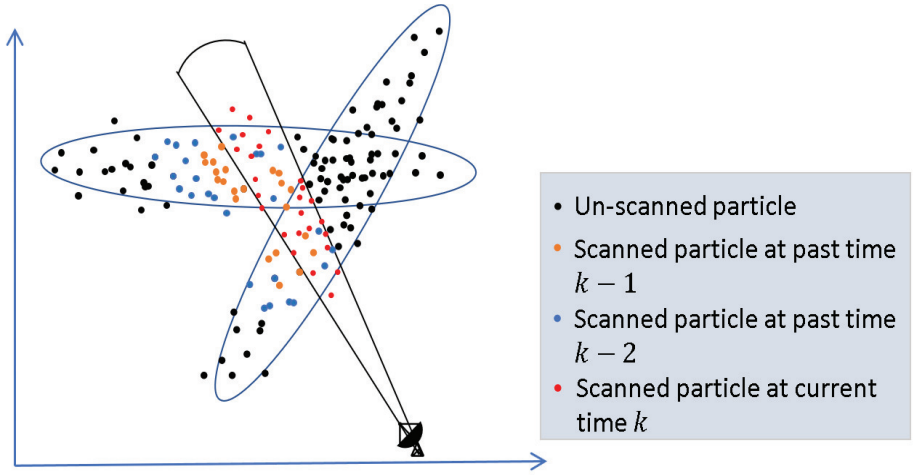

Figure 3.7: Illustration of particles scanned by the radar at different times

All the red points represent the part of the target existence that is illuminated by the radar. $\bar{O}(i)$ denotes whether or not one point $\xi_{p,i}$ is included inside the scan area. Using equation (3.2.17),

$$\mathrm{Jz}(\xi_{p,i}) = \mathrm{E}[H_k(\xi_{p,i}) R_s^{-1} H_k(\xi_{p,i})'] \tag{3.3.11}$$

The expected measurement contribution from this scan is given by

$$\mathrm{E}\mathbf{J}_Z = \frac{p_d \bar{p}_g p_n}{\hat{N}_p} \sum_{i=1}^{N_p} \bar{O}(i) \mathbf{J}_{Z_i} \tag{3.3.12}$$

and $\bar{p}_g \approx \frac{\hat{N}_p}{N_p} p_g$, where N_p is the total number of points used to represent the distribution, $\hat{N}_p$ is the number of points covered by one scan beam, and p_n is the ratio of new particles scanned to the total number of particles scanned.

An example of a practical scenario is illustrated in Fig.3.8. Twelve particles are used to represent the target existence distribution, and three scans are included. At

time $k-2$, the central part of the area of interest is scanned and six out of twelve particles are illuminated. This is taken as the first scan, so $p_n = 1$ as all the particles are scanned for the first time. Then, at time $k-1$, there is a new covariance matrix from the propagation of the target state. The beam moves to the left of the area of

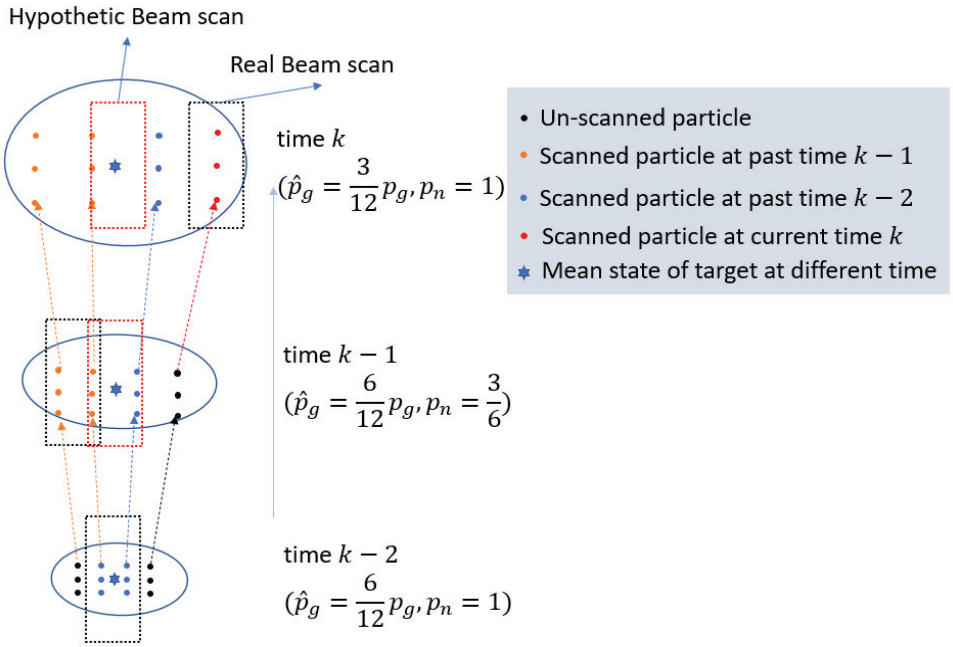

Figure 3.8: Illustration of beam scheduler for targets in motion

interest and six particles are scanned but three of them are scanned for the second time, thus $p_n = 3/6$. For the current scan at time k that illuminates the right part of the area of interest, three new particles are included, thus $p_n = 1$. From the process described in the figure, it can be seen that p_n denotes the ratio of new information to the total information obtained in the scan. This parameter, p_n, ensures that the radar goes through the area of interest instead of only focusing on the subregion that provides the highest $\mathbf{J}_Z$. Without using p_n in the formula, the radar tends to point to the central part around the mean target state (shown as the red rectangle in

Fig.3.8) as it provides the higher p_g. Although it will return a high reward, the other regions with high target existence possibilities are ignored, which may result in missed detections, especially for the scenarios with highly maneuvering targets. This is a new problem arising from pencil-beam scheduling as only a small section of the area of interest can be covered with a single scan. Thus, finding a good combination of scans to not only increase the tracking accuracy but also the target detection possibility is vital.

The expected FIM is given by

$$\mathrm{E}\mathbf{J} = \mathbf{J}_X + \mathrm{E}\mathbf{J}_Z \tag{3.3.13}$$

where $\mathbf{J}_X$ is calculated as in equation (3.2.15).

To provide an optimal beam scheduler that aids the tracker with minimum track drops, errors, and resources (time), multiple objects are adopted.

1. Accuracy:

$$\begin{aligned} &\min_{S} \ \max_{q} \ \{\mathrm{EPCRLB}_{q,t}\} \\ &\text{s.t.} \quad t \in (t_{\text{start}}, t_{\text{start}} + t_{\text{plan}}) \end{aligned} \tag{3.3.14}$$

2. Measurement contribution (Reward):

$$\max_{S} \ \min_{q} \ \{\sum_{s=1}^{N_S} O(s,q)\mathrm{E}\mathbf{J}_{Z\,s,q}\} \tag{3.3.15}$$

where $O(s,q)$ equals one or zero depending on whether or not the target q is

illuminated by sth single narrow beam scan and $\mathrm{E}\mathbf{J}_{Zs,q}$ is the expected measurement contribution calculated with aforementioned Monte-Carlo approach.

3.3.4 Complexity Analysis

The complexity of the task scheduler incorporated in beam scheduler 1 is $\mathcal{O}(Q \times N)$. The search volume is enlarged when the number of radar nodes and/or targets is increased. The beam scheduler itself does not consume much computational budget, once the target existence area is calculated, the scanning pattern can be obtained.

The complexity of beam scheduler 2 is of the order of $\mathcal{O}(N^1_{pop} \times N^2_{pop})$, where N^1_{pop} and N^2_{pop} are the population size of the first and the second level respectively. N^2_{pop} is independent of the problem size while N^1_{pop} is proportional to the value of $Q \times N$. Note that the complexity of GA is also relevant to the GA parameters. The complexity grows with the increase of maximum iteration times. With the increase in the problem size, more combinations of radar-to-target assignment need to be investigated.

The complexity of beam scheduler 3 is of the order of $\mathcal{O}(Q \times N \times N_p/\beta)$, where N_p is the number of particles that represent the distribution of *each* target and β is the beamwidth. When β is large enough to cover the whole area of interest, beam scheduler 3 reduces to a normal-beam scheduling strategy.

3.4 Simulation

In this section, numerical results are presented to demonstrate the performance of the proposed strategies. Assume a phased array radar system with $N = 2$ radar nodes is used to track $Q = 3$ airborne targets. The radar nodes are located at $(-10, 5)$

km and $(5, -10)$ km. The area is surveilled for 50 frames with the time interval $\Delta T = 1$s. The targets' motions are modeled by two dynamic models: the constant velocity (CV) model and the constant turn (CT) model with the turn rate known. Each target will perform two turning maneuvers during the surveillance period. The detailed information on targets is provided in Table 3.1 and their trajectories are shown in Fig.3.9. The beamwidth of the pencil-beam is set to $\beta = 0.15°$.

Table 3.1: Initial Target States

Target Index	1	2	3
Position (km)	(30,35)	(-40,25)	(-25,-20)
Velocity (m/s)	(-200,-250)	(300,0)	(100,25)
Turning Interval 1 (s)	(10,20)	(5,20)	(10,15)
Turn Rate 1(°)	3	4	-4
Turning Interval 2 (s)	(35,45)	(25,35)	(35,45)
Turn Rate 2(°)	-3	2	5

For the hierarchical cooperative GA used in the beam schedulers, the number of groups (first-level population size) is 15. Each group has 101 individuals. The probabilities of crossover $P_c = 0.6$ and the probability of mutation $P_m = 0.6$. Each group stops evolving if it reaches the maximum of 30 iterations or if there is no improvement within the latest five generations. For the optimal beam scheduler, each target's distribution is represented by $N_p = 500$ particles. All results are averaged over 100 Monte Carlo runs.

3.4.1 Comparison among ABS Strategies

From Fig.3.10, there are no significant differences between the worst-case PCRLB offered by the three algorithms, although the optimal beam scheduler obtains a slightly lower PCRLB. Table 3.2 presents detailed data for the PCRLB of the three beam

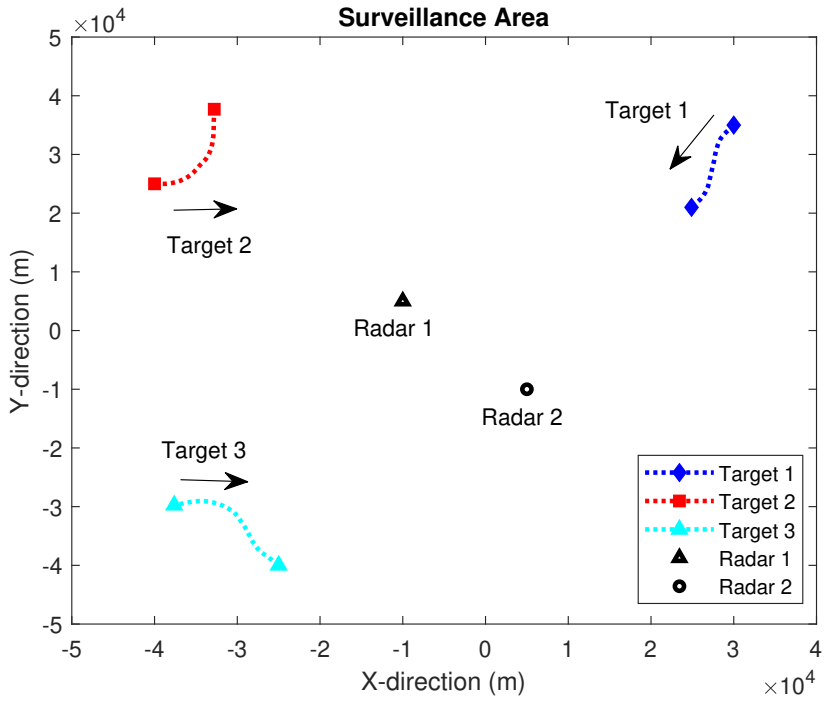

Figure 3.9: Layout of target trajectories and radar deployment

scheduler algorithms at different frames. Note the bold numbers, the optimal solution already gives a lower PCRLB for target 1 though it does not change the worst-case PCRLB. This is because the worst-case PCRLB comes from the target that is not tracked.

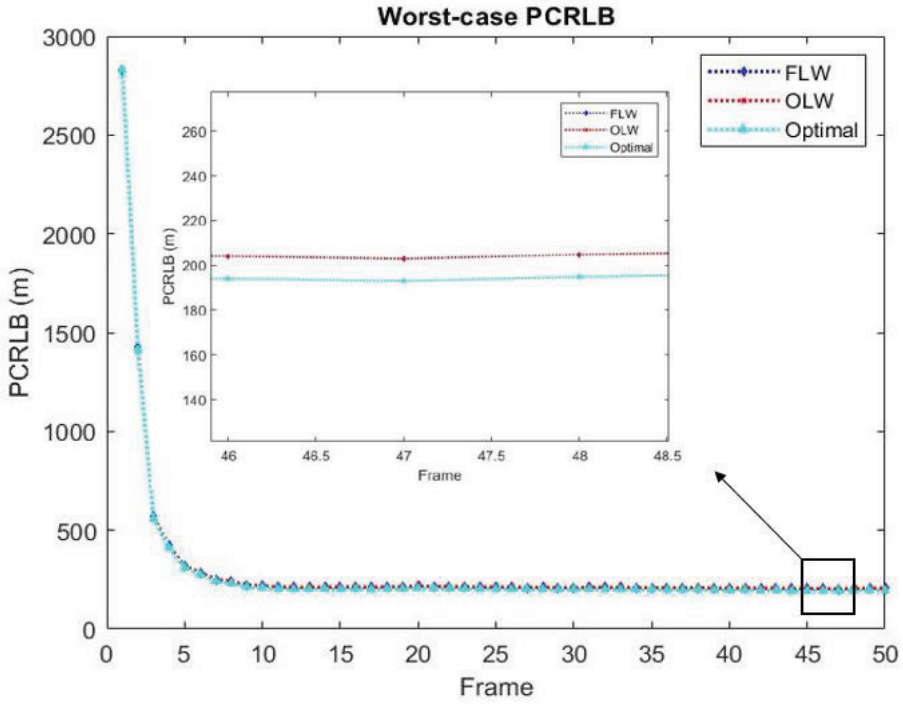

Figure 3.10: Worst-case PCRLB

To demonstrate the effectiveness of proposed strategies, an information reduction factor (IRF) ξ_q is defined to describe how much information was obtained from imperfect observation. The proposed beam schedulers essentially try to maximize this factor.

Table 3.2: PCRLB of Each Target

Time Index	Algorithm	PCRLB of Target No.			Worst-case PCRLB
		1	2	3	
2	FLW	693.6	1424.2	558.5	1424.2
	OLW	693.6	1424.2	558.5	1424.2
	Optimal	693.6	1424.2	558.5	1424.2
3	FLW	**470.1**	428.3	558.5	558.5
	OLW	**467.8**	428.3	558.5	558.5
	Optimal	**466.5**	428.2	558.5	558.5
...					...
50	FLW	192.5	189.0	206.5	206.5
	OLW	192.6	189.0	206.4	206.4
	Optimal	192.6	187.9	197.6	197.6

For the linear wipe strategies, ξ_q is expressed as the actual probability of detection

$$\xi = \bar{p}_d = 1 - \prod_{i=1}^{M_S}(1 - p_g^i p_d) \tag{3.4.1}$$

For the EPCRLB-based optimal solution, ξ_q is defined as the expected measurement contribution, $\mathrm{E}\mathbf{J}_Z$, over the total measurement contribution $\mathbf{J}_Z$. Since they are both matrices, their trace is used as their scalar metric to perform the division.

$$\xi = \frac{\mathrm{trace}(\mathrm{E}\mathbf{J}_Z)}{\mathrm{trace}(\mathbf{J}_Z)} \tag{3.4.2}$$

For simplicity, the target index q is omitted in the equations of ξ_q above.

Fig.3.11 shows the IRF of target 1 over the entire surveillance period. Note that at time step $k = 1$, the IRFs are all set to 0. It can be seen from the figure that the

optimal solution offers significantly better IRF than the linear wipe strategies. The average IRFs over the 50 time steps are given in Table 3.3. In practice, a large IRF will guarantee a high probability of detection.

Table 3.3: Average Information Reduction Factor

Strategy	FLW	OLW	Optimal
Average IRF	0.4613	0.5183	0.7854

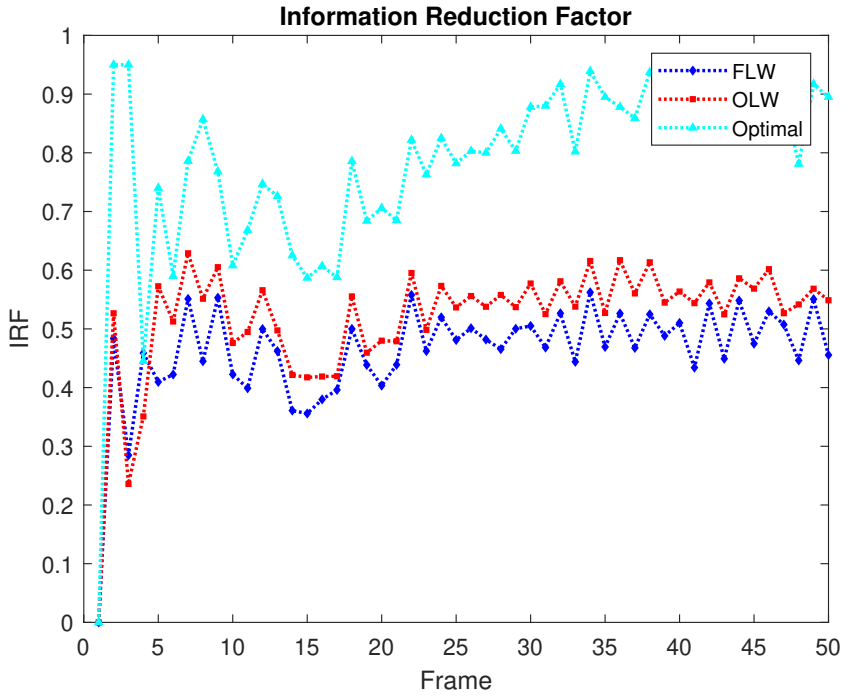

Figure 3.11: Information reduction factor for Target 1 using the proposed beam scheduler strategies

3.4.2 Performance of the Multitarget Tracker

The optimal beam scheduler offers a higher IRF and thus, a lower PCRLB. However, PCRLB is only a theoretically lower bound and may not be achieved in real-life cases,

$$\text{RMSE}_k = \left[\frac{1}{N_{MC}} \sqrt{\sum_{j=1}^{N_{MC}} \max_q \left[\left(x_q^k - \hat{x}_q^{k,j} \right)^2 + \left(y_q^k - \hat{y}_q^{k,j} \right)^2 \right]} \right] \tag{3.4.3}$$

hence the actual estimation error of the tracker is of more importance in practice.

The performance of the multitarget tracker is evaluated by the worst-case RMSE

Fig.3.12 shows the worst-case RMSE of all three tracks, along with the PCRLB offered by the optimal beam scheduler. The actual estimation errors for the optimal beam scheduler are smaller when compared to the other two strategies. Table 3.4 gives the worst-case RMSE at selected time intervals.

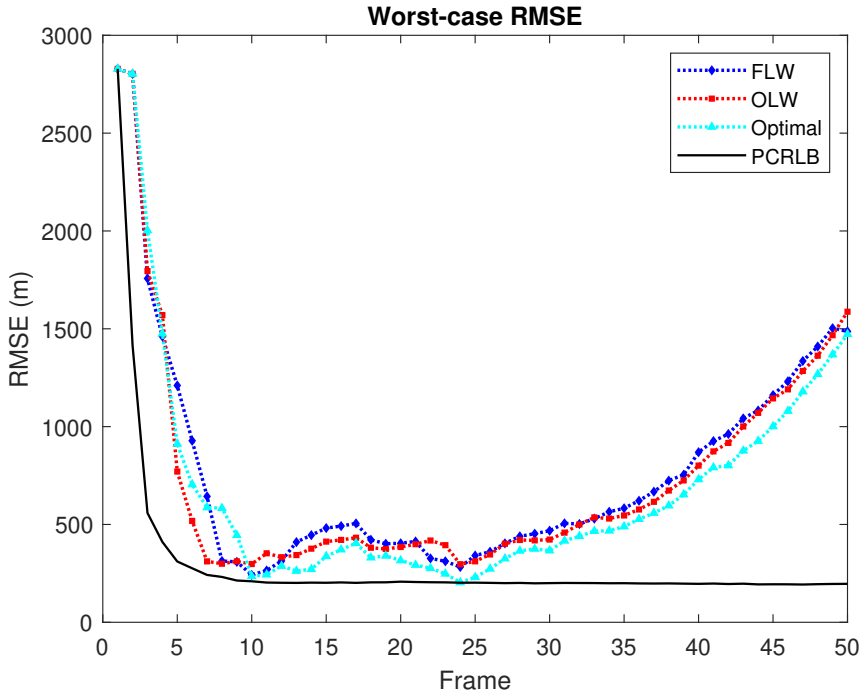

Figure 3.12: Worst-case RMSE for the proposed beam scheduler strategies

Note that the number of radars is less than the number of targets, so there will be targets whose state and covariance are only predicted by the tracker but not updated

Table 3.4: Worst-case RMSE of Target Position Estimation

Time Index	Worst-case Position RMSE (m)		
	FLW	OLW	Optimal
5	1210.3	**508.2**	961.9
15	481.5	392.3	**387.4**
25	341.1	257.2	**235.5**

due to missed measurements. At time $k = 1$, since target 2 has the least PCRLB and therefore, is not being tracked, its state will only be predicted and the error from the motion model is preserved, so the worst-case estimation error remains high.

The RMSE of target 3 is presented in Fig.3.13, which shows a better convergence than the worst-case RMSE.

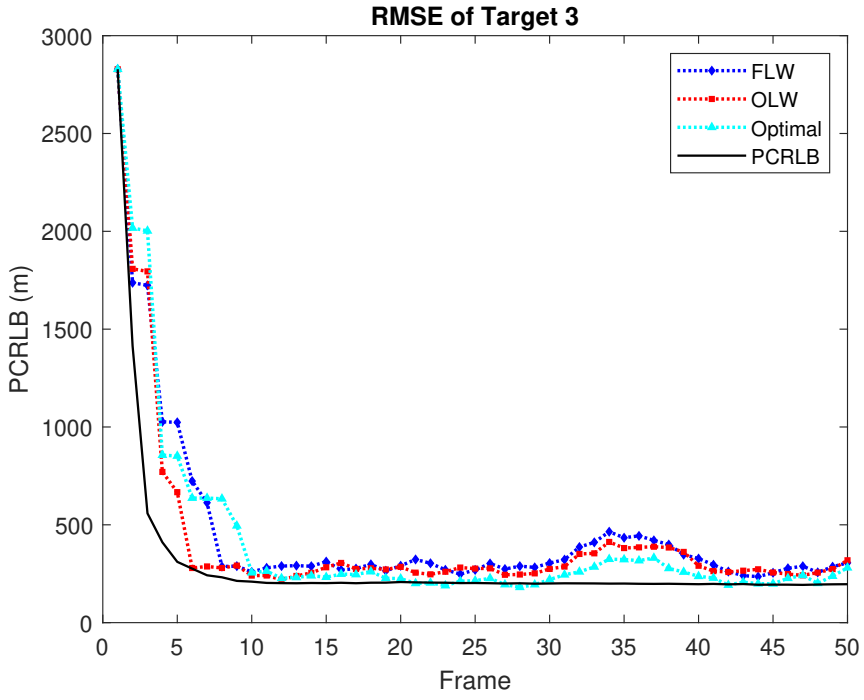

Figure 3.13: The RMSE for target 3 using the developed beam scheduling strategies

3.4.3 Evaluation of algorithm speed

To evaluate the efficiency of the proposed algorithms, each algorithm's run time was recorded. All simulations are conducted using MATLAB R2019a on a laptop with a Core™ i5 2.6 GHz CPU and 8 GB RAM.

Table 3.5: Average Time Cost

Strategy	FLW	OLW	Optimal
Time spent per frame (s)	0.0042	1.2181	0.5462

Table 3.5 gives the average time cost of the three algorithms. Due to the hierarchical structure of HGA, the open-loop line wipe beam scheduling strategy takes a considerably longer time. It can be fastened by decreasing the population size and the maximum number of generations. Furthermore, intelligent operations can be utilized to reduce the time of deficient evolution, e.g., eliminating groups with low average fitness.

Though the EPCRLB-based optimal solution takes less time than the open-loop linear wipe strategy, its computational cost is high compared with real-time requirements. In practice, sub-optimal strategies may be adopted to save time and budget.

3.5 Conclusion

An adaptive beam scheduling problem for cooperative phased array radars with pencil beams was presented and addressed. Traditional phased array radar schedulers have challenges with pencil-beams as they do not cover the area of interest due to their narrow beamwidth. Therefore, a more precise beam scheduler that controls the steering direction and operation time of the radar beam needs to be developed. In

this paper, the problems of tracking with pencil-beam and of beam scheduling were presented and three beam scheduling strategies namely fixed linear wipe, open-loop liner wipe and EPCRLB-based optimal solution were developed. The concept of expected PCRLB was proposed and the predictive EPCRLB was adopted as a criterion to minimize. Numerical simulations were presented along with results that showed the EPCRLB-based optimal solution beam scheduler achieved a lower worst-case PCRLB and a smaller estimation error for the tracker working with it.

This work can be further extended by considering the following issues. First, the scheduling of wide fan-beams can be jointly considered by adding the performance metrics of target detection into the optimization. More mission and corresponding beam types can be incorporated in the future. Second, the simultaneous multibeam (SM) working mode of PARs where a PAR can simultaneously launch multiple beams could be explored. In this working mode, the issue of power allocation that determines how much power a radar assigns to each beam can be incorporated into the resource management problem. In parallel, the duration of each beam can also be studied to get better SNR.

Chapter 4

Joint PRF Set Selection and Waveform Design for Pulsed Doppler Radars

4.1 Introduction

4.1.1 Background and Motivation

Pulsed Doppler radar systems use a train of pulses to reject clutter returns and achieve good range and Doppler resolutions. Adaptive design of burst pulses and waveform is a fundamental component in resource management to ensure detection capability and tracking accuracy[46]. Pulsed Doppler radar systems suffer from ambiguities, blind zones, and multipaths. Typically, burst parameters can be designed to resolve range or Doppler resolution, but not both simultaneously. The strategy to transmit pulses with a set of pulse repetition frequencies (PRF) is adopted to compromise the

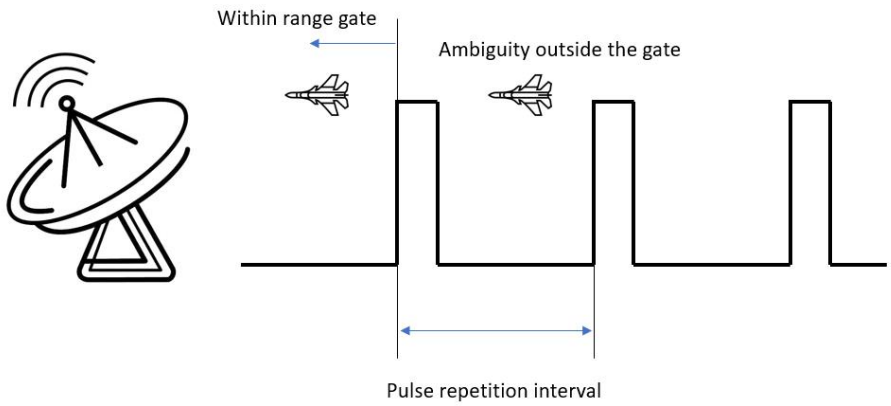

Figure 4.1: Range ambiguity in pulsed Doppler radar

drawbacks of low PRF systems and high PRF systems. With a proper selection of the PRF scheme, the blind zone rate can be significantly reduced. This problem has been examined in works [32, 31, 6, 91, 35, 3, 13, 89].

The problem of PRF set selection is typically applied to target monitoring and localization scenarios. In the context of target tracking, however, maneuvering targets make sudden and unpredictable moves. Therefore, they can fall into blind zones and the solution of finding an optimal set of PRF and generating a good blind zone map may not be favorable for the radar system. In this paper, we extend the PRF set selection problem and incorporate waveform design.

Considerable interest has been drawn to the issue of waveform selection[39, 65, 70, 44, 37, 36]. In [55], the adaptive waveform selection in a multistatic radar system is studied and the transmitted waveforms are selected from the library to minimize the tracking mean squared error. [65] implements a fractional Fourier transform on a base waveform to obtain the waveform library. A joint transmit resource management and waveform selection problem is addressed, and a fast solution based on particle swarm

optimization (PSO) is developed in [72]. Waveform selection problems are further extended by jointly considering other resource management problems such as power allocation[92] and beam assignment[94, 99].

The waveform selection issues are mathematically formulated into optimization problems, where one or multiple objective functions are minimized subject to system constraints[10]. The tracking accuracy is optimized by minimizing the posterior Cramér-Rao lower bound (PCRLB), which is defined to be the inverse of Fisher information matrix (FIM) and gives a mean squared error bound on the performance of any unbiased estimator [8, 25, 82]. The PCRLB is independent of the estimation algorithm and can be calculated recursively [86].

Genetic algorithm (GA) is a heuristic search technique inspired by the process of natural evolution, which offers fast and near-optimal solutions at a modest computational cost compared to an exhaustive search. Due to the time budget, it is more favorable for the system to obtain a suboptimal result than to wait for the global optimum. Therefore, GA is widely used in the selection of PRF scheme selection [3, 31, 89, 32] or resource management problems that are NP-hard[77, 73, 64]. Besides GA, other heuristic algorithms such as simulated annealing (SA)[2] or PSO[72] can also be used.

In this paper, two formulations and corresponding solutions are proposed. Firstly, a dual-objective problem is formulated, and the solver uses non-dominated sorting genetic algorithm II (NSGA-II) to find the Pareto optimum. Secondly, the problem is solved sequentially by obtaining a blind zone map where all targets are visible during consecutive intervals and then optimizing the waveform selection.

4.1.2 Main Contributions

This paper makes the following contributions:

1) *A joint PRF selection and waveform design (JPSSWD) problem is analyzed and formulated.* The novel problem of jointly optimizing the global detection capability and ensuring current tracking accuracy is addressed. Solutions to the problem seek to prevent target under tracking from falling into blind zones by adaptively selecting the PRF scheme and minimizing the tracking accuracy through proper waveform tailoring.

2) *Algorithms based on genetic algorithms are proposed to solve the problem in real-time.* Searching for an optimal combination of PRFs requires an enormous time, and thus, may not meet the real-time requirements. Therefore, we develop solution techniques based on GA to obtain quick solutions. Numerical results show the efficiency of the proposed strategies.

3) *A JPSSWD-based multitarget tracking framework is developed.* We develop a closed-loop signal processing framework to handle real-time tracking scenarios. An interacting multiple model (IMM) unscented Kalman filter (UKF) is used to deal with maneuvering multiple target tracking. Fig. 4.2 illustrates details of the framework.

The remainder of the paper is organized as follows. Section II gives preliminary knowledge of ambiguity, target tracking, and PCRLB. Two mathematical formulations and corresponding solution techniques are presented in Section III. Numerical simulations are demonstrated in Section IV and conclusions are given in Section V.

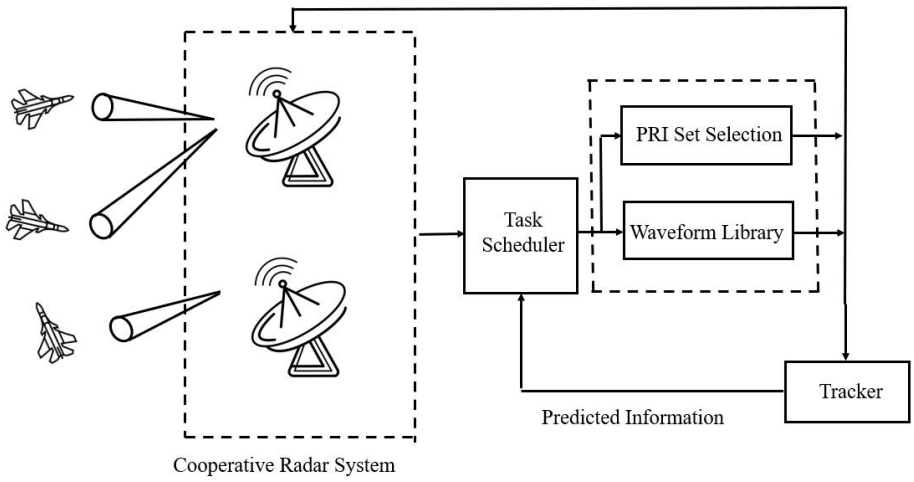

Figure 4.2: JPSSWD-based multitarget tracking framework in a cooperative radar system

4.2 Background and Problem Description

4.2.1 Ambiguities and Blind Zones

Pulsed Doppler radars have shown the capability to discriminate targets from large clutter returns by using multiple pulses. However, the issue of ambiguity arises with the use of multiple pulses. When the radar is transmitting a pulse while a target return arrives, it will fail to receive the returning signal. This is referred to as the ambiguity through eclipse, which yields the failure to detect the target's range. If the target's Doppler shift is close to a multiple of the radar's PRF, the velocity of the target will be hard to detect. The range and Doppler ambiguities result in the blind zones of a radar. If a target's range or Doppler shift falls into blind zones, it will be challenging for the radar to detect the target. Low PRF radars have an unambiguous range while having limited capacity for velocities. On the opposite, high PRF radars have clear Doppler intervals but highly ambiguous ranges, as shown in Fig.4.3.

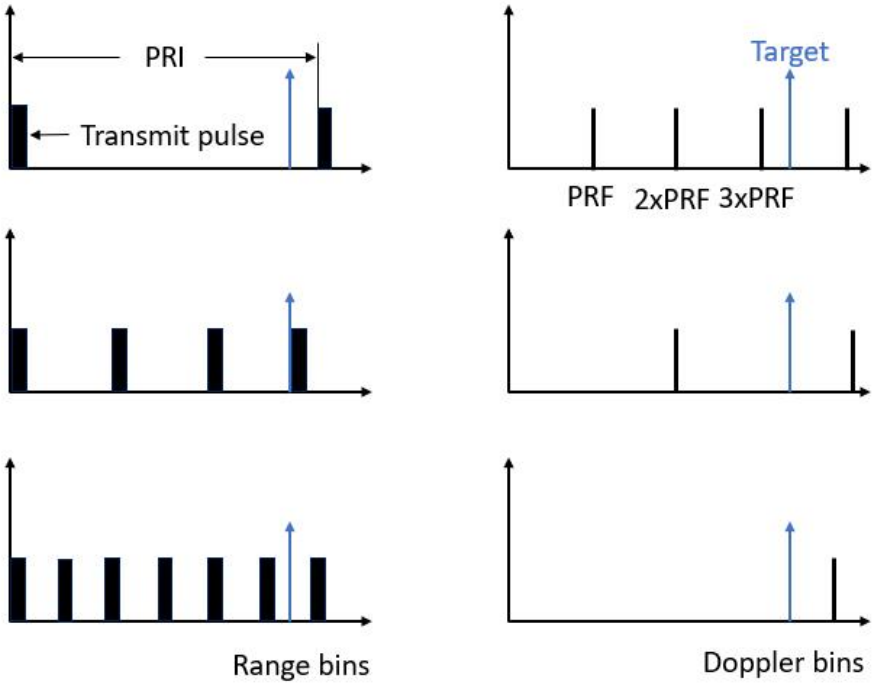

Figure 4.3: Ambiguities in pulsed Doppler radar

Generally, medium PRF radars are selected as a compromise solution to overcome the drawbacks of both low and high PRF radars. However, the ambiguities are simply confined to an acceptable level but not ideally resolved. Furthermore, the system still suffers from a number of blind zones where targets will be completely undetectable. To alleviate these problems, the radar system may operate on multiple PRFs. The radar transmits pulses with N different PRFs and a target is considered detected if it is observable by more than M PRFs, which is known as a M of N scheme. In the literature[13, 3], M and N are typically set to 3 and 8, while in the industry, they are selected to be smaller due to system constraints.

To ensure a proper PRF scheme, the decodability must be satisfied. For a M of N PRF set to be decodable, the lowest common multiple (LCM) of any set of M PRIs from N PRIs must be greater than the time delay of the maximum range of interest. Similarly, the LCM of any set of M PRFs from N PRFs must be greater than the Doppler bandwidth.

Fig.4.4 shows the blind map of a system with a single PRF and Fig.4.5 show the blind map of that with a 3 of 8 PRF set. The gray areas in Fig.4.5 are marginal detectable areas where targets are seen by exactly M PRFs. It can be seen that the detecting ability is significantly improved with a multiple PRF scheme.

4.2.2 Signal Model

Consider a distributed pulsed Doppler radar network with N spatially diverse radar nodes. The position of the nth node is denoted by (x_n, y_n). There are Q airborne targets to be tracked. The qth target is initially located at $(x_{q,1}, y_{q,1})$ with an initial velocity $(\dot{x}_{q,1}, \dot{y}_{q,1})$. At time step k, the qth target is located at $(x_{q,k}, y_{q,k})$ with velocity

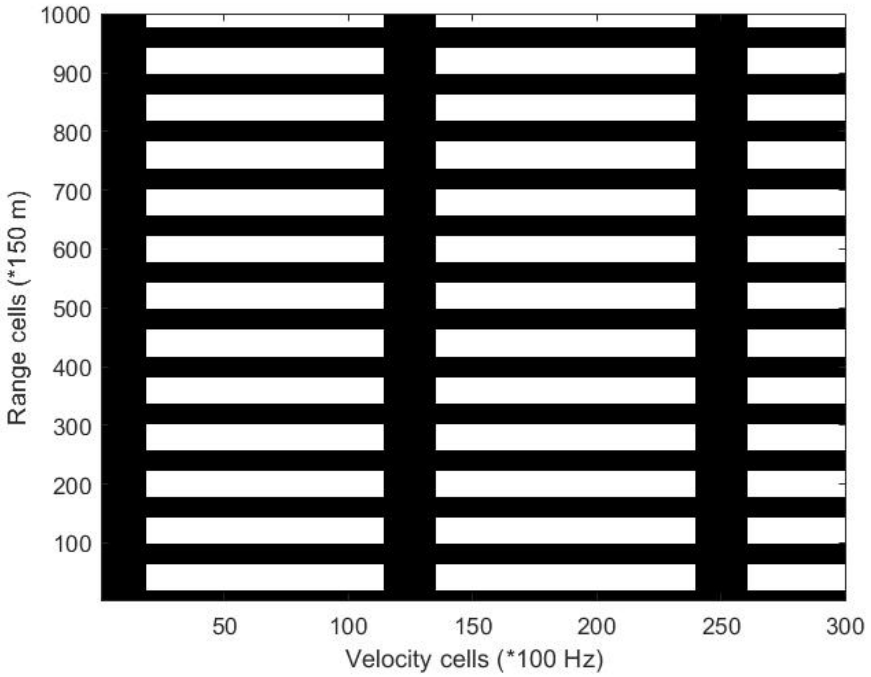

Figure 4.4: Blind map of a single PRF

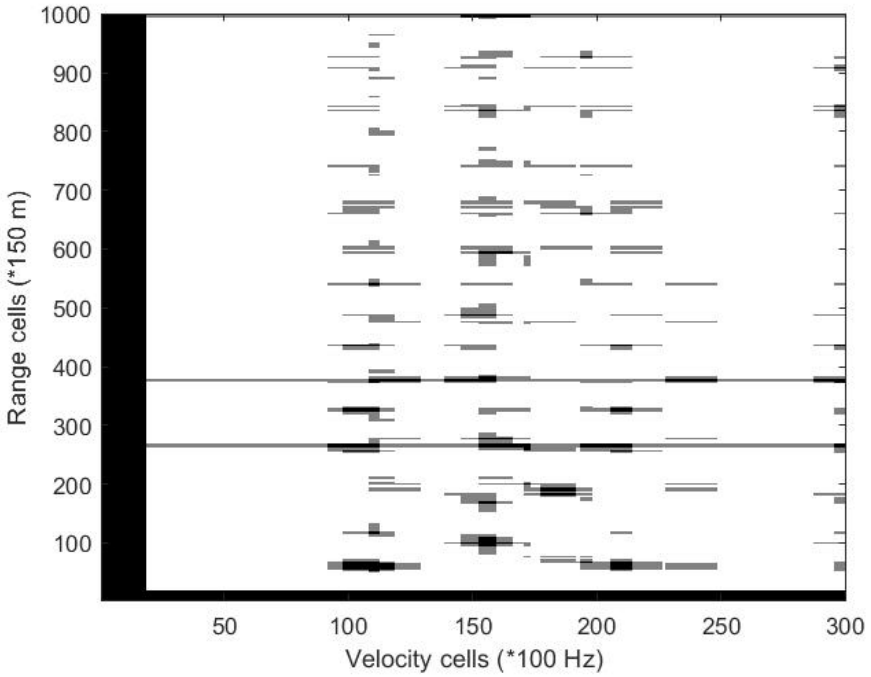

Figure 4.5: Blind map of a PRF set

$(\dot{x}_{q,k}, \dot{y}_{q,k})$.

For simplicity, the following assumptions are made.

1. Each radar node transmits a narrow-band signal to track one single target.
2. The number of radar nodes N is less than the number of targets Q, i.e., there will always be targets that are not illuminated by any radar in each time step.
3. The number of targets is known and remains constant. All tracks are already confirmed.

The transmit signal of the nth radar node is given by:

$$s_{n,k}(t) = \sqrt{P_{n,k}} E_{n,k}(t) e^{-j2\pi f_c t} \tag{4.2.1}$$

where f_c is the carrier frequency, and $P_{n,k}$ is the transmit power of radar node n at time step k.

The term $E_{n,k}(t)$ is the normalized complex envelope of the transmit signal with unit power, which can be expressed by

$$E_{n,k}(t) = \big(\frac{1}{\pi\lambda_{n,k}^2}\big)^{\frac{1}{4}} \exp\big[-\big(\frac{1}{2\lambda_{n,k}^2} - j2\pi b_{n,k}\big)t^2\big] \tag{4.2.2}$$

where $b_{n,k}$ is the the frequency modulation rate, $b_{n,k} = W_{n,k}/2T_{n,k}$, $W_{n,k}$ is the bandwidth of the transmit waveform, $T_{n,k}$ is the effective pulse length and $\lambda_{n,k}$ is the Gaussian pulse length parameter. The effective pulse length is approximated with $T_{n,k} = 7.4338\lambda_{n,k}$ [55].

The signal received by the nth receiver is an attenuated version of the transmit

signal, which is delayed by

$$\begin{aligned} r_{n,k}(t) =& h_{q,k}\sqrt{\alpha_{n,q,k}P_{n,k}}E_{n,k}(t-\tau_{n,q,k})e^{-j2\pi f_{n,q,k}t} \\ &+ \omega_{n,k}(t) \end{aligned} \tag{4.2.3}$$

The term $\alpha_{n,q}^{k} \propto 1/(R_{n,q,k})^4$ denotes the variation in the signal strength due to loss effects along the signal transmission path, where $R_{n,q,k}$ is the range from the nth radar to the qth target. $h_{q,k}$ denotes the target RCS, also referred to as reflectivity, which is a random variable. $\omega_{n,k}$ is a zero-mean complex Gaussian noise. $\tau_{n,q,k}$ and $f_{n,q,k}$ denote the time delay and Doppler shift of target q with respect to radar n, respectively.

4.2.3 Target Dynamics

Let $\mathbf{x}_q^k = [x_{q,k}, \dot{x}_{q,k}, y_{q,k}, \dot{y}_{q,k}]^T$ denote the state vector of the qth target, where $[x_{q,k}, y_{q,k}]$ and $[\dot{x}_{q,k}, \dot{y}_{q,k}]$ denote the position and velocity of the target, respectively.

The state space model that describes the qth target's motion is given by:

$$\mathbf{x}_{q,k+1} = \mathbf{F}_k\mathbf{x}_{q,k} + \mathbf{w}_{q,k} \tag{4.2.4}$$

where $\mathbf{x}_{q,k} = [x_{q,k}, y_{q,k}, \dot{x}_{q,k}, \dot{y}_{q,k}]^T$ is the column state vector of the qth target, and $[x_{q,k}, y_{q,k}]$ and $[\dot{x}_{q,k}, \dot{y}_{q,k}]$ denote the position and velocity of the target, respectively. $\mathbf{F}_k$ denotes the state transition matrix. $\mathbf{w}_{q,k}$ is the process noise assumed to be the model input to control the evolution of target state $\mathbf{x}_{q,k}$. $\mathbf{w}_k$ is the process noise that describes the inaccuracy of the motion model. It is assumed to be zero-mean

Gaussian distributed with a known covariance $\mathbf{\Gamma}_k$.

$$\mathbf{\Gamma}_k = \kappa \mathbf{I}_2 \otimes \begin{bmatrix} \frac{1}{3}T^3 & \frac{1}{2}T^2 \\ \frac{1}{2}T^2 & T \end{bmatrix} \tag{4.2.5}$$

where κ is the intensity of process noise.

In this paper, we consider two target dynamic models: constant velocity (CV) and constant turn (CT) with a known turn rate.

For the CV model, the transition matrix is given by:

$$\mathbf{F}_k = \mathbf{I}_2 \otimes \begin{bmatrix} 1 & T \\ 0 & 1 \end{bmatrix} \tag{4.2.6}$$

where $\otimes$ is the Kronecker operator, and $\mathbf{I}_2$ denotes the 2×2 identity matrix.

For the CT model, the transition matrix is given by:

$$\mathbf{F}_k = \begin{bmatrix} 1 & \frac{\sin \omega T}{\omega} & 0 & -\frac{1-\cos \omega T}{\omega} \\ 0 & \cos \omega T & 0 & -\sin \omega T \\ 0 & \frac{1-\cos \omega T}{\omega} & 1 & \frac{\sin \omega T}{\omega} \\ 0 & \sin \omega T & 0 & \cos \omega T \end{bmatrix} \tag{4.2.7}$$

4.2.4 Measurement Model

Let $\mathbf{Z}_{q,k}$ be the stacked measurements of target q from multiple radar nodes at the kth time step, it has the form $\mathbf{Z}_{q,k} = [\mathbf{z}_{1,q,k}^T, ..., \mathbf{z}_{n,q,k}^T, ..., \mathbf{z}_{N,q,k}^T]^T$, where the measurement

obtained by the nth radar $\mathbf{z}_{n,q,k}$ is given by:

$$\mathbf{z}_{n,q,k} = \begin{cases} h_n(\mathbf{x}_{q,k}) + \mathbf{v}_{n,q,k} & \text{if originated from target } q \\ \upsilon_{n,q,k} & \text{if false alarm} \end{cases} \tag{4.2.8}$$

where h_n is the nonlinear observation function. The measurements consist of three components: the range measurement $R_{n,q,k}$, the $f_{n,q,k}$ and the bearing $\theta_{n,q,k}$, i.e.,

$$h_n(\mathbf{x}_{q,k}) = [R_{n,q,k}, f_{n,q,k}, \theta_{n,q,k}]^T \tag{4.2.9}$$

$$\begin{cases} R_{n,q,k} = \sqrt{(x_{n,q,k} - x_n)^2 + (y_{n,q,k} - y_n)^2} \\ f_{n,q,k} = \frac{\dot{x}_{n,q,k}(x_{n,q,k} - x_n) + \dot{y}_{n,q,k}(y_{n,q,k} - y_n)}{R_{n,q,k}} \\ \theta_{n,q}^k = \arctan\left(\frac{y_{n,q,k} - y_n}{x_{n,q,k} - x_n}\right) \end{cases} \tag{4.2.10}$$

$\mathbf{v}_{n,q,k}$ is the measurement noise, which is assumed to be a zero-mean Gaussian random variable with covariance $\mathbf{\Sigma}_{n,q,k}$. It is assumed the observation error covariance can reach the Cramér-Rao lower bound (CRLB) for the radar estimates $\mathbf{C}_{n,k}$, given by:

$$\mathbf{C}_{n,k} = \frac{1}{\mathrm{SNR}_{n,k}} \begin{bmatrix} 2\lambda_{n,k}^2 & -4b_{n,k}\lambda_{n,k}^2 & 0 \\ -4b_{n,k}\lambda_{n,k}^2 & \frac{1}{2\pi^2\lambda_{n,k}^2} + 8b_{n,k}^2\lambda_{n,k}^2 & 0 \\ 0 & 0 & \sigma_\theta^2 \end{bmatrix} \tag{4.2.11}$$

The frequency modulate rate $b_{n,k}$ and the Gaussian pulse length parameter $\lambda_{n,k}$ constitute the waveform parameter $\mathbf{\Omega}_{n,k}$. The signal-to-noise-ratio for the nth radar at time step k $\mathrm{SNR}_{n,k}$ is a function of the radar's transmit power and dwell time and

does not depend on the waveform parameter $\mathbf{\Omega}_{n,k}$. Therefore, it is assumed to be a certain value throughout the course of this paper.

Generally, the probability of detection P_d of each target is always less than unity due to the inevitable interference. Furthermore, clusters in the surveillance area will result in false alarms, which are assumed to be a zero-mean Gaussian random variable uniformly distributed in the measurement space (within the observation volume V) with their number being a Poisson-distributed variable, given by

$$p(n_{fa}) = \frac{e^{-\lambda V}(\lambda V)^{n_{fa}}}{n_{fa}!} \tag{4.2.12}$$

where n_{fa} is the number of false alarms, λ is the spatial density, that is, the average number of false alarms within each frame.

4.2.5 FIM and PCRLB

The Cramér-Rao lower bound (CRLB), defined to be the inverse of the Fisher information matrix (FIM), provides a lower bound of the error covariance matrix of any unbiased estimator for a certain parameter. The posterior Cramér-Rao lower bound (PCRLB) gives a measure of the achievable accuracy for dynamic state estimation. Under the assumption of Gaussian measurement noise, the estimation error asymptotically approaches the PCRLB in high SNR[57]. PCRLB is often utilized as a criterion to minimize in resource management problems due to its independence in tracking algorithms. Let $\hat{\mathbf{x}_k}$ be an unbiased estimate of $\mathbf{x}_k$ based on the measurement $\mathbf{z}_k$, $\mathbf{C}_k$ be the error covariance matrix, and $\mathbf{J}(\mathbf{x}_k)$ be the FIM, we have

$$\mathbf{C}_k = \mathbb{E}[(\hat{\mathbf{x}}_k - \mathbf{x}_k)(\hat{\mathbf{x}}_k - \mathbf{x}_k)^T] \geq \mathbf{J}_(\mathbf{x}_k)^{-1} \tag{4.2.13}$$

where $\mathbb{E}$ denotes expectation operator.

The FIM can be calculated with the following recursion[86].

$$\mathbf{J}_k = \mathbf{J}_X(\mathbf{x}_k) + \mathbf{J}_Z(\mathbf{x}_k) \tag{4.2.14}$$

$\mathbf{J}_X(\mathbf{x}_k)$ and $\mathbf{J}_Z(\mathbf{x}_k)$ are referred to as the prior knowledge and the measurement contribution at time step k, respectively.

$$\begin{cases} \mathbf{J}_X(\mathbf{x}_k) = \mathbf{D}_{k-1}^{22} - \mathbf{D}_{k-1}^{21}(\mathbf{J}_k + \mathbf{D}_{k-1}^{11})^{-1}\mathbf{D}_{k-1}^{12} \\ \mathbf{J}_Z(\mathbf{x}_k) = \mathbb{E}\{-\Delta_{\mathbf{x}_k}^{\mathbf{x}_k} \ln p(\mathbf{z}_k|\mathbf{x}_k)\} \end{cases} \tag{4.2.15}$$

where

$$\begin{cases} \mathbf{D}_{k-1}^{11} = \mathbb{E}\{-\Delta_{\mathbf{x}_{k-1}}^{\mathbf{x}_{k-1}} \ln p(\mathbf{x}_k|\mathbf{x}_{k-1}\} \\ \mathbf{D}_{k-1}^{12} = \mathbb{E}\{-\Delta_{\mathbf{x}_k}^{\mathbf{x}_{k-1}} \ln p(\mathbf{x}_k|\mathbf{x}_{k-1}\} = (\mathbf{D}_{k-1}^{21})^T \\ \mathbf{D}_{k-1}^{22} = \mathbb{E}\{-\Delta_{\mathbf{x}_k}^{\mathbf{x}_k} \ln p(\mathbf{x}_k|\mathbf{x}_{k-1}\} \end{cases} \tag{4.2.16}$$

The prior information can be calculated by:

$$\mathbf{J}_X(\mathbf{x}_k) = [\mathbf{\Gamma}_{k-1} + \mathbf{F}_k\mathbf{J}(\mathbf{x}_{k-1})^{-1}\mathbf{F}_{k-1}^T]^{-1} \tag{4.2.17}$$

The measurement contribution is given by

$$\mathbf{J}_{Z_n}(\mathbf{x}_k) = \mathbb{E}\{\mathbf{H}_{q,k}^T \Sigma_{q,k}^{-1} \mathbf{H}_{q,k}\} \tag{4.2.18}$$

where $\mathbf{H}_{q,k} = [\Delta_{\mathbf{x}_q^k} h_n^T(\mathbf{x}_q^k)]^T$ is the Jacobian matrix of the measurement function $h_n(\mathbf{x}_q^k)$ with respect to the target state $\mathbf{x}_q^k$. and $\mathbb{E}$ denotes expectation with respect to the target state.

4.2.6 IMM-UKF filter

1) Unscented Kalman Filter: Kalman filter (KF) is an optimal LMSE tracking algorithm in linear systems[8]. Extended Kalman filter (EKF) and unscented Kalman filter (UKF) were developed to deal with the nonlinearity between the observation vector and the target state vector. UKF has been proven to offer better performance than EKF and, therefore, is adopted as the tracking algorithm in this paper.

The UKF uses unscented transform (UT) to approximate nonlinear transformation. The main idea of UT is to use a set of samples, referred to as sigma points σ_k^i, with corresponding weights w^i, to represent the state distribution $\mathbf{x}_k$.

When we generate a set of sigma points (typically 5) to approximate the distribution of the target's estimated state, the prediction is completed by predicting all sigma points and adding them up by weight.

$$\mathbf{x}_{k+1}^- = \sum_i w^i \cdot \mathbf{F}_k \sigma_k^i \tag{4.2.19}$$

$$P_{k+1}^- = \sum_i w^i \cdot [\mathbf{x}_{k+1}^- - \sigma_k^i] \cdot [\mathbf{x}_{k+1}^- - \sigma_k^i]^T + \mathbf{\Gamma}_k \tag{4.2.20}$$

where the superscript $-$ denotes prediction.

Similarly, the prediction of measurements is a weighted summation of each sigma point's predicted measurements:

$$\mathbf{z}_{k+1}^- = \sum_i w^i \cdot h(\sigma_k^i) \tag{4.2.21}$$

In the update step, firstly, the innovation is obtained by

$$S_{k+1} = \sum_i w^i \cdot [\mathbf{z}^-_{k+1} - \mathbf{z}_{k+1}] \cdot [\mathbf{z}^-_{k+1} - \mathbf{z}_{k+1}]^T + \mathbf{\Sigma}_{k+1} \tag{4.2.22}$$

The Kalman filter gain is given by

$$K_{k+1} = (\sum_i w^i \cdot [\mathbf{x}^-_{k+1} - \sigma^i_k] \cdot [\mathbf{z}^-_{k+1} - \mathbf{z}_{k+1}]^T) \cdot S^{-1}_{k+1} \tag{4.2.23}$$

Finally, filter gain is used to update the predicted state and covariance.

$$\hat{\mathbf{x}}_{k+1} = \mathbf{x}^-_{k+1} + K_{k+1} \cdot [\mathbf{z}^-_{k+1} - \mathbf{z}_{k+1}] \tag{4.2.24}$$

$$\hat{P}_{k+1} = P^-_{k+1} - K_{k+1} \cdot S_{k+1} \cdot K^T_{k+1} \tag{4.2.25}$$

2) Interacting Multiple Model: The UKF can only handle a single motion model. In our assumed scenario where a target has multiple dynamic models, the interacting multiple model (IMM) algorithm is used.

The core idea of IMM is to run multiple tracking filters in parallel, where each filter is responsible for a specific motion model, and the final estimate of state and covariance is a weighted combination of the estimates from individual local filters. i.e.,

$$\hat{\mathbf{x}}_k = \sum_{j=1}^{J} \mu^{j-}_k \hat{\mathbf{x}}^j_k \tag{4.2.26}$$

$$\hat{P}_k = \sum_{j=1}^{J} \mu^{j-}_k \{\hat{P}^j_k + [\hat{\mathbf{x}}_k - \hat{\mathbf{x}}^j_k] \cdot [\hat{\mathbf{x}}_k - \hat{\mathbf{x}}^j_k]^T\} \tag{4.2.27}$$

where J is the number of motion models, j is the model index and μ_k^{j-} is the model probability.

3. Cooperative Multitarget Tracking: In this paper, we adopt a cooperative tracking framework instead of independent tracking where tracks of a target are initialized and maintained separately by multiple radar nodes.

In a cooperative tracking framework, only one single track is maintained for each target. If there is more than one detection from different radars (or from false alarms), a detection-to-track data association is performed[52] to decide which measurement the system will adopt and then pass to the filter. Probabilistic data association (PDA) is used if multiple detections occur.

A target may receive no measurement at a time step due to one or more of the following reasons: (1) the target falls into the blind zone; (2) the radar's imperfect detection due to interference; (3) the target is not assigned to any radar nodes, the reader is reminded that it is assumed that number of radars is smaller than the number of targets. When a target has no measurement in a tracking interval, the tracker will simply predict the target's state and covariance and use them as the filter output. For more information about IMM, UKF, and PDA, the reader is referred to [8].

4.3 JPSSWD Strategies

Mathematically speaking, the JPSSWD problem can be formulated as a bi-objective optimization problem subject to several system constraints. At every time step k, optimization will be made to determine the selection of the PRF scheme τ_k, the task assignment matrix U_k, and the waveform parameter of all radar nodes $\mathbf{\Omega}_k =$

$[\mathbf{\Omega}_{1,k}, \mathbf{\Omega}_{2,k}, ..., \mathbf{\Omega}_{n,k}]$.

U_k is the radar-to-target assignment matrix, such that

$$U_k = \begin{bmatrix} u_{11} & & u_{1Q} \\ & \ddots & \\ u_{N1} & & u_{NQ} \end{bmatrix}_{N \times Q} \tag{4.3.1}$$

where $u_{n,q}$ takes value 1 if the qth target is assigned to the nth radar and 0 otherwise. We assumed every radar would be assigned to only one tracking task, hence, U_k satisfies $\sum_{n \in R} u_{n,q} = 1$.

4.3.1 Objective

The JPSSWD problem aims to jointly optimize the overall detection ability and the tracking accuracy. The metric for the detection ability is the total blind rate, which is a function of the PRF scheme only, denoted as $\mathcal{F}_1(\tau_k)$. The metric for the tracking accuracy is the worst-case PCRLB, which is a function of the task assignment scheme and the waveform parameter, denoted as $\mathcal{F}_2(\tau_k, U_k, \mathbf{\Omega}_k)$. Note that the PCRLB is dependent on the blind zone map of the radar. For targets in the areas where the radar is blind due to its specific PRF scheme, no information will be obtained. Therefore, $\mathcal{F}_2$ is also dependent on the PRF scheme τ_k.

$\mathcal{F}_1$ is calculated after the blind zone map is generated based on a given PRF scheme[13, 3].

As previously stated in **??**, PCRLB gives a theoretically achievable lower optimum for any unbiased estimator. Therefore, we adopt PCRLB as the criterion to minimize. In the assumed scenario where the number of radar nodes is smaller than the number

of targets to be tracked, we use worst-case PCRLB as an objective.

$$\mathcal{F}_2 = \max\ (\mathbf{J}_{q,k})^{-1} \tag{4.3.2}$$

where $\mathbf{J}_{q,k}$ is the predicted FIM of the qth target.

Since the targets have different motion models, the predicted FIM of a target is calculated as follows[8]:

$$\mathbf{J}_{q,k} = \sum_{j=1}^{J} \mu_k^{j-} \mathbf{J}_X^j + \mathbf{J}_Z \tag{4.3.3}$$

where μ_k^{j-} is the predicted probability of motion model j at time step k, and $\mathbf{J}_X^j$ is the prior information related with the jth model.

Remark 1: The calculation of the measurement contribution (4.2.18) requires an expectation operation and is computationally expensive. A general approach to handle this is to approximate the measurement contribution using the Jacobian evaluated with the predicted state estimation.

$$\mathbf{J}_Z(\mathbf{x}_k) = \{\mathbf{H}_{q,k}^T \Sigma_{q,k}^{-1} \mathbf{H}_{q,k}\}\Big|_{\mathbf{x}_{k|k-1}} \tag{4.3.4}$$

Remark 2: PCRLB is a matrix whose diagonal elements give the optimally achievable lower bounds for the variances on the estimations of the target's position and velocity in x and y coordinates. Generally, as adopted in this paper, we utilize $\sqrt{C_k(1,1) + C_k(3,3)}$ as a scalar metric to evaluate PCRLB, where $C_k(1,1)$ and $C_k(3,3)$ denote the first and third elements on the diagonal of the PCRLB, which represent the lower bounds on the variances of the target's estimated positions on x and y coordinates, respectively. Some papers use the trace of PCRLB matrices as a scalar

metric, which is also reasonable. The lower bounds on the variances of the target's estimated velocities are neglected in this paper since they are generally much smaller than those of estimated positions.

4.3.2 Constraints

The optimization of radar parameter configurations is restricted by system configurations. In the JPSSWD problem, both PRF set and waveform parameters are chosen from given libraries.

1) *Constraints on PRF scheme:* The PRF scheme τ_k is a set of M frequencies of the transmitted signal. Each of them is constrained by a minimum frequency f_{min} and a maximum frequency f_{max}.

$$\tau_k = f_1, f_2, ..., f_M, \;\; f_i \in (f_{min}, f_{max}), \;\; i = 1, 2, ..., M \tag{4.3.5}$$

Note the decodability of the PRF scheme needs to be satisfied for the range and Doppler ambiguities to be resolved [13, 3], as aforementioned.

2) *Constraints on waveform parameter:* The waveform parameter of the nth radar node $\Omega_{n,k}$ consists of the frequency modulation rate $b_{n,k}$ and the Gaussian pulse length $\lambda_{n,k}$, each of them must be chosen from their specific range, i.e.,

$$b_{n,k} \in (b_{min}, b_{max}), \;\; \lambda_{n,k} \in (\lambda_{min}, \lambda_{max}) \tag{4.3.6}$$

3) *Constraints on target assignment:* Each radar node can only track one target at a time. We define a binary assignment variable $u_{n,q}$ to represent if target q is tracked

by radar n.

$$u_{n,q} = \begin{cases} 1 & \text{if target } q\text{assigned to radar } n \\ 0 & \text{otherwise} \end{cases} \tag{4.3.7}$$

It is assumed that the number of radars is smaller than the number of targets. Therefore, for the radar-to-target assignment matrix (4.3.1), each row adds up to 1.

$$\sum_{q=1}^{Q} u_{n,q} = 1, \ n = 1, 2, ..., N \tag{4.3.8}$$

4.3.3 Strategy 1: Bi-Objective Pareto Optimization

The JPSSWD problem is formulated below as a bi-objective optimization problem that seeks to jointly optimize the total blind rate and tracking accuracy.

$$\begin{aligned} \min \quad & \mathbb{F}(\tau_k, U_k, \mathbf{\Omega}_k) =< \mathcal{F}_1(\tau_k), \mathcal{F}_2(\tau_k, U_k, \mathbf{\Omega}_k) > \\ \text{s.t.} \quad & u_{n,q} \in \{0, 1\} \\ & \sum_{q=1}^{Q} u_{n,q} = 1 \leq M \\ & f_i \in (f_{min}, f_{max}) \\ & b_{n,k} \in (b_{min}, b_{max}) \\ & \lambda_{n,k} \in (\lambda_{min}, \lambda_{max}) \end{aligned} \tag{4.3.9}$$

We can see that each frequency in the PRF scheme and waveform parameters are chosen from continuous ranges while the task assignment variables are binary.

Therefore, the problem (4.3.9) is a mixed-integer nonlinear programming (MINLP) problem, which is typically NP-hard and requires enormous search trees.

To ensure the problem is solved in real-time, it is favorable to obtain a near-optimal solution quickly than to wait for the global optimum. In this paper, we adopt the genetic algorithm (GA) as a fast and effective heuristic approach. GA was developed to solve problems with a single objective. To handle the bi-objective problem, the non-dominated sorting genetic algorithm II (NSGA-II) is used.

GA is inspired by the process of natural selection and the survival of the fittest candidates. Candidate solutions are called individuals, and the set of individuals is referred to as the population. Each individual is described by a chromosome, which consists of several sections called genes. Through decoding, a string of genes represents a specific decision variable in the problem. The fitness of each individual is evaluated by a fitness function. In this bi-objective problem, the fitness functions are $\mathcal{F}_1$ and $\mathcal{F}_2$.

Remark 3: The encoding method that deciphers genes into decision variables needs to be selected properly. In this paper, we use real number encoding where a single gene, which is a real number, represents a decision variable, e.g., a PRF is encoded into a random number between 0 and 1. Gray encoding that represents a variable with a string of binary genes can also be used. This method sacrifices efficiency for local search capability since the randomness introduced during evolution is smaller due to the long length of chromosomes.

The parallel searches performed among all individuals are called generations. In each generation, three operations that mimic natural evolution are performed: selection, crossover, and mutation.

The fitness function is evaluated in every generation. The constraints (4.3.5), (4.3.6) and (4.3.8) are automatically satisfied during the generation of chromosomes.

The selection operation chooses individuals with high fitness values and copies them into the next generation, while those with low fitness will be eliminated. Roulette wheel and tournament schemes are the most used strategies for selection [64, 56]. In this paper, a binary tournament selection is adopted.

The crossover operation exchanges traits of two individuals referred to as parent individuals. A random locus is selected, and the subsequences before and after that locus are exchanged between two chromosomes. Crossover is performed with a probability P_c, i.e., a fraction P_c of the new generation is bred by crossover.

Each gene has a probability of P_m to mutate. In the mutation operation, binary variables are flipped and continuous variables are replaced by a random value.

Elitism is adopted to preserve individuals with high fitness values. After the selection operation, several highly fitted individuals will be directly to the next generation without participating in the crossover and mutation operations.

The traditional GA, however, only applies to single-objective problems. In a multi-objective case, an individual has multiple fitness functions. If all the fitness values of individual a are greater than b, then a is said to be dominated by b, i.e., a is completely inferior to b. The purpose of multi-objective optimization is to find a curve, referred to as the Pareto optimal front, where all the points dominate any other points in the solution space.

To handle the multi-objective problem, a non-dominated sorting GA-II (NSGA-II) [14] was developed. Each chromosome has two more attributes: non-dominated rank and crowding distance. The non-dominated rank gives the level of domination of the

individual. Individuals from lower non-dominated ranks dominate those from higher ranks. Crowding distance describes the similarity of a certain individual with others from the same non-dominated rank. Individuals with higher crowding distances are clustered and generally more optimal.

In NSGA-II, the normal selection operation is advanced to non-dominated selection. At first, individuals are sorted into different non-dominated ranks by evaluating whether they are dominated by other individuals in the population. Until all individuals are ranked, then their crowding distances are calculated. Fig.4.6 shows the flow chart of the NSGA-II algorithm.

4.3.4 Strategy 2: Two-Step Solution Methodology

Although the Pareto optimum obtained previously remains a feasible solution in general scenarios, the issue of blind zones still exists. In a multi-radar system, a radar node may optimally configure its PRF scheme by ignoring targets that are currently tracked by other nodes, which may result in those targets falling into blind zones. As aforementioned, the main focus of this paper is to maintain the system's high tracking accuracy while avoiding the blindness of current targets. Therefore, in this subsection, we give priority to the detectability of targets and formulate the optimization into a two-step problem.

1. Configure the PRF scheme and generate the blind map: In this step, we solve the problem of PRF selection with GA. The fitness function is given by

$$\min \quad \mathbb{F}(\tau_k) = \mathcal{F}_1(\tau_k) + \mathcal{P}(\tau_k) \tag{4.3.10}$$

where $\mathcal{P}(\tau_k)$ is a penalty function, which takes value 0 if all targets are visible to all

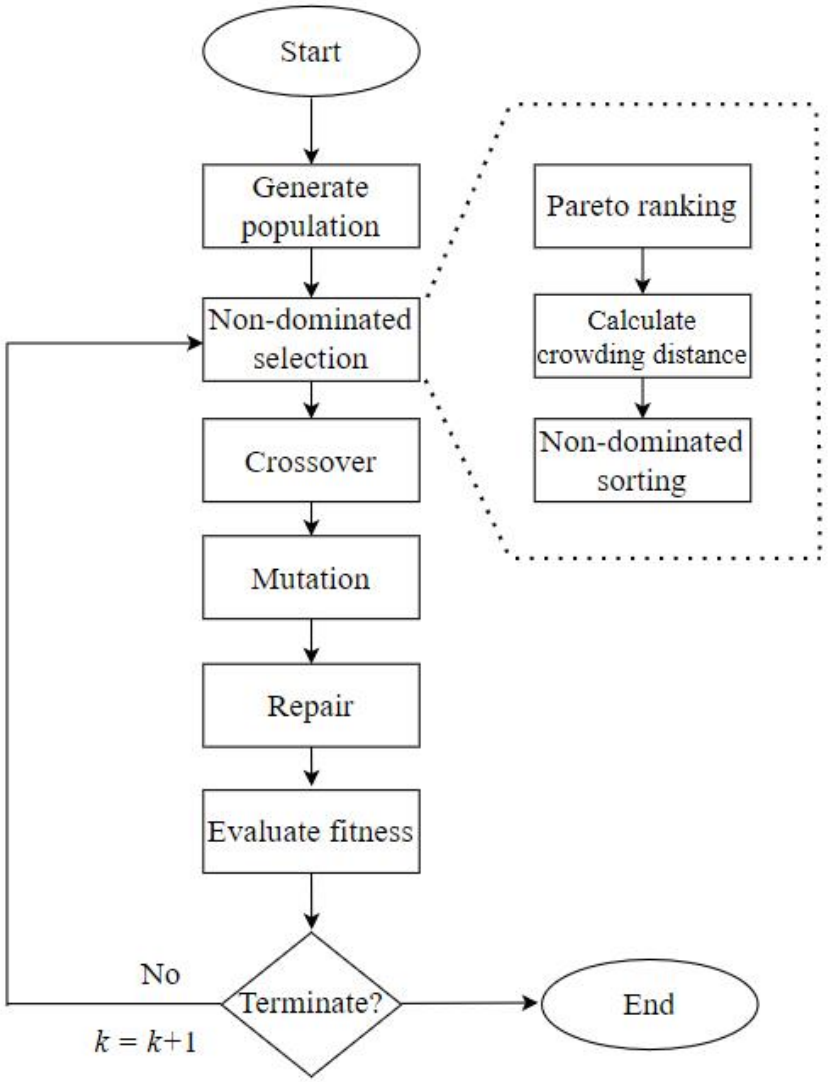

Figure 4.6: Block diagram of the NSGA-II algorithm

radars, and grows large quickly when a radar's blind zone approaches any target's existence region (TER).

2. Waveform selection: Solve the following waveform selection problem:

$$\min \quad \mathbb{F}(\tau_k, U_k, \mathbf{\Omega}_k) = \mathcal{F}_2(\tau_k, U_k, \mathbf{\Omega}_k) \tag{4.3.11}$$

The solution is obtained with a grid search over the variable space [55]. This approach is computationally cheaper than gradient-based methods [75].

The two-step methodology is referred to as genetic algorithm followed by grid search (GA-GS). A diagram is presented as Fig.4.7, and a pseudo-code is given in Algorithm.3. Note the time index k is omitted in the algorithm section.

Algorithm 3 Two-Step GA-GS Algorithm

Input:

Estimates of all targets $\hat{\mathbf{x}}_q$, $\hat{P}_q$. System configuration parameters, Maximum iteration $i_{\max}$

Output:

PRF scheme τ, Task assignment matrix U, Waveform parameter $\mathbf{\Omega} = b, \lambda$

Generate random population representing the PRF scheme
Evaluate individual fitness and selection
while $i < i_{\max}$ **do**
    Crossover
    Mutation
    Selection by fitness value
end while
Obtain τ and generate the blind map
Enumerate all possible task assignment schemes and form a set **U**
for Each U in **U do**
    Identify a search direction in the solution space (b, λ) in which $\mathcal{F}_2$ descends most quickly
    Linearly search until converged
end for

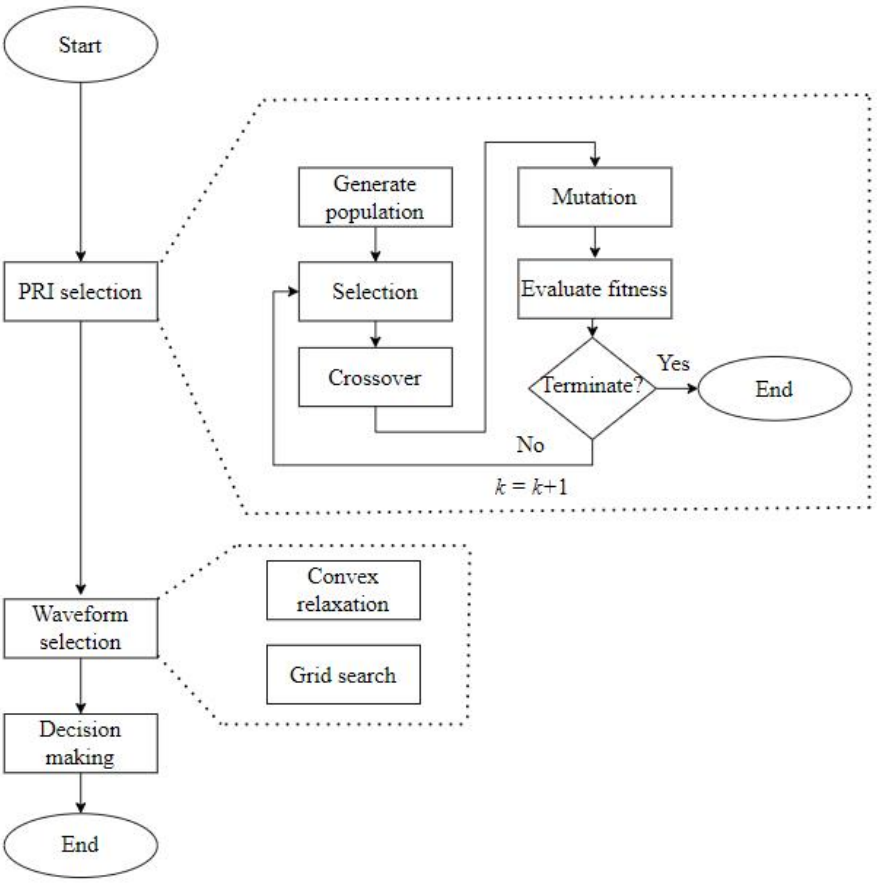

Figure 4.7: Block diagram of the GA-GS algorithm

4.4 Simulation

In this section, numerical experiments are conducted to demonstrate the performance of the proposed strategies and compare them against other simple strategies. Assume a pulsed Doppler radar system with $N = 2$ radar nodes is used to track $Q = 4$ airborne targets. The radar nodes are located at $(-10, 5)$ km and $(5, -10)$ km. We track the targets for 50 frames with the time interval $\Delta T = 1$s. The targets' motions are modeled by two dynamic models: the constant velocity (CV) model and the constant turn (CT) model with the turn rate known. Each target will perform two turning maneuvers during the surveillance period. The detailed information of targets is provided in Table 4.1 and their trajectories are shown in Fig.4.8.

Table 4.1: Initial Target States

Target Index	1	2	3	4
Position (km)	(20,25)	(-20,15)	(-15,-30)	(25,-20)
Velocity (m/s)	(-200,-250)	(300,0)	(-200,-300)	(250,-250)
Turning Interval 1 (s)	(10,20)	(5,20)	(10,15)	(5,20)
Turn Rate 1(°)	3	4	-4	-6
Turning Interval 2 (s)	(35,45)	(25,35)	(30,45)	(40,50)
Turn Rate 2(°)	-3	2	5	-1

A 2 of 6 PRF scheme is to be determined. The 6 PRIs are chosen from the interval (50,100) μs. The Gaussian pulse length parameter is chosen from the interval (10,100) μs. The bandwidth is chosen from the interval (0.1,1) MHz.

When selecting the PRF scheme and generating the blind zone map, we use the radar parameters, e.g., bin size and blind range due to eclipsing, etc., as in [3].

In the GA method, the number of population is 101. The probabilities of crossover $P_c = 0.6$ and the probability of mutation $P_m = 0.1$. The maximum generation is 30.

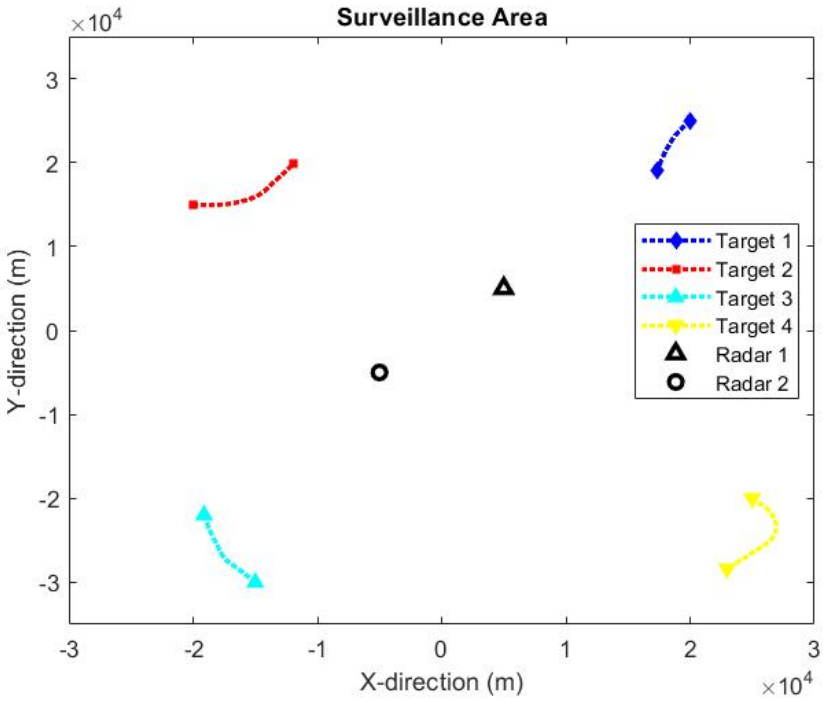

Figure 4.8: Layout of target trajectories and radar deployment

Table 4.2: Worst-case PCRLB (m)

Frame	2	3	4	5	6	7
NSGA-II	47.4	45.4	40.1	39.7	40.8	43.2
GA-GS	40.9	34.3	29.8	26.5	28.8	31.3
FPS	633.5	633.3	632.9	633.0	47.6	43.4
FW	1792.9	1414.2	1414.2	1266.2	641.7	106.9

The population stops evolving if no improvement in individual fitness is found within the next five generations.

The two proposed strategies, NSGA-II and GA-GS, and compared with the following two simple strategies:

1.Fixed PRF Scheme (FPS): When the surveillance starts, the system optimizes the PRF scheme τ_1 to minimize the total blind rate. The system will keep using this PRF scheme throughout the tracking process, whether or not any target falls into the blind zone. Each time step, the system will optimize the waveform parameter $\mathbf{\Omega_k}$ to minimize the worst-case PCRLB.

2.Fixed Waveform Parameter (FW): Every radar selects an optimal waveform parameter from the library and uses it throughout the surveillance. Each time step, the system will adapt the PRF scheme accordingly by preventing targets from falling into blind zones.

All the results are averaged over 100 Monte Carlo runs.

4.4.1 Performance of Different JPSSWD Strategies

The worst-case PCRLB obtained by four strategies is shown in Fig.4.9. Table 4.2 gives selected results from intervals 2 to 7.

It can be seen that the two proposed algorithms offer better performance than the

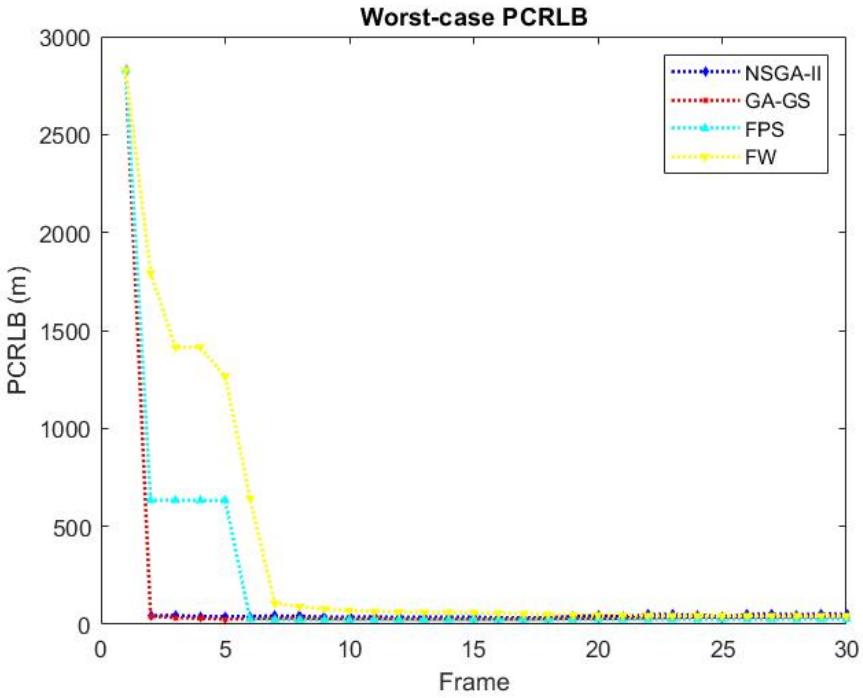

Figure 4.9: Worst-case PCRLB obtained with different strategies

Table 4.3: Blind zone rate

Strategy	NSGA-II	GA-GS	FPS	FW
Blind zone rate (%)	13.41	14.08	13.09	13.67

other two simple strategies. It is noteworthy that the PCRLBs obtained with the FW strategy remain relatively high, especially in the first 10 intervals. That is because the FW does not optimize waveform parameters and uses the same configuration throughout the entire surveillance, which yields the impact of waveform optimization in the context of target tracking.

Table 4.3 gives the average blind zone rate during the 30 tracking intervals and Table 4.4 gives the average tracking lost. Note that only missed detections due to imperfect measurement or blind zones are counted as lost track; those that result from task assignment are not counted. For example, if target 1 is not assigned to any radar nodes at time step 2, then it's not a lost track; target 3, however, is tracked by radar 1, but falls into its blind zone, and thus no measurement is obtained, then target 3 is a lost track at that time step.

Results show that the GA-GS strategy has slightly larger blind zone rates than the others, but has a significantly reduced tracking loss. That's because the GA-GS adds a large penalty value to the objective if any target falls into the blind zone. The GA-GS strategy successfully avoids tracking loss due to radar blindness, at a small cost of global blind rate. The FPS strategy has the lowest blind rate because it selects the optimal PRF scheme at the beginning of the surveillance and does not adapt accordingly. Its high tracking loss rate indicates it is not a feasible strategy in target tracking.

Table 4.4: Track lost

Strategy	NSGA-II	GA-GS	FPS	FW
Track lost (%)	31.33	19.08	38.67	37.33

$$\mathrm{RMSE}_k = \left[\frac{1}{N_{MC}} \sqrt{\sum_{j=1}^{N_{MC}} \max_q \left[\left(x_q^k - \hat{x}_q^{k,j} \right)^2 + \left(y_q^k - \hat{y}_q^{k,j} \right)^2 \right]} \right] \tag{4.4.1}$$

4.4.2 Evaluation of the IMM-UKF Tracker

The result of the optimization problem only gives a theoretically achievable optimum. In practice, however, the actual tracking accuracy is more important to the system. Therefore, the tracking performance of the IMM-UKF is compared with different JPSSWD strategies applied.

The performance of the multitarget tracker is evaluated by the worst-case root mean squared error (RMSE).

The worst-case RMSE obtained with different JPSSWD strategies are shown in Fig.4.10 and the RMSE values at selected time steps are given in Table 4.5.

It can be seen that, consistent with the theoretical PCRLB value, systems with relatively lower PCRLB offer smaller RMSE and, hence, better tracking accuracy.

There are increments in RMSE during the initial few time intervals. That is because the number of radars is smaller than the number of targets and there are always targets that are not being tracked. The state and covariance of those targets are simply predicted and the errors accumulate due to the noise of their motion models. Since we use worst-case RMSE as a performance metric, the increments come from those targets that are not tracked.

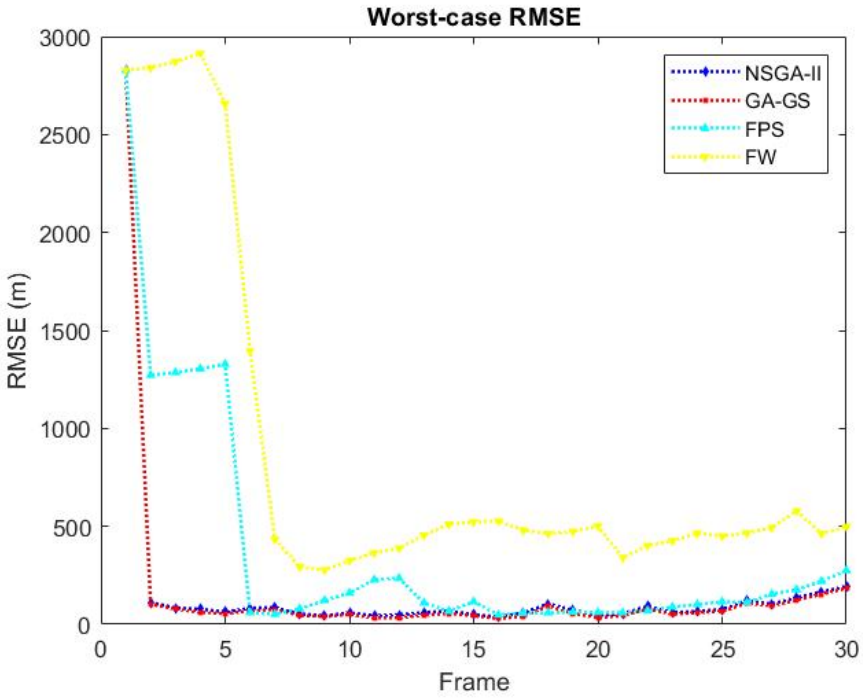

Figure 4.10: Worst-case RMSE obtained with different strategies

Table 4.5: Worst-case RMSE (m)

Frame	2	3	4	5	6	7
NSGA-II	177.8	149.2	52.5	46.2	51.9	48.1
GA-GS	103.1	77.5	61.7	55.3	68.2	76.7
FPS	1271.5	1285.5	1304.4	1327.6	60.5	51.5
FW	2841.2	2871.5	2914.7	1396.4	432.9	293.2

4.5 Conclusion

A joint PRF selection and waveform design problem for cooperative pulsed Doppler radars was addressed. The primary objective of the problem is to jointly maintain a high tracking accuracy and high detection ability by simultaneously optimizing several radar burst parameters, including PRF scheme, waveform bandwidth, and pulse width. Two different formulations and corresponding solutions are proposed. The bi-objective formulation is solved by an NSGA-II and the two-step formulation is solved by a GA-GS algorithm. Numerical results illustrate the effectiveness of the proposed strategies.

It is shown that genetic algorithms and methods based on it offer quick and feasible solutions for NP-hard problems.

Chapter 5

Conclusions and Future Works

5.1 Conclusions

PCRLB-based resource management algorithms for multisensor-multitarget tracking were studied in this thesis. PCRLB, which gives a theoretically achievable lower bound on the mean squared error for any unbiased estimator, is used as the performance metric to minimize in the context of multisensor-multitarget tracking.

First, a joint path planning and power allocation in a multistatic radar system is addressed. The coordination and management of both receivers and transmitters over a finite time horizon are considered and formulated into a weighted-sum optimization problem. A modified GA with a custom pre-selection operator is used to solve the nonconvex problem. The pre-selection operator can improve the distribution of the population and accelerate the algorithm.

Next, an adaptive beam scheduling problem for accurate tracking with pencil-beams is studied. Pencil-beams, with narrow beamwidth and concentrated power, offer efficient high-precision tracking performance but can cause partial observations.

The concept of EPCRLB is proposed and used as a criterion to optimize. An open-loop linear wipe strategy that uses PCRLB as the criterion and the optimal strategy that uses EPCRLB are proposed and compared. A HGA is used as part of the open-loop linear wipe beam scheduler to solve the optimization problem. Results show that both strategies offer better performance but the optimal scheduler, which takes advantage of the EPCRLB to guide the steering of beams, is a quicker and more efficient strategy.

Finally, a joint PRF set selection and waveform design problem is discussed. To resolve range and Doppler ambiguities and avoid radar blindness, two formulations and corresponding solution methodologies are developed. Numerical simulations are conducted to illustrate the performance and advantages of the proposed strategies.

5.2 Future Works

In the research of radar resource management, there are always more aspects to explore. Integrated and comprehensive resource management in the context of target tracking and detection has been a trend in any resource-aware radar system. For future research, this thesis can be extended in the following ways:

1. Detection capability enhancement: This thesis focuses on the scenario of target tracking, while target detection is also an important problem to address [52, 15]. The mathematical models of the relations between target detection ability and radar parameters or resources can be explored in depth. The performance metrics for detection can be utilized alone, or jointly considered with metrics for target tracking to formulate a multi-objective optimization problem. It is a

prospective fashion to extend the research in Chapter 3 by considering target detection with fan-beams.

2. Resource management in multi-functional radar: Phased array radars have shown potential in performing various kinds of tasks [49, 50] and related resource management problems are worth addressing. Research can be continued for radar systems that execute missions of different priorities and/or types. Task prioritization or scheduling can also be incorporated into these resource management problems.

3. Comprehensive burst parameter design and beamforming: In Chapter 4, as in the literature, only limited types of waveform parameters are studied and then optimized to improve system performance [55, 39, 44]. More detailed and more accurate mathematical descriptions between waveform parameters and system performance metrics can be studied, and hence, used to support more comprehensive and effective resource management optimizations.

Bibliography

[1] C. W. Ahn and R. S. Ramakrishna. Elitism-based compact genetic algorithms. *IEEE Transactions on Evolutionary Computation*, 7(4):367–385, 2003.

[2] S. Ahn, H. Lee, and B. Jung. Medium prf set selection for pulsed doppler radars using simulated annealing. In *2011 IEEE RadarCon (RADAR)*, pages 090–094. IEEE, 2011.

[3] C. M. Alabaster, E. J. Hughes, and J. H. Matthew. Medium PRF radar PRF selection using evolutionary algorithms. *IEEE Transactions on Aerospace and Electronic Systems*, 39(3):990–1001, 2003.

[4] G. Alirezaei, M. Reyer, and R. Mathar. Optimum power allocation in sensor networks for passive radar applications. *IEEE Transactions on Wireless Communications*, 13(6):3222–3231, 2014.

[5] M. S. Arulampalam, S. Maskell, N. Gordon, and T. Clapp. A tutorial on particle filters for online nonlinear/non-Gaussian Bayesian tracking. *IEEE Transactions on Signal Processing*, 50(2):174–188, 2002.

[6] J. Bae and N. A. Goodman. Adaptive PRF selection technique for multiple targets in track-before-detect. In *2013 5th IEEE International Workshop*

on Computational Advances in Multi-Sensor Adaptive Processing (CAMSAP), pages 448–451. IEEE, 2013.

[7] Y. Bar-Shalom, F. Daum, and J. Huang. The probabilistic data association filter. *IEEE Control Systems Magazine*, 29(6):82–100, 2009.

[8] Y. Bar-Shalom, X. R. Li, and T. Kirubarajan. *Estimation with Applications to Tracking and Navigation: Theory Algorithms and Software*. John Wiley & Sons, 2004.

[9] S. S. Blackman. Multiple hypothesis tracking for multiple target tracking. *IEEE Aerospace and Electronic Systems Magazine*, 19(1):5–18, 2004.

[10] S. Boyd, S. P. Boyd, and L. Vandenberghe. *Convex Optimization*. Cambridge university press, 2004.

[11] M. A. Bruna, K. F. Bing, and M. Minges. Airborne bistatic radar trajectory optimization for ground geolocation accuracy maximization. In *2017 IEEE Radar Conference (RadarConf)*, pages 1608–1613, 2017.

[12] D. A. Castanon. Approximate dynamic programming for sensor management. In *Proceedings of the 36th IEEE Conference on Decision and Control*, volume 2, pages 1202–1207. IEEE, 1997.

[13] P. G. Davies and E. J. Hughes. Medium PRF set selection using evolutionary algorithms. *IEEE Transactions on Aerospace and Electronic Systems*, 38(3):933–939, 2002.

[14] K. Deb, A. Pratap, S. Agarwal, and T. Meyarivan. A fast and elitist multiobjective genetic algorithm: NSGA-II. *IEEE transactions on evolutionary computation*, 6(2):182–197, 2002.

[15] Z. Ding. A survey of radar resource management algorithms. In *2008 Canadian Conference on Electrical and Computer Engineering*, pages 001559–001564. IEEE, 2008.

[16] K. Dogancay. Online optimization of receiver trajectories for scan-based emitter localization. *IEEE Transactions on Aerospace and Electronic Systems*, 43(3):1117–1125, 2007.

[17] K. Doğançay. Single-and multi-platform constrained sensor path optimization for angle-of-arrival target tracking. In *2010 18th European Signal Processing Conference*, pages 835–839. IEEE, 2010.

[18] K. Dogancay. UAV path planning for passive emitter localization. *IEEE Transactions on Aerospace and Electronic systems*, 48(2):1150–1166, 2012.

[19] A. J. Fenn, D. H. Temme, W. P. Delaney, and W. E. Courtney. The development of phased-array radar technology. *Lincoln Laboratory Journal*, 12(2):321–340, 2000.

[20] E. Frew. Receding horizon control using random search for UAV navigation with passive, non-cooperative sensing. In *AIAA guidance, navigation, and control conference and exhibit*, page 5864, 2005.

[21] S. Ghosh, R. R. Rajkumar, J. Hansen, and J. Lehoczky. Integrated QoS-aware

resource management and scheduling with multi-resource constraints. *Real-Time Systems*, 33(1-3):7–46, 2006.

[22] H. Godrich, A. P. Petropulu, and H. V. Poor. Power allocation strategies for target localization in distributed multiple-radar architectures. *IEEE Transactions on Signal Processing*, 59(7):3226–3240, 2011.

[23] E. Hanle. Survey of bistatic and multistatic radar. *IEE Proceedings F - Communications, Radar and Signal Processing*, 133(7):587–595, 1986.

[24] S. He, H.-S. Shin, and A. Tsourdos. Trajectory optimization for target localization with bearing-only measurement. *IEEE Transactions on Robotics*, 2019.

[25] M. Hernandez, T. Kirubarajan, and Y. Bar-Shalom. Multisensor resource deployment using Posterior Cramér-Rao bounds. *IEEE Transactions on Aerospace and Electronic Systems*, 40(2):399–416, 2004.

[26] M. L. Hernandez. Optimal sensor trajectories in bearings-only tracking. In *Proceedings of the Seventh International Conference on Information Fusion*, volume 2, pages 893–900, 2004.

[27] A. O. Hero and D. Cochran. Sensor management: Past, present, and future. *IEEE Sensors Journal*, 11(12):3064–3075, 2011.

[28] M. W. Hofbaur and B. C. Williams. Hybrid estimation of complex systems. *IEEE Transactions on Systems, Man, and Cybernetics, Part B (Cybernetics)*, 34(5):2178–2191, 2004.

[29] S.-M. Hong and Y.-H. Jung. Optimal scheduling of track updates in phased

array radars. *IEEE transactions on Aerospace and Electronic Systems*, 34(3):1016–1022, 1998.

[30] R. Huang and G. V. Zaruba. Static path planning for mobile beacons to localize sensor networks. In *Fifth annual IEEE international conference on pervasive computing and communications workshops (PerComW'07)*, pages 323–330. IEEE, 2007.

[31] E. J. Hughes and C. M. Alabaster. Medium PRF radar PRF optimisation using evolutionary algorithms. In *Proceedings of the 2003 IEEE Radar Conference (Cat. No. 03CH37474)*, pages 192–197. IEEE, 2003.

[32] E. J. Hughes and C. M. Alabaster. Novel PRF Schedules for medium PRF radar. In *2003 Proceedings of the International Conference on Radar (IEEE Cat. No. 03EX695)*, pages 678–683. IEEE, 2003.

[33] A. Irci, A. Saranli, and B. Baykal. Study on Q-RAM and feasible directions based methods for resource management in phased array radar systems. *IEEE Transactions on Aerospace and Electronic Systems*, 46(4):1848–1864, 2010.

[34] A. Izquierdo-Fuente and J. Casar-Corredera. Optimal radar pulse scheduling using a neural network. In *Proceedings of 1994 IEEE International Conference on Neural Networks (ICNN'94)*, volume 7, pages 4588–4591. IEEE, 1994.

[35] M. Jevtić, N. Zogović, and S. Graovac. Evolutionary multi-objective optimisation of the pulse burst waveform in solid-state vhf moving target detection radar. *IET Radar, Sonar & Navigation*, 13(12):2093–2101, 2019.

[36] B. Jin, J. Guo, B. Su, D. He, and Z. Zhang. Adaptive waveform selection for maneuvering target tracking in cognitive radar. *Digital Signal Processing*, 75:210–221, 2018.

[37] B. Jiu, H. Liu, L. Zhang, Y. Wang, and T. Luo. Wideband cognitive radar waveform optimization for joint target radar signature estimation and target detection. *IEEE Transactions on Aerospace and Electronic Systems*, 51(2):1530–1546, 2015.

[38] P.-S. Kang and C.-G. Lee. Coordinated search and track by multiple phased array radars. In *Proceedings. RTAS 2004. 10th IEEE Real-Time and Embedded Technology and Applications Symposium, 2004.*, pages 227–235. IEEE, 2004.

[39] D. J. Kershaw and R. J. Evans. Optimal waveform selection for tracking systems. *IEEE Transactions on Information Theory*, 40(5):1536–1550, 1994.

[40] E. F. Knott. *Radar cross section measurements*. Springer Science & Business Media, 2012.

[41] P. D. Konstantinova, A. Udvarev, and T. Semerdjiev. A study of a target tracking algorithm using global nearest neighbor approach. In *Compsystech*, volume 3, pages 290–295, 2003.

[42] F. Koohifar, A. Kumbhar, and I. Guvenc. Receding horizon multi-UAV cooperative tracking of moving RF source. *IEEE Communications Letters*, 21(6):1433–1436, 2016.

[43] T.-W. Kuo, Y.-S. Chao, C.-F. Kuo, and C. Chang. Real-time dwell scheduling

of component-oriented phased array radars. *IEEE Transactions on Computers*, 54(1):47–60, 2005.

[44] B. La Scala, W. Moran, and R. Evans. Optimal adaptive waveform selection for target detection. In *2003 Proceedings of the International Conference on Radar (IEEE Cat. No. 03EX695)*, pages 492–496. IEEE, 2003.

[45] Z. Li, J. Xie, H. Zhang, H. Xiang, and Z. Zhang. Adaptive sensor scheduling and resource allocation in netted collocated mimo radar system for multi-target tracking. *IEEE Access*, 8:109976–109988, 2020.

[46] W. H. Long and K. A. Harriger. Medium PRF for the AN/APG-66 radar. *Proceedings of the IEEE*, 73(2):301–311, 1985.

[47] Y. Lu, C. Han, Z. He, S. Liu, and Y. Wang. Adaptive JSPA in distributed colocated MIMO radar network for multiple targets tracking. *IET Radar, Sonar & Navigation*, 13(3):410–419, 2018.

[48] E. Mazor, A. Averbuch, Y. Bar-Shalom, and J. Dayan. Interacting multiple model methods in target tracking: a survey. *IEEE Transactions on aerospace and electronic systems*, 34(1):103–123, 1998.

[49] S. Miranda, C. Baker, K. Woodbridge, and H. Griffiths. Knowledge-based resource management for multifunction radar: a look at scheduling and task prioritization. *IEEE Signal Processing Magazine*, 23(1):66–76, 2006.

[50] S. Miranda, C. Baker, K. Woodbridge, and H. Griffiths. Fuzzy logic approach for prioritisation of radar tasks and sectors of surveillance in multifunction radar. *IET Radar, Sonar & Navigation*, 1(2):131–141, 2007.

[51] P. Moo and Z. Ding. *Adaptive radar resource management*. Academic Press, 2015.

[52] P. W. Moo and Z. Ding. Coordinated radar resource management for networked phased array radars. *IET Radar, Sonar & Navigation*, 9(8):1009–1020, 2015.

[53] A. S. Narykov, O. A. Krasnov, and A. Yarovoy. Algorithm for resource management of multiple phased array radars for target tracking. In *Proceedings of the 16th International Conference on Information Fusion*, pages 1258–1264. IEEE, 2013.

[54] N. H. Nguyen and K. Doğançay. Optimal geometry analysis for multistatic TOA localization. *IEEE Transactions on Signal Processing*, 64(16):4180–4193, 2016.

[55] N. H. Nguyen, K. Dogancay, and L. M. Davis. Adaptive waveform selection for multistatic target tracking. *IEEE Transactions on Aerospace and Electronic Systems*, 51(1):688–701, 2015.

[56] I. K. Nikolos, E. S. Zografos, and A. N. Brintaki. UAV path planning using evolutionary algorithms. In *Innovations in intelligent machines-1*, pages 77–111. Springer, 2007.

[57] R. Niu, R. S. Blum, P. K. Varshney, and A. L. Drozd. Target localization and tracking in noncoherent multiple-input multiple-output radar systems. *IEEE Transactions on Aerospace and Electronic Systems*, 48(2):1466–1489, 2012.

[58] R. Niu, P. Willett, and Y. Bar-Shalom. Matrix CRLB scaling due to measurements of uncertain origin. *IEEE Transactions on Signal Processing*, 49(7):1325–1335, 2001.

[59] A. Orman, C. N. Potts, A. Shahani, and A. Moore. Scheduling for a multi-function phased array radar system. *European Journal of operational research*, 90(1):13–25, 1996.

[60] A. Paris, I. Del Portillo, B. Cameron, and E. Crawley. A genetic algorithm for joint power and bandwidth allocation in multibeam satellite systems. In *2019 IEEE Aerospace Conference*, pages 1–15. IEEE, 2019.

[61] R. R. Pitre, X. R. Li, and R. Delbalzo. UAV route planning for joint search and track missions—An information-value approach. *IEEE Transactions on Aerospace and Electronic Systems*, 48(3):2551–2565, 2012.

[62] K. Punithakumar, T. Kirubarajan, and M. Hernandez. Multisensor deployment using PCRLBs, incorporating sensor deployment and motion uncertainties. *IEEE Transactions on Aerospace and Electronic Systems*, 42(4):1474–1485, 2006.

[63] S. Ragi and E. K. Chong. UAV path planning in a dynamic environment via partially observable Markov decision process. *IEEE Transactions on Aerospace and Electronic Systems*, 49(4):2397–2412, 2013.

[64] V. Roberge, M. Tarbouchi, and G. Labonté. Comparison of parallel genetic algorithm and particle swarm optimization for real-time UAV path planning. *IEEE Transactions on industrial informatics*, 9(1):132–141, 2012.

[65] C. O. Savage and B. Moran. Waveform selection for maneuvering targets within an IMM framework. *IEEE Transactions on Aerospace and Electronic Systems*, 43(3):1205–1214, 2007.

[66] W. W. Schmaedeke. Information-based sensor management. In *Signal processing, sensor fusion, and target recognition II*, volume 1955, pages 156–164. International Society for Optics and Photonics, 1993.

[67] K. M. Scott, W. C. Barott, and B. Himed. Illuminator selection statistics using atsc passive radar with a mobile receiver. In *2018 IEEE Radar Conference (RadarConf18)*, pages 0981–0986. IEEE, 2018.

[68] T. A. Severson and D. A. Paley. Distributed multitarget search and track assignment with consensus-based coordination. *IEEE Sensors Journal*, 15(2):864–875, 2014.

[69] M. Shaghaghi and R. S. Adve. Machine learning based cognitive radar resource management. In *2018 IEEE Radar Conference (RadarConf18)*, pages 1433–1438. IEEE, 2018.

[70] N. Sharaga, J. Tabrikian, and H. Messer. Optimal cognitive beamforming for target tracking in mimo radar/sonar. *IEEE Journal of Selected Topics in Signal Processing*, 9(8):1440–1450, 2015.

[71] J. She, F. Wang, and J. Zhou. A novel sensor selection and power allocation algorithm for multiple-target tracking in an lpi radar network. *Sensors*, 16(12):2193, 2016.

[72] C. Shi, Y. Wang, S. Salous, J. Zhou, and J. Yan. Joint transmit resource management and waveform selection strategy for target tracking in distributed phased array radar network. *IEEE Transactions on Aerospace and Electronic Systems*, 58(4):2762–2778, 2021.

[73] J. d. Silva Arantes, M. d. Silva Arantes, C. F. Motta Toledo, O. T. Júnior, and B. C. Williams. Heuristic and genetic algorithm approaches for UAV path planning under critical situation. *International Journal on Artificial Intelligence Tools*, 26(01):1760008, 2017.

[74] A. Sinha, T. Kirubarajan, and Y. Bar-Shalom. Autonomous surveillance by multiple cooperative UAVs. In *Signal and Data Processing of Small Targets 2005*, volume 5913, page 59131V. International Society for Optics and Photonics, 2005.

[75] S. P. Sira, A. Papandreou-Suppappola, and D. Morrell. Dynamic configuration of time-varying waveforms for agile sensing and tracking in clutter. *IEEE Transactions on Signal Processing*, 55(7):3207–3217, 2007.

[76] T. L. Song and D. Mušicki. Target existence based resource allocation. *IEEE Transactions on Signal Processing*, 58(9):4496–4506, 2010.

[77] A. Sonmez, E. Kocyigit, and E. Kugu. Optimal path planning for UAVs using genetic algorithm. In *2015 International Conference on Unmanned Aircraft Systems (ICUAS)*, pages 50–55. IEEE, 2015.

[78] P. Stinco, M. Greco, F. Gini, and A. Farina. Sensor selection in PCL radar

systems based on bistatic PCRLB. In *2012 Tyrrhenian Workshop on Advances in Radar and Remote Sensing (TyWRRS)*, pages 41–45. IEEE, 2012.

[79] D. Stromberg and P. Grahn. Scheduling of tasks in phased array radar. In *Proceedings of International Symposium on Phased Array Systems and Technology*, pages 318–321. IEEE, 1996.

[80] Z. Sun, J. Wu, J. Yang, Y. Huang, C. Li, and D. Li. Path planning for GEO-UAV bistatic SAR using constrained adaptive multiobjective differential evolution. *IEEE Transactions on Geoscience and Remote Sensing*, 54(11):6444–6457, 2016.

[81] R. Tharmarasa, A. Chatterjee, Y. Wang, T. Kirubarajan, J. Berger, and M. C. Florea. Closed-loop multi-satellite scheduling based on hierarchical mdp. In *2019 22th International Conference on Information Fusion (FUSION)*, pages 1–7. IEEE, 2019.

[82] R. Tharmarasa, T. Kirubarajan, M. L. Hernandez, and A. Sinha. PCRLB-based multisensor array management for multitarget tracking. *IEEE Transactions on Aerospace and Electronic Systems*, 43(2):539–555, 2007.

[83] R. Tharmarasa, T. Kirubarajan, and T. Lang. Joint path planning and sensor subset selection for multistatic sensor networks. In *2009 IEEE Symposium on Computational Intelligence for Security and Defense Applications*, pages 1–8, 2009.

[84] R. Tharmarasa, T. Kirubarajan, J. Peng, and T. Lang. Optimization-based

dynamic sensor management for distributed multitarget tracking. *IEEE Transactions on Systems, Man, and Cybernetics, Part C (Applications and Reviews)*, 39(5):534–546, 2009.

[85] R. Tharmarasa, T. Kirubarajan, A. Sinha, and T. Lang. Decentralized sensor selection for large-scale multisensor-multitarget tracking. *IEEE Transactions on Aerospace and Electronic systems*, 47(2):1307–1324, 2011.

[86] P. Tichavsky, C. H. Muravchik, and A. Nehorai. Posterior Cramér-Rao bounds for discrete-time nonlinear filtering. *IEEE Transactions on signal processing*, 46(5):1386–1396, 1998.

[87] G. van Keuk and S. S. Blackman. On phased-array radar tracking and parameter control. *IEEE Transactions on aerospace and electronic systems*, 29(1):186–194, 1993.

[88] R. B. Washburn, M. Schneider, and J. Fox. Stochastic dynamic programming based approaches to sensor resource management. In *Proceedings of the Fifth International Conference on Information Fusion. FUSION 2002.(IEEE Cat. No. 02EX5997)*, volume 1, pages 608–615. IEEE, 2002.

[89] D. Wiley, S. Parry, C. Alabaster, and E. Hughes. Performance comparison of PRF schedules for medium PRF radar. *IEEE transactions on aerospace and electronic systems*, 42(2):601–611, 2006.

[90] J. Wu, H. Wang, N. Li, P. Yao, Y. Huang, and H. Yang. Path planning for solar-powered UAV in urban environment. *Neurocomputing*, 275:2055–2065, 2018.

[91] X.-G. Xia. Doppler ambiguity resolution using optimal multiple pulse repetition frequencies. *IEEE Transactions on Aerospace and Electronic systems*, 35(1):371–379, 1999.

[92] M. Xie, W. Yi, T. Kirubarajan, and L. Kong. Joint node selection and power allocation strategy for multitarget tracking in decentralized radar networks. *IEEE Transactions on Signal Processing*, 66(3):729–743, 2017.

[93] S. Xu and K. Doğançay. Optimal sensor placement for 3-D angle-of-arrival target localization. *IEEE Transactions on Aerospace and Electronic Systems*, 53(3):1196–1211, 2017.

[94] J. Yan, H. Liu, B. Jiu, B. Chen, Z. Liu, and Z. Bao. Simultaneous multibeam resource allocation scheme for multiple target tracking. *IEEE Transactions on Signal Processing*, 63(12):3110–3122, 2015.

[95] J. Yan, H. Liu, W. Pu, S. Zhou, Z. Liu, and Z. Bao. Joint beam selection and power allocation for multiple target tracking in netted colocated mimo radar system. *IEEE Transactions on Signal Processing*, 64(24):6417–6427, 2016.

[96] J. Yan, W. Pu, J. Dai, H. Liu, and Z. Bao. Resource allocation for search and track application in phased array radar based on pareto bi-objective optimization. *IEEE Transactions on Vehicular Technology*, 68(4):3487–3499, 2019.

[97] P. Zhan, D. W. Casbeer, and A. L. Swindlehurst. Adaptive mobile sensor positioning for multi-static target tracking. *IEEE Transactions on Aerospace and Electronic Systems*, 46(1):120–132, 2010.

[98] H. Zhang, J. Xie, J. Ge, Z. Zhang, and B. Zong. A hybrid adaptively genetic algorithm for task scheduling problem in the phased array radar. *European Journal of Operational Research*, 272(3):868–878, 2019.

[99] H. Zhang, J. Xie, J. Shi, T. Fei, J. Ge, and Z. Zhang. Joint beam and waveform selection for the mimo radar target tracking. *Signal Processing*, 156:31–40, 2019.

[100] Z. Zhang, J. Zhou, F. Wang, W. Liu, and H. Yang. Multiple-target tracking with adaptive sampling intervals for phased-array radar. *Journal of Systems Engineering and Electronics*, 22(5):760–766, 2011.